STRUCTURAL STUDIES OF CHAPERONES AND CHAPERONE-TIP INTERACTIONS FROM THE TYPE III SECRETION SYSTEMS OF *YERSINIA* AND *PSEUDOMONAS*

By

SUKANYA CHAUDHURY

Submitted to the graduate degree program in Molecular Biosciences
and the Graduate Faculty of the University of Kansas
in partial fulfillment of the requirements for the degree of
Doctor of Philosophy.

Chairperson Roberto N. De Guzman, PhD

Committee members Susan M. Egan, PhD

David Davido, PhD

P. Scott Hefty, PhD

Mark Richter, PhD

David Weis, PhD

Date Defended: 04/15/2013

The Dissertation Committee for Sukanya Chaudhury
certifies that this is the approved version of the following dissertation:

STRUCTURAL STUDIES OF CHAPERONES AND CHAPERONE-TIP INTERACTIONS FROM THE TYPE III SECRETION SYSTEMS OF *YERSINIA* AND *PSEUDOMONAS*

Chairperson _____ Roberto N. De Guzman, PhD

Date approved: 04/24/2013

Abstract

Many Gram-negative bacteria assemble a complex nanomachine, the type III secretion system (T3SS) to inject virulence proteins directly into eukaryotic cells to initiate infection. The T3SS is composed of structural and non-structural proteins. The structural component of the T3SS is a needle apparatus composed of a membrane embedded basal structure, an external needle, a tip complex that caps the needle and a translocon. Chaperones are small cytoplasmic proteins that assist in the assembly and proper operation of the T3SS. They serve as important regulators of secretion and sequester effector proteins and other structural components while inside the bacterial cytosol.

Yersinia pestis is the causative agent of plague that in the past has caused worldwide pandemics, and is considered a potential agent of bioterrorism. *Pseudomonas aeruginosa* is an opportunistic pathogen that is most frequently associated with nosocomial infections of immuno-compromised patients. A key factor in the pathogenesis of *Y. pestis* and *P. aeruginosa* is that they harbor the T3SS, which enables them to inject virulent effector proteins that hijack the host cellular machinery and facilitate the survival of these bacteria inside the host cells.

An important component of the *Y. pestis* and the *P. aeruginosa* T3SS is the LcrG/PcrG family of chaperone proteins, which form a complex with the T3SS tip proteins LcrV and PcrV. They also function as important regulators of effector secretion and facilitate the translocation of effector proteins into the targeted host cells. The atomic structures of members of the LcrG/PcrG family of chaperone proteins are currently unknown. Further, how they interact with their cognate tip proteins is poorly understood. Here, I show by CD and NMR spectroscopy that the chaperones,

LcrG and PcrG, lack compact tertiary structures. However, they are not completely disordered but contain secondary structure dominated by at least two major α-helices from residues Val-16 to Gly-41 and Glu-55 to Ser-76 in PcrG, and residues Asp-7 to Gly-38 and Ala-59 to Arg-73 in LcrG. NMR backbone dynamics studies show that the helices in the chaperones have semi-rigid flexibility and they tumble as a single entity with similar backbone dynamics. Thus the LcrG/PcrG family of T3SS chaperone proteins is partially folded. The conformational dynamics perhaps contribute to their functional versatility, which is a characteristic signature of many flexible proteins. Overall, the LcrG/PcrG family of proteins can be added to a growing list of partially folded proteins that play important roles in the bacterial type III secretion systems. The NMR titration data indicate that the tip proteins induce a global change in the overall structure of the chaperones upon complex formation. Further, the C-terminus of LcrG (Ser-52 to Ile-67) was identified to be important in blocking the secretion of Yop effectors in the *Y. pestis* T3SS.

Also described here is a crystal structure of LcrV, at a higher resolution (1.65 Å) than the previously described structure 1R6F. This current structure contains native residues in the N-terminal domain of LcrV as opposed to the original crystal structure, 1R6F, which was solved using triple mutations (K40A/D41A/K42A) in the N-terminal domain. The current structure should prove useful in future studies of the LcrV-translocon interaction.

The work presented in this dissertation provides the first structural insight into the conformation and dynamics of the LcrG/PcrG family of chaperones in solution and upon complex formation. This has enhanced our understanding of the mechanism by which these chaperones perform their multiple roles in regulating the type III secretion system.

ACKNOWLEDGEMENTS

First and foremost, I would like to thank my mentor, Dr. Roberto N. De Guzman for introducing me to the world of structural biology and NMR. Without his mentorship, guidance and unstinted support, none of this would have been possible. It was a pleasure, privilege and honor to work under his apprenticeship.

I would like to thank all past and current members of the De Guzman lab; it was a pleasure to work with all of them. Specially, I would like to thank Dr. Fernando Estrada and Dr. Yu Wang for all the stimulating discussions we shared. I would like to specially thank my lab colleagues Srirupa Chatterjee, Kawaljeet Kaur and Andrew Mc Shan for making the lab a great place to do science.

I would like to acknowledge The Department of Molecular Biosciences at the University of Kansas, which provided me with support and unparallel environments to work in. I would like to thank all the professors who taught me at KU. I would especially like to thank all my committee members for providing their valuable time and advice. I would like to acknowledge Dr. Scott Lovell and Dr. Asokan Anbanandam for their help and support

Last but not the least a special vote of thanks to my family members and my in-laws who stood like a rock behind me at all times. None of this would have been possible without the constant love, encouragement and support of my parents Sumit and Shipra Chaudhury and my sister Spandana. Finally, my husband Srayanta has supported and guided me throughout and has always remained my biggest strength.

Table of Contents

LIST OF TABLES

LIST OF FIGURES

LIST OF ABBREVIATIONS

T3SS	Type III Secretion System
Yop	*Yersinia* Outer Proteins
LCR	Low Ca^{+2} Response
HSQC	Heteronuclear Single Quantum Coherence
CD	Circular Dichroism
NMR	Nuclear Magnetic Resonance
IPTG	Isopropyl-β-D-thiogalactopyranoside
STEM	Scanning Transmission Electron Microscopy
SPR	Surface Plasmon Resonance
FP	Fluorescence Polarization
T_1	Longitudinal Relaxation Time
T_2	Transverse Relaxation Time
OM	Outer Membrane
IM	Inner Membrane

I dedicate this to my husband, son and parents

CHAPTER 1: Introduction

A key step involved in the pathogenesis of many bacteria is the secretion of virulence factors from the bacterial cytoplasm into the host cell. Accordingly, a number of complex protein translocation systems have evolved to aid the secretion process. Among them, the type III secretion system (T3SS) is utilized by many pathogenic Gram-negative bacteria to deliver effector proteins into the cytosol of targeted host cells (*1*). In this dissertation, the T3SS of two model organisms, *Yersinia pestis* and *Pseudomonas aeruginosa,* are chosen for structural studies of tip proteins (LcrV/PcrV) and their chaperones (LcrG/PcrG).

1.1 Yersinia pestis, etiological agent of plague

The Gram-negative bacterium *Yersinia pestis* is the causative agent of plague, a widespread zoonotic disease. The three main plague pandemics have caused large-scale social devastation in the past, claiming over 200 million deaths worldwide (*2*). Although it is not a major public health problem in the modern era, there are annual outbreaks of plague that occur throughout the world with ~2000-3000 (*3*) reported cases each year and it is considered a potential agent of bioterrorism (*4*). Rodents and fleas are the primary carriers of *Y. pestis*. Following the bite of an infected rat flea, *Y. pestis* multiplies in the lymph node causing bubonic plague. The infection can then spread into the bloodstream causing septicemic plague, and finally aerosol transmission of the bacteria by infected individuals causes pneumonic plague (*5*). Although bubonic plague can be successfully treated with antibiotics, pneumonic plague is almost invariably fatal (*4, 5*). The rapid development of pneumonic plague has made effective treatments with antibiotics difficult (*4, 5*).

1.2 Pseudomonas aeruginosa, an opportunistic pathogen

Pseudomonas aeruginosa is a ubiquitous Gram-negative pathogen and is capable of colonizing and infecting a large number of mammalian tissues (*6*). It is an opportunistic pathogen and is a common cause of nosocomial infections in immuno-compromised patients. It is commonly associated with patients suffering from sepsis, cystic fibrosis, pneumonia, urinary tract infections, wounds, and burns (*6, 7*). Despite treatment with potent antibiotics, the mortality rate is approximately 40% in cases of acute infections (*7*). The growing number of multi-drug resistant isolates of *P. aeruginosa* is a major concern for public health.

1.3 The Type III Secretion System

Both *Y. pestis* and *P. aeruginosa* harbor a contact-mediated protein-export apparatus, the T3SS, which is also referred to as an injectisome. The T3SS plays a key role in their pathogenesis and allows these bacteria to inject virulence proteins directly into the eukaryotic cells to initiate infection (*1, 8, 9*). The T3SS has been identified in plant, animal, and insect pathogens (*1, 8, 9*). Among these are many Gram-negative bacteria including *Salmonella, Shigella, Yersinia, Pseudomonas, Burkholderia, Escherichia* and *Chlamydia spp.* The T3SS present in these animal pathogens can be grouped into three families, *(i)* the Ysc- family of T3SS includes the *Yersinia* Ysc, the *Pseudomonas* Psc, and the *Aeromonas* Asc, *(ii)* the Inv-Mxi-Spa family includes the *Salmonella (Salmonella* Pathogenicity Island-1 i.e. SPI-1) and *Shigella* systems, and *(iii)* the Ssa-Esc family includes the *Salmonella* (*Salmonella* Pathogenicity Island-2 i.e. SPI-2), enteropathogenic *E. coli* (EPEC) and the enterohemorrhagic *E. coli* (EHEC) systems (*10*). The Ysc-family of T3SS is the focus in this dissertation.

About 25 different proteins are required for the proper functioning of the T3SS, which is composed of both structural and non-structural proteins (*1*). The structural proteins are needed to assemble the needle apparatus, which consists of a membrane embedded basal structure, an external needle that protrudes from the bacterial surface, and a tip complex that caps the needle. Upon host cell contact, a translocon is assembled between the needle tip complex and the host cell, serving as a gateway for translocation of effector proteins by creating a pore in the host cell membrane. Following delivery into the host cytoplasm, effectors initiate and maintain infection by manipulating host cell biology, such as cell signaling, intracellular trafficking, cytoskeletal dynamics, inflammatory response, and inhibition of phagocytosis. Finally, chaperones play an important role in the assembly, function and regulation of the different T3SS components, namely the effectors, translocon, needle and tip proteins (*1*).

1.4 The Type III Secretion System in Yersinia pestis

In *Y. pestis* the genes for the T3SS, which is also referred to as the Ysc-Yop system, is encoded on a 70-kb plasmid called pCD1 (*8, 9, 11*). The T3SS allows *Y. pestis* to inject effector Yops (*Yersinia* outer proteins) into the cytosol of eukaryotic cells **(Figure 1-1)**. The six known effector Yops (YopH, T, E, O, P/J, and M) then collectively act towards disturbing the dynamics of the cytoskeleton, preventing phagocytosis and blocking the production of pro-inflammatory cytokines, adhesion molecules and chemokines; thereby favoring the survival and multiplication of *Y. pestis* inside the host cells (*8, 9*). The needle apparatus consists of a basal body that spans the peptidoglycan layer and the two bacterial membranes. The basal body is composed of an outer membrane (OM) ring formed by the secretin protein YscC, an inner membrane (IM) ring

formed by two proteins, YscD and YscJ, an export apparatus composed of five different proteins YscV, U, R, T and S and an ATPase, YscN (*12*). The external part of the Ysc needle apparatus is made up of a hollow needle with a diameter of ~20 Å (*8*). The needle is formed by the helical polymerization of a small protein, YscF (*8*). On the distal end of the needle sits the tip complex formed by several copies of the tip protein, LcrV (*8, 13*). Upon host cell contact, two hydrophobic proteins, YopB and YopD, assemble the translocon, which forms a pore in the host cell membrane to allow the passage of effectors inside the host cells (*8*). LcrV, YopB and YopD are indispensable for the delivery of the effectors into the host cell (*8*). Several of these Yops need the assistance of specialized chaperones for their efficient secretion through the injectisome (*8*). Likewise, while inside the bacterial cytosol, the tip protein LcrV is chaperoned by a smaller protein, LcrG (95 residues). Analysis of these two proteins, LcrV and LcrG, forms an integral part of my dissertation.

1.5 The Type III Secretion System in Pseudomonas aeruginosa

The T3SS in *P. aeruginosa* is encoded by ~36 chromosomal genes present in five operons, together with 6 other genes scattered throughout the chromosome (*14*). The overall architecture of the T3SS in *P. aeruginosa* is similar to the Ysc-Yop system in *Y. pestis* **(Figure 1-1)**. Similar to the *Yersinia* system, the base is composed of an OM ring formed by the secretin PscC, and an IM ring formed by the lipoprotein, PscJ (*14*). The ATPase, PscN, energizes the export of substrates through the secretion channel (*14*). Likewise the external needle is composed of PscF,

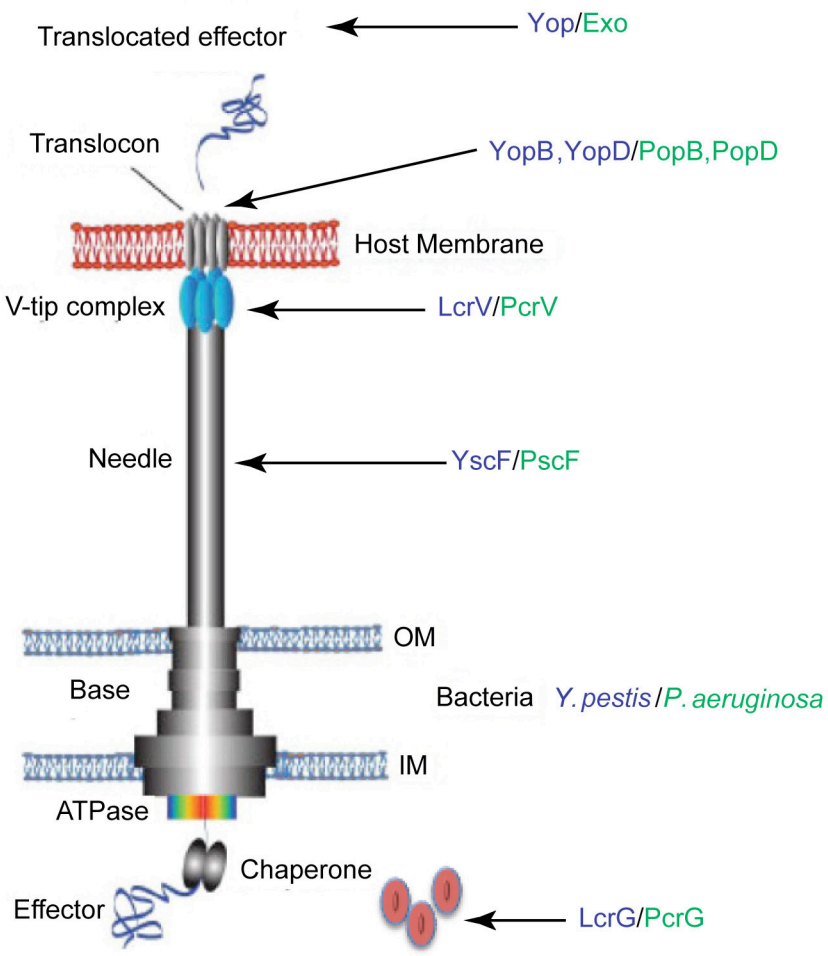

Figure 1-1. Schematic of the T3SS of *Y. pestis* and *P. aeruginosa*. The names of the respective proteins that assemble the different parts of the T3SS are colored in blue for *Y. pestis* and green for *P. aeruginosa.* The base spans the bacterial outer (OM) and inner membrane (IM). The needle is formed by the polymerization of YscF/PscF. LcrV/PcrV forms the pentameric V-tip complex that sits on top of the needle. YopB, YopD/PopB, PopD assemble the translocon. An effector protein (blue ribbon) is transferred through the T3SS and delivered to the host cells. LcrG and PcrG function as chaperones of the respective tip proteins LcrV and PcrV. This figure is modified from (*15*).

the tip complex is formed by PcrV, and the hydrophobic proteins PopB and PopD assemble to form the translocon (*14*). Upon assembly of the T3SS, *P. aeruginosa* utilizes this system to inject effector proteins into the host cell. The four known effector proteins (ExoS, T, U and Y) then disrupt the epithelial barrier, inhibit wound repair, induce apoptosis and prevent bacterial uptake by phagocytes (*7*). Similar to *Yersinia*, chaperones play an important role in assisting effectors, needle protein, translocon protein and the tip protein (*14*). The tip protein of *P. aeruginosa* T3SS, PcrV is chaperoned by a small protein, PcrG (98 amino acids) (*16, 17*). Analysis of the structure and function of these two proteins PcrV and PcrG forms an integral part of my dissertation.

1.6 V-tip proteins, roles, structure and assembly

The *Yersinia* LcrV and the *Pseudomonas* PcrV belong to the same T3SS family and can be grouped together as V-tip proteins (*1, 10, 15*). LcrV and PcrV share ~37% sequence identity with each other (*15*). The tip proteins play an important role in the pathogenicity of *Y. pestis* and *P. aeruginosa.* Deletion mutants of the genes encoding the tip proteins, LcrV or PcrV were avirulent in mice (*15, 18-22*) and non-cytotoxic during infection of cultured epithelial or phagocytic cells (*17, 23-25*). The tip proteins have multifunctional roles. Firstly, due to their extracellular localization, they function as host cell sensors (*10, 15, 17, 26*). Secondly, they serve as a platform for the assembly of the translocon (*23, 25, 27*). LcrV and PcrV help in the proper insertion of the translocon proteins YopB/YopD and PopB/PopD, respectively in the host cell membranes, and thereby assist in the formation of functional pore complexes (*23, 25, 27*). Thirdly, they are important for the translocation of effector proteins into the host cytosol (*10, 17,*

24, 27, 28) and they also regulate the secretion of effectors into the host cell (*10, 15, 17, 26*). This mechanism of regulation of effector secretion is different between PcrV and LcrV and will be discussed in the following sections.

The 2.2 Å crystal structure of LcrV (*29*) represents what is currently known about the atomic structure of the LcrV/PcrV family of tip proteins **(Figure 1-2)**. This crystal structure was solved using an LcrV construct containing triple mutations (K40A/D41A/K42A) (*29*). The overall structure of LcrV can be described as "dumbbell-shaped" consisting of a central coiled coil connected by two globular domains (*29*). The central coiled coil motif of LcrV is a distinct structural feature that is highly conserved among all the known tip protein structures like SipD (*Salmonella*) (*30, 31*), BipD (*Burkholderia*) (*32, 33*) and IpaD (*Shigella*) (*32*). Comparisons of these tip protein structures, however, point to the absence of an N-terminal α-helical hairpin in LcrV. The N-terminal α-helical hairpin folds independently in SipD and IpaD (*34, 35*) and functions as a self-chaperone by preventing the self-oligomerization of BipD and IpaD (*32*). Additionally, the N-terminal α-helical hairpin hinders the interaction between the needle protomer PrgI and the tip protein SipD (*31*). Due to the absence of this N-terminal α-helical hairpin in LcrV, it is suggested that a small cytoplasmic protein, LcrG that functions as the chaperone for LcrV adopts a similar α-helical hairpin structure (*26, 32*). Likewise, the LcrG homolog in *Pseudomonas*, PcrG functions as a chaperone for the PcrV tip protein and is hypothesized to adopt an α-helical hairpin structure. The absence of an intra-molecular chaperoning domain in LcrV and PcrV hints at divergent assembly processes at the needle tip between the *Salmonella*/*Shigella* and the *Yersinia*/*Pseudomonas* species.

Low resolution electron micrographs of the *Yersinia* LcrV tip were obtained by *Mueller et al. (13)*, where they visualized LcrV as a well-defined structure at the tip of the needle **(Figure 1-2)**. Interestingly, both *pcrV* (*Pseudomonas)* and *acrV* (*Aeromonas)* could successfully complement an *lcrV* deletion by forming tip structures on *Yersinia* needles (*13*). This highlighted the structural and functional conservation among members of the V-tip protein family. The structure of the *Yersinia* LcrV tip complex showed a distinct head, neck, and a base (*13*). Broz *et al.* (*27*) concluded that the LcrV N-terminal globular domain forms the base, the C- terminal globular domain forms the head, and the coiled coil region forms the neck. The base was also shown to be responsible for the correct insertion of the *Yersinia* translocon protein YopB into the host cell membrane (*27*). Broz *et al.* (*27*), used the low-resolution structural data from the scanning transmission electron microscopy (STEM) (*13*) and multiple copies of the LcrV crystal structure (*29*) to fit the low-resolution density map to obtain a model of the tip complex. In the model of Broz *et al. (27)* LcrV is oriented where the N and C-termini point towards the needle, while the coiled coil domain is oriented inwards. Five LcrV monomers were found to be the best fit in this model. Broz *et al.* concluded that the *Yersinia* tip complex is formed by an LcrV pentameric ring (*27*).

1.7 Chaperones of the tip proteins

The architecture of the N-terminal domain of the V-tip proteins is different from other tip proteins of the T3SS families. Significantly, the V-tip proteins do not have any intra-molecular self-chaperoning domain (*15, 26*). It is suggested that two other relatively smaller cytoplasmic proteins, LcrG (95 amino acids) and PcrG (98 amino acids), serve as cognate chaperones for the

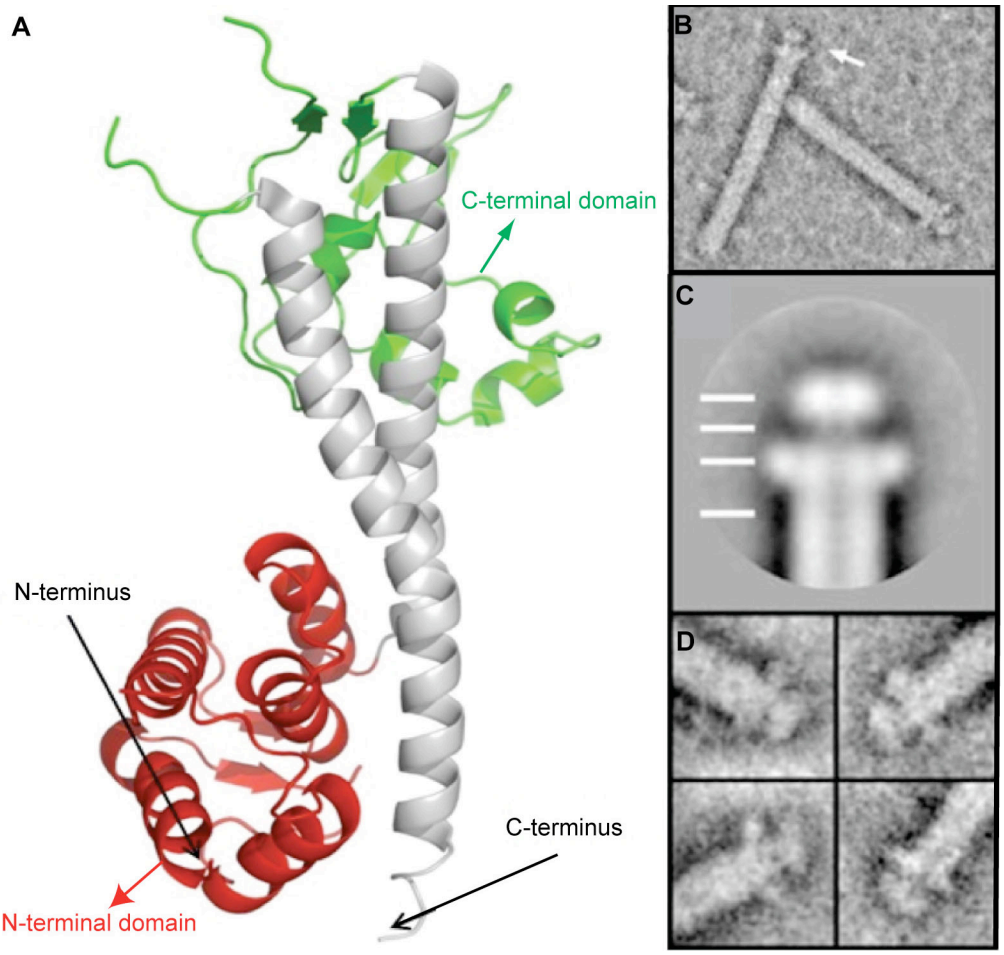

Figure 1-2. **(A)** Crystal structure of LcrV (*29*). The globular N-terminal domain is colored red, the central coiled coil is colored gray, and the mixed α/β domain is colored green. Scanning transmission electronmicrographs (STEM) showing **(B)** LcrV forms a well-defined structure (white arrow) at the tip of the needle. **(C)** the three distinct parts (head, neck and base) formed by the LcrV tip complex. **(D)** typical single images of the tip complexes formed by LcrV. Figures **B, C** and **D** are taken from (*13*).

V-tip proteins LcrV and PcrV, respectively (*15,17, 26*). LcrG and PcrG share about 40% sequence identity with each other (*16*). The chaperones and the V-tip proteins are all part of the same operon (*10, 17*). LcrG and PcrG are referred to as export chaperones and they facilitate the secretion of their respective tip proteins (*17, 36*). An *lcrG* deletion leads to significant decrease in LcrV secretion, which is restored upon complementation with wild type *lcrG* (*36*). Additionally, an LcrG mutant (A16R) that has lost the capacity to bind LcrV led to defective LcrV secretion (*17, 37*). Similarly both deletion of *pcrG* and a PcrG mutant (V16R) that can no longer bind to PcrV, led to a significant defect in PcrV export (*17*).

Other than facilitating secretion of the V-tip proteins, the LcrG/PcrG chaperones have additional regulatory roles in the T3SS of *Y. pestis* and *P. aeruginosa*. LcrG functions as a negative regulator of Yop secretion, i.e. increased levels of LcrG results in blockage of Yop secretion (*37-41*). LcrG also plays a facilitative role in targeting both effector Yops and translocator Yops (YopD) into the host cells (*36, 42*). LcrG does not have a direct role in targeting of Yops, rather it is an indirect effect of facilitating the secretion of LcrV, which then acts as the assembly platform for the translocator Yops, thereby allowing the secretion of Yop effectors. Like LcrG, PcrG acts as negative regulator of effector secretion and assists in the translocation of effectors into the host cells (*17, 43*).

1.8 Regulation of Yop secretion by LcrG and LcrV

In *Y. pestis*, the 70kb plasmid that encodes the T3SS is also called the **l**ow-**C**Ca^{+2} **r**esponse (LCR) virulence plasmid (*2, 11, 37, 41, 44*). *In vitro,* millimolar concentrations of Ca^{+2} maintain basal level of expression and almost no secretion of Yops (*37, 41, 44*). Removal of Ca^{+2} leads to full

induction of expression and secretion of Yops (*37, 41, 44*). Due to the dependence of *Yersinia* T3SS on Ca^{+2}, this regulatory mechanism is designated as the LCR. The absence of Ca^{+2} provides an unidentified signal that mimics the presence of host cell contact, which leads to the induction of LCR (*41*).

The secretion of Yops by the *Y. pestis* T3SS is a highly regulated process, and Yops are secreted *in vivo* only upon contact with the host cells (*45*). Several proteins are involved in regulating Yop secretion, among which, LcrG and LcrV play important roles in this process. The current model that explains the regulation of Yop secretion by LcrG and LcrV is the "Titration" model **(Figure 1-3**) proposed by Nilles and coworkers (*37, 39, 41*). In this model, the absence of host cell contact or in the presence of Ca^{+2}, LcrG blocks the T3SS from the cytoplasmic face and prevents secretion of Yops **(Figure 1-3)**. Upon host cell contact or in the absence of Ca^{+2}, there is an upregulation of the expression of LcrV, which then titrates away LcrG by forming a stable LcrG-LcrV complex **(Figure 1-3)**. This relieves the negative block thereby allowing the secretion of Yops. Thus, LcrV controls secretion of effectors from the cytoplasm through its interaction with LcrG. Hence, if LcrG-LcrV interaction is blocked, LcrG cannot be titrated away from the T3SS resulting in a constitutive blockage of secretion of Yops regardless of host cell contact or Ca^{+2} concentration **(Figure 1-3)**.

1.9 Regulation of effector secretion by PcrG and PcrV

As in *Y. pestis*, removal of Ca^{+2} *in vitro*, or the presence of host cell contact can trigger the secretion of effectors by the *P. aeruginosa* T3SS (*43, 46, 47*). The regulation of effector secretion by PcrG and PcrV are not well characterized as compared to the *Yersinia* counterparts.

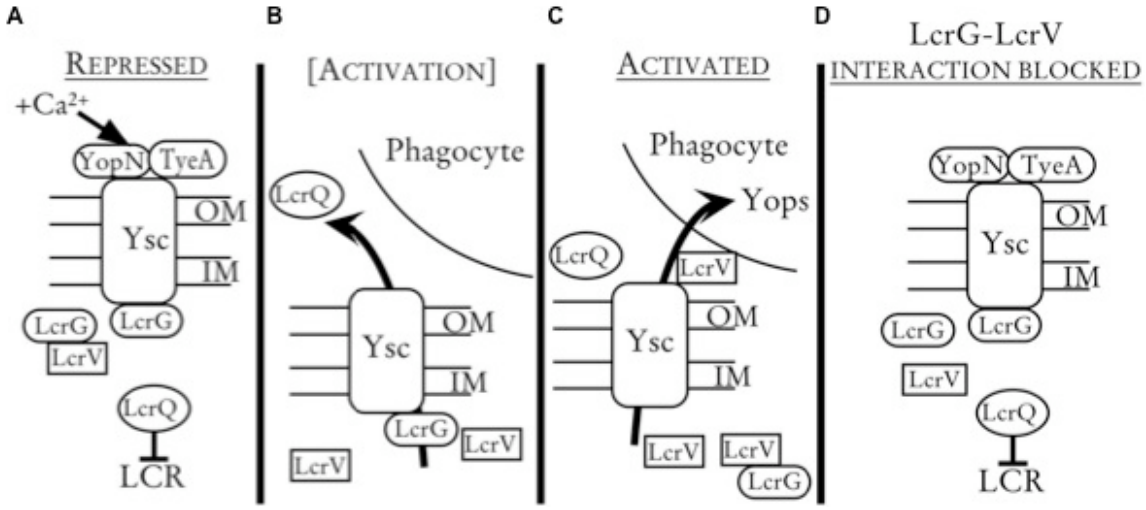

Figure 1-3. The LcrG titration model. **(A)** In the presence of millimolar amounts of Ca^{+2}, the Ysc is blocked by LcrG from the cytoplasm, and two other proteins YopN and TyeA from the cell surface. This secretion block retains LcrQ, a negative regulator, in the cell resulting in the repression of LCR regulated genes. **(B)** Upon host cell contact, LcrQ is released and higher levels of LcrV are produced. **(C)** Due to higher levels of LcrV, it titrates away LcrG from the Ysc by forming a stable LcrG-LcrV complex. This removes the negative block thereby allowing the Yops to be secreted into the host cells. **(D)** If the LcrG-LcrV interaction is blocked, then LcrG cannot be titrated away from the Ysc, thereby blocking secretion of Yops. This figure is taken from (*37*).

Deletion of *pcrG* and *pcrV* led to upregulation of effector export (*17, 46*), and both these deletions had an additive effect on secretion of effectors (*17*). Lee and coworkers (*17*) proposed a model that explains the regulation of effector secretion by PcrG and PcrV **(Figure 1-4)**. According to this model, the export of PcrV and its assembly at the needle tip, together with the interaction of PcrG with an unknown cytoplasmic component of the T3SS, turns off the secretion of effectors **(Figure 1-4)**. However, host cell contact induces a conformational change in the needle tip, which is propagated to the base of the apparatus, thereby releasing PcrG and triggering the secretion of effectors **(Figure 1-4)**. Thus, unlike the *Yersinia* model, where LcrV controls the secretion of effectors from the cytoplasm, PcrV controls the secretion of effectors by assembling at the needle tip. But similat to *Yersinia* LcrG, *Pseudomonas* PcrG also controls secretion of effectors from the cytoplasm. However, a PcrG point mutant (V16R) that was incapable of binding to PcrV, could control the secretion of effectors (*17*). Contrastingly, an LcrG mutant (A16R) that was unable to bind to LcrV, constitutively blocked the secretion of Yop effectors (*37*). Hence, contrary to the *Yersinia* model, where the LcrG-LcrV complex is important in the regulation of effector secretion, the PcrG-PcrV complex is suggested to be not important for regulation of effector secretion by the *P. aeruginosa* T3SS (*17*). Thus, unlike LcrG, PcrG controls secretion of effectors in a PcrV independent manner.

1.10 Biophysical properties of the chaperones and the chaperone-tip complexes

Knowledge about the three-dimensional structure of the chaperones or the chaperone-tip complexes is scant. Results from Circular Dichroism (CD) have shown that LcrG and PcrG are α-helical proteins (*16, 48*). Nanao *et al.* (*16*) has reported that the α-helicity of PcrG increases while in complex with PcrV, indicating that the structure of PcrG is somewhat stabilized upon

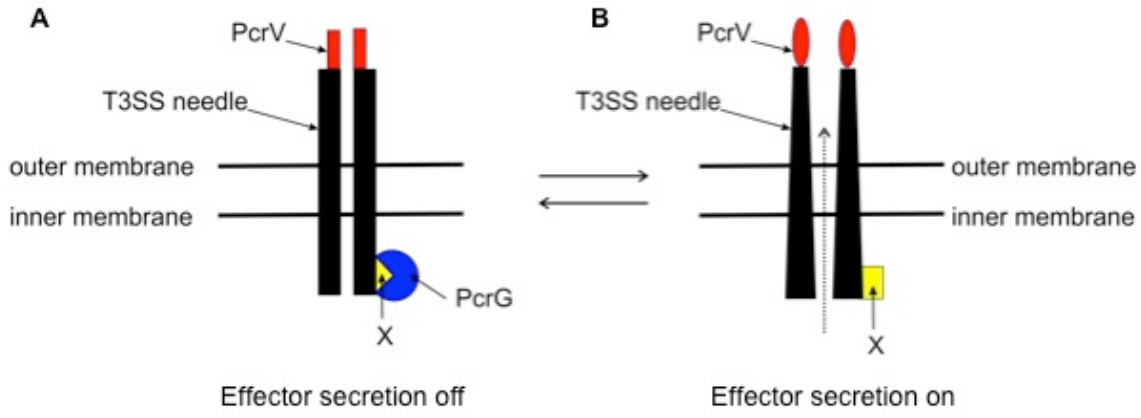

Figure 1-4. **(A)** The export of PcrV (red) and its assembly at the needle tip, together with interaction of PcrG (blue) with an unknown cytoplasmic component (X shown in yellow) of the T3SS, turns off secretion of effectors. **(B)** Host cell contact induces a conformational change in the needle tip, which is propagated to the base of the apparatus thereby releasing PcrG and triggering secretion of effectors. This figure is modified from (*17*).

complex formation with PcrV (*16*). Temperature scanning CD measurements showed that PcrG unfolds in a non-cooperative manner without a clear melting temperature (*16*). Based on the coiled coil nature of the self-chaperoning domains of IpaD, BipD and SipD; the helical nature of LcrG and PcrG; and the computational prediction (COILS Algorithim predicted that Asp-7 to Ala-35 of LcrG forms a coiled coil) (*40, 48*), it has been suggested in the literature that LcrG and PcrG form a coiled coil structure (*26*). Further, others have proposed that the interaction between the V-tip proteins (LcrV/PcrV) and their chaperones (LcrG/PcrG) are mediated by coiled coil domains (*40, 48*).

A direct interaction between LcrG and LcrV has been previously demonstrated by yeast-two-hybrid assay (*40*), chemical cross-linking and co-purification studies (*39*), surface plasmon resonance (SPR) (*48*), and ELISA (*48*). Using yeast-two-hybrid assay, it was demonstrated that the N-terminal region of LcrG is involved in the protein-protein interaction with residues Asp-7 to Thr-40 being the minimal region of LcrG required for binding to LcrV (**Figure 1-5**) (*40*). The coiled coil domain of LcrV was identified to be the site of protein-protein interaction with LcrG (*48, 49*). The dissociation constant (K_d) of the LcrG-LcrV interaction was estimated to be ~140 nM, which was determined by SPR (*48*). On the other hand, for the PcrG-PcrV complex, K_d of binding was estimated to be ~15.6 nM using SPR (*16*). Lee *et al.* (*17*) provided the first evidence using pull down and effector export assay that the two separate functions of PcrG, namely, the regulation of effector secretion and binding to its cognate tip protein, can be assigned to the two distinct halves of PcrG. The N-terminus of PcrG was demonstrated to be critical for binding PcrV, while the C-terminus was responsible for regulation of effector secretion, but both the halves of PcrG were required for efficient export of PcrV (**Figure 1-5**)

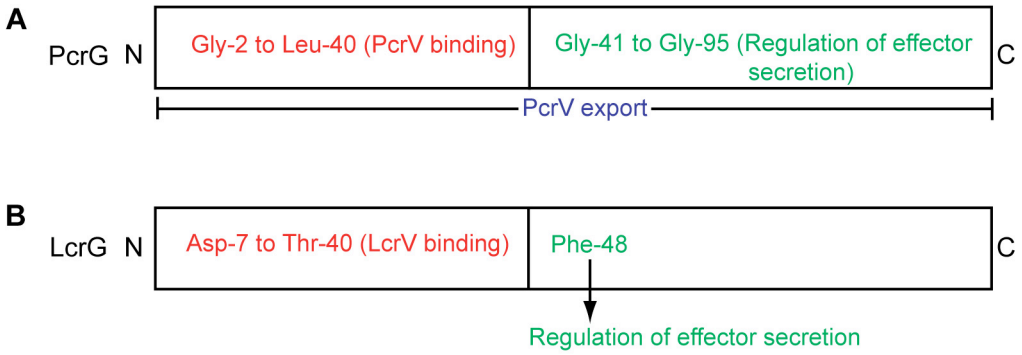

Figure 1-5. **(A)** Linear representation of PcrG showing the PcrV-binding region (red), the secretion regulation region (green), and the PcrV-export region (blue). **(B)** Linear representation of LcrG showing the LcrV-binding region (red) and the residue important for regulation of secretion (green). "N" and "C" denote the N and C termini of the two proteins.

(*17*). However, there was no evidence showing that the C-terminus of LcrG is important for the regulation of Yop secretion, while preliminary data suggests that Phe-48 in LcrG might be important for this regulatory function (**Figure 1-5**) (*40*).

1.11 Conclusion

There is a dearth of structural knowledge about the chaperones and the chaperone-tip complexes of the V-tip protein family. Specifically, critical questions remain unanswered, among them: i) The structure of V-tip chaperones, LcrG and PcrG; ii) The atomic-level detail of LcrG-LcrV and PcrG-PcrV interactions including the key residues involved in complex formation; and iii) Structural aspects of LcrG and PcrG which help them achieve their functional versatility. Accordingly, the primary aim of this research was to determine the three-dimensional structures of LcrG and PcrG and to characterize their interactions with their cognate tip proteins LcrV and PcrV by NMR spectroscopy. The subsequent chapters in this dissertation include, NMR characterization of the structure and dynamics of the V-tip chaperones and their complex: LcrG (Chapter 4), PcrG (Chapter 6), the LcrG-LcrV complex (Chapter 5) and the PcrG-PcrV complex (Chapter 6). The crystal structure of LcrV without the triple mutations in the N-terminal domain and at a higher resolution of 1.65 Å is also reported (Chapter 3). The N-terminal domain of LcrV was suggested to be the site of protein-protein interaction with the translocon (*27*), and hence this current structure of LcrV reported here will be useful.

Overall, the research in this dissertation has contributed new knowledge towards understanding the structural behavior of V-tip chaperones and how they interact with their respective V-tip proteins. The knowledge gained about their structures sheds light on their functional versatility.

In addition, this research has provided a refined crystal structure of LcrV with native residues in the N-terminal domain that will be useful in future structural studies of the protein-protein interaction of LcrV.

1.12 References

1. Cornelis, G. R. (2006) The type III secretion injectisome, *Nat. Rev. Microbiol. 4*, 811-825.
2. Perry, R. D., and Fetherston, J. D. (1997) Yersinia pestis--etiologic agent of plague, *Clin Microbiol Rev 10*, 35-66.
3. http://www.upmc-biosecurity.org/website/our_work/biological-threats-and-epidemics/fact_sheets/plague.html.
4. Riedel, S. (2005) Plague: from natural disease to bioterrorism, *Proc (Bayl Univ Med Cent) 18*, 116-124.
5. Titball, R. W., and Oyston, P. C. (2007) A plague upon fibrin, *Nat Med 13*, 253-254.
6. Lyczak, J. B., Cannon, C. L., and Pier, G. B. (2000) Establishment of *Pseudomonas aeruginosa* infection: lessons from a versatile opportunist, *Microbes Infect. 2*, 1051-1060.
7. Engel, J., and Balachandran, P. (2009) Role of Pseudomonas aeruginosa type III effectors in disease, *Curr Opin Microbiol 12*, 61-66.
8. Cornelis, G. R. (2002) The *Yersinia* Ysc-Yop 'type III' weaponry, *Nat Rev Mol Cell Biol 3*, 742-752.
9. Cornelis, G. R. (2002) *Yersinia* type III secretion: send in the effectors, *J. Cell Biol. 158*, 401-408.

10. Mueller, C. A., Broz, P., and Cornelis, G. R. (2008) The type III secretion system tip complex and translocon, *Mol. Microbiol. 68*, 1085-1095.

11. Perry, R. D., Straley, S. C., Fetherston, J. D., Rose, D. J., Gregor, J., and Blattner, F. R. (1998) DNA sequencing and analysis of the low-Ca2+-response plasmid pCD1 of *Yersinia pestis* KIM5, *Infect. Immun. 66*, 4611-4623.

12. Diepold, A., Wiesand, U., and Cornelis, G. R. (2011) The assembly of the export apparatus (YscR,S,T,U,V) of the Yersinia type III secretion apparatus occurs independently of other structural components and involves the formation of an YscV oligomer, *Mol Microbiol 82*, 502-514.

13. Mueller, C. A., Broz, P., Muller, S. A., Ringler, P., Erne-Brand, F., Sorg, I., Kuhn, M., Engel, A., and Cornelis, G. R. (2005) The V-antigen of *Yersinia* forms a distinct structure at the tip of injectisome needles, *Science 310*, 674-676.

14. Hauser, A. R. (2009) The type III secretion system of Pseudomonas aeruginosa: infection by injection, *Nat. Rev. Microbiol. 7*, 654-665.

15. Sato, H., and Frank, D. W. (2011) Multi-Functional Characteristics of the *Pseudomonas aeruginosa* Type III Needle-Tip Protein, PcrV; Comparison to Orthologs in other Gram-negative Bacteria, *Front. Microbiol. 2*, 142.

16. Nanao, M., Ricard-Blum, S., Di Guilmi, A. M., Lemaire, D., Lascoux, D., Chabert, J., Attree, I., and Dessen, A. (2003) Type III secretion proteins PcrV and PcrG from Pseudomonas aeruginosa form a 1:1 complex through high affinity interactions, *BMC.Microbiol. 3*, 21.

17. Lee, P. C., Stopford, C. M., Svenson, A. G., and Rietsch, A. (2010) Control of effector export by the Pseudomonas aeruginosa type III secretion proteins PcrG and PcrV, *Mol. Microbiol. 75*, 924-941.

18. Skrzypek, E., and Straley, S. C. (1995) Differential effects of deletions in lcrV on secretion of V antigen, regulation of the low-Ca2+ response, and virulence of Yersinia pestis, *J Bacteriol 177*, 2530-2542.

19. Sato, H., Hunt, M. L., Weiner, J. J., Hansen, A. T., and Frank, D. W. (2011) Modified needle-tip PcrV proteins reveal distinct phenotypes relevant to the control of type III secretion and intoxication by Pseudomonas aeruginosa, *PLoS One 6*, e18356.

20. Carter, P. B., Zahorchak, R. J., and Brubaker, R. R. (1980) Plague virulence antigens from Yersinia enterocolitica, *Infect Immun 28*, 638-640.

21. Price, S. B., Cowan, C., Perry, R. D., and Straley, S. C. (1991) The Yersinia pestis V antigen is a regulatory protein necessary for Ca2(+)-dependent growth and maximal expression of low-Ca2+ response virulence genes, *J Bacteriol 173*, 2649-2657.

22. Sawa, T., Yahr, T. L., Ohara, M., Kurahashi, K., Gropper, M. A., Wiener-Kronish, J. P., and Frank, D. W. (1999) Active and passive immunization with the Pseudomonas V antigen protects against type III intoxication and lung injury, *Nat Med 5*, 392-398.

23. Goure, J., Pastor, A., Faudry, E., Chabert, J., Dessen, A., and Attree, I. (2004) The V antigen of *Pseudomonas aeruginosa* is required for assembly of the functional PopB/PopD translocation pore in host cell membranes, *Infect. Immun. 72*, 4741-4750.

24. Pettersson, J., Holmstrom, A., Hill, J., Leary, S., Frithz-Lindsten, E., von Euler-Matell, A., Carlsson, E., Titball, R., Forsberg, A., and Wolf-Watz, H. (1999) The V-antigen of

Yersinia is surface exposed before target cell contact and involved in virulence protein translocation, *Mol Microbiol 32*, 961-976.

25. Goure, J., Broz, P., Attree, O., Cornelis, G. R., and Attree, I. (2005) Protective anti-V antibodies inhibit Pseudomonas and Yersinia translocon assembly within host membranes, *J.Infect.Dis. 192*, 218-225.

26. Blocker, A. J., Deane, J. E., Veenendaal, A. K., Roversi, P., Hodgkinson, J. L., Johnson, S., and Lea, S. M. (2008) What's the point of the type III secretion system needle?, *Proc. Natl. Acad. Sci. U.S.A. 105*, 6507-6513.

27. Broz, P., Mueller, C. A., Muller, S. A., Philippsen, A., Sorg, I., Engel, A., and Cornelis, G. R. (2007) Function and molecular architecture of the Yersinia injectisome tip complex, *Mol. Microbiol. 65*, 1311-1320.

28. Galan, J. E., and Wolf-Watz, H. (2006) Protein delivery into eukaryotic cells by type III secretion machines, *Nature 444*, 567-573.

29. Derewenda, U., Mateja, A., Devedjiev, Y., Routzahn, K. M., Evdokimov, A. G., Derewenda, Z. S., and Waugh, D. S. (2004) The structure of *Yersinia pestis* V-antigen, an essential virulence factor and mediator of immunity against plague, *Structure 12*, 301-306.

30. Chatterjee, S., Zhong, D., Nordhues, B. A., Battaile, K. P., Lovell, S. W., and De Guzman, R. N. (2011) The Crystal Structure of the Salmonella Type III Secretion System Tip Protein SipD in Complex with Deoxycholate and Chenodeoxycholate, *Protein Sci. 20*, 75-86.

31. Lunelli, M., Hurwitz, R., Lambers, J., and Kolbe, M. (2011) Crystal structure of PrgI-SipD: insight into a secretion competent state of the type three secretion system needle tip and its interaction with host ligands, *PLoS Pathog. 7*, e1002163.

32. Johnson, S., Roversi, P., Espina, M., Olive, A., Deane, J. E., Birket, S., Field, T., Picking, W. D., Blocker, A. J., Galyov, E. E., Picking, W. L., and Lea, S. M. (2007) Self-chaperoning of the type III secretion system needle tip proteins IpaD and BipD, *J. Biol. Chem. 282*, 4035-4044.

33. Erskine, P. T., Knight, M. J., Ruaux, A., Mikolajek, H., Wong Fat Sang, N., Withers, J., Gill, R., Wood, S. P., Wood, M., Fox, G. C., and Cooper, J. B. (2006) High Resolution Structure of BipD: An Invasion Protein Associated with the Type III Secretion System of *Burkholderia pseudomallei*, *J. Mol. Biol. 363*, 125-136.

34. Espina, M., Ausar, S. F., Middaugh, C. R., Picking, W. D., and Picking, W. L. (2006) Spectroscopic and calorimetric analyses of invasion plasmid antigen D (IpaD) from *Shigella flexneri* reveal the presence of two structural domains, *Biochemistry 45*, 9219-9227.

35. Espina, M., Ausar, S. F., Middaugh, C. R., Baxter, M. A., Picking, W. D., and Picking, W. L. (2007) Conformational stability and differential structural analysis of LcrV, PcrV, BipD, and SipD from type III secretion systems, *Protein Sci. 16*, 704-714.

36. Fields, K. A., Nilles, M. L., Cowan, C., and Straley, S. C. (1999) Virulence role of V antigen of Yersinia pestis at the bacterial surface, *Infect.Immun. 67*, 5395-5408.

37. Matson, J. S., and Nilles, M. L. (2001) LcrG-LcrV interaction is required for control of Yops secretion in *Yersinia pestis*, *J. Bacteriol. 183*, 5082-5091.

38. Skrzypek, E., and Straley, S. C. (1993) LcrG, a secreted protein involved in negative regulation of the low-calcium response in *Yersinia pestis*, *J. Bact. 175*, 3520-3528.

39. Nilles, M. L., Williams, A. W., Skrzypek, E., and Straley, S. C. (1997) Yersinia pestis LcrV forms a stable complex with LcrG and may have a secretion-related regulatory role in the low-Ca2+ response, *J Bacteriol 179*, 1307-1316.

40. Matson, J. S., and Nilles, M. L. (2002) Interaction of the *Yersinia pestis* type III regulatory proteins LcrG and LcrV occurs at a hydrophobic interface, *BMC Microbiol. 2*, 16.

41. Nilles, M. L., Fields, K. A., and Straley, S. C. (1998) The V antigen of Yersinia pestis regulates Yop vectorial targeting as well as Yop secretion through effects on YopB and LcrG, *J Bacteriol 180*, 3410-3420.

42. Sarker, M. R., Sory, M. P., Boyd, A. P., Iriarte, M., and Cornelis, G. R. (1998) LcrG is required for efficient translocation of Yersinia Yop effector proteins into eukaryotic cells, *Infect Immun 66*, 2976-2979.

43. Sundin, C., Thelaus, J., Broms, J. E., and Forsberg, A. (2004) Polarisation of type III translocation by Pseudomonas aeruginosa requires PcrG, PcrV and PopN, *Microb. Pathog. 37*, 313-322.

44. Straley, S. C., Plano, G. V., Skrzypek, E., Haddix, P. L., and Fields, K. A. (1993) Regulation by Ca2+ in the Yersinia low-Ca2+ response, *Mol Microbiol 8*, 1005-1010.

45. Pettersson, J., Nordfelth, R., Dubinina, E., Bergman, T., Gustafsson, M., Magnusson, K. E., and Wolf-Watz, H. (1996) Modulation of virulence factor expression by pathogen target cell contact, *Science 273*, 1231-1233.

46. McCaw, M. L., Lykken, G. L., Singh, P. K., and Yahr, T. L. (2002) ExsD is a negative regulator of the Pseudomonas aeruginosa type III secretion regulon, *Mol Microbiol 46*, 1123-1133.

47. Rietsch, A., Vallet-Gely, I., Dove, S. L., and Mekalanos, J. J. (2005) ExsE, a secreted regulator of type III secretion genes in Pseudomonas aeruginosa, *Proc Natl Acad Sci U S A 102*, 8006-8011.

48. Lawton, D. G., Longstaff, C., Wallace, B. A., Hill, J., Leary, S. E., Titball, R. W., and Brown, K. A. (2002) Interactions of the type III secretion pathway proteins LcrV and LcrG from *Yersinia* pestis are mediated by coiled-coil domains, *J. Biol. Chem. 277*, 38714-38722.

49. Hamad, M. A., and Nilles, M. L. (2007) Structure-function analysis of the C-terminal domain of LcrV from *Yersinia pestis*, *J. Bacteriol. 189*, 6734-6739.

CHAPTER 2: Materials and Methods

2.1 Subcloning, Protein Expression, and Purification

2.1.1 LcrG constructs

DNA fragments encoding full-length LcrG, (residues 1-95; henceforth referred to as $LcrG^{FL}$) and truncated LcrG (residues 7-73; henceforth referred to as $LcrG^{7-73}$) were PCR amplified from the *Yersinia pestis* plasmid pCD1 (*1*) and subcloned into a pET-21a vector (Novagen) using NdeI and BamHI as the restriction sites. The vector was modified to encode an N-terminal His_6-tagged GB1 domain followed by a tobacco etch virus (TEV) protease site. GB1 (56 residues) is the B1 immunoglobulin binding domain from *Streptococcus* protein G that functions as a solubility enhancement tag (*2, 3*), and a GB1 expression plasmid (obtained from Peter E. Wright, Scripps Research Institute, La Jolla, California) was used for subcloning. The TEV protease site allows the cleavage of the target protein from the His_6-GB1 tag. For protein expression, the expression plasmids were transformed in *E. coli* BL21 (DE3) DNAY cells. The gene product of *E. coli dnaY* is an arginine tRNA corresponding to a rare arginine codon, thereby allowing the overproduction of this rare tRNA product. The freshly transformed colonies were used to inoculate a 50 mL LB overnight starter culture at 37 °C using 30 µg/mL kanamycin and 100 µg/mL carbenicillin as antibiotics. Isotopically ^{15}N-labeled proteins were obtained by using the cell pellet from the overnight growth as the inoculum in a 1 L M9 minimal media supplemented with 1 g/L of ^{15}N-ammonium chloride (Isotec). Cells were grown at 37 °C until A_{600} was ~0.6 to 0.8, induced with 1 mM isopropyl-β-D-thiogalactopyranoside (IPTG), and cell growth was

continued at 15 °C overnight in a shaker-incubator (to a final A_{600} ~2.0). The cells were diluted to obtain this A_{600} reading. Cells were harvested by centrifugation at 4,000 rpm (using the centrifuge Sorvall RC 5C Plus from Thermo Scientific) for 10 minutes and the pellet was resuspended in ~30 ml of binding buffer (500 mM NaCl, 20 mM Tris-HCl, 5 mM imidazole, pH 8.0). Cells were kept on ice, ~300 µl of 1 mM phenylmethylsulfonyl fluoride (PMSF) was added, and the cells were lysed by sonication using a Branson Digital Sonifier for 3 minutes of 2 seconds long pulses at 80% power followed by 20 seconds gaps. Cellular debris was removed by centrifugation of the cell lysate, and 600 µl of 5% polyethyleneimine (PEI) was added to the supernatant to precipitate the nucleic acids. The mixture was centrifuged at 13,000 rpm (using the centrifuge Sorvall RC 5C Plus from Thermo Scientific) for 10 minutes, and the supernatant was loaded onto a pre-charged Ni^{+2} affinity column, which was equilibrated with ~35 ml of binding buffer. The column was washed with ~100 ml of binding buffer, and the fusion protein was eluted using ~60 ml of elution buffer (500 mM NaCl, 20 mM Tris, 250 mM imidazole, pH 8.0). The fusion protein was then digested by placing the protein in a dialysis tubing with 250 µl of 0.06 mM recombinant Tobacco Etch Virus (TEV) protease (*4*), and the dialysis tubing was placed in 1 L of TEV buffer (50 mM Tris-HCl, 20 mM NaCl, 1 mM DTT, 0. 5 mM EDTA, pH 8.0) overnight at room temperature. The digested protein mixture was dialyzed again in 1 L binding buffer and passed through a second Ni^{+2} affinity column. Recombinant $LcrG^{FL}$/$LcrG^{7-73}$ were in the flow-through and column wash while the GB1 fusion tag was retained in the column. Recombinant $LcrG^{FL}$ and $LcrG^{7-73}$ contained a three residue (GHM) N-terminal cloning artifact after TEV cleavage. Recombinant proteins were concentrated using Amnicon Ultra 3K

(Milipore) and protein concentration was determined by absorbance at A_{280} using a Nanodrop (Thermo Fischer).

Site-directed mutants ($LcrG^{7-73}$ C34S, $LcrG^{7-73}$ C34A and $LcrG^{FL}$ C34S) were generated by the Stratagene QuickChange Kit and confirmed by DNA sequencing. All the LcrG mutants were expressed and purified by nickel affinity chromatography as described above. Unlabeled proteins were expressed by using the overnight LB starter growth to inoculate a 1 L LB medium. $LcrG^{7-73}$ C34S and $LcrG^{FL}$ C34S were also purified as $^{15}N/^{13}C$ double-labeled proteins by growing the cells in 1 L M9 minimal media supplemented with 1 g/L of ^{15}N-ammonium chloride and 2.0 g/L ^{13}C D-glucose. In this dissertation, "labeled" proteins refer to isotopically labeled proteins unless otherwise mentioned. Nine point mutants (I56N, K57E, K57L, R61E, R61L, I67N, K68E, K68L and L63N) and five deletion mutants (Δ52-57, Δ58-62, Δ63-67, Δ68-73, Δ52-73) of the LcrG 52-73 region (details of the mutants can be found in chapter 5) were generated by the Stratagene QuickChange Kit in pBAD vector for the *Yersinia* Yop secretion assay.

2.1.2 LcrV construct

In the crystal structure of LcrV determined by Derewenda *et al.* (*5*), the extreme N and C-terminal residues of LcrV (residues 23-27 and 323-326) lacked electron density and therefore were disordered. Therefore, a truncated LcrV spanning residues 28-322 was subcloned for protein expression. DNA fragment encoding LcrV residues 28-322 was PCR amplified from the *Y. pestis* plasmid pCD1 (*1*) and subcloned into a modified pET-21a vector as described in section 2.1.1. The C273S point mutation was introduced in the LcrV construct by the Stratagene

QuickChange Kit and confirmed by DNA sequencing. Hence the LcrV construct generated was $LcrV^{28-322}$ C273S. Since there is only one LcrV construct used, $LcrV^{28-322}$ C273S will be referred to as LcrV throughout this dissertation. Derewenda *et al.* (*5*) also introduced a C273S point mutation in LcrV to prevent the dimerization of LcrV and to improve the purification of recombinant LcrV. LcrV was expressed and purified by nickel affinity chromatography as described in section 2.1.1.

2.1.3 PcrG constructs

DNA fragments encoding full-length PcrG (residues 1-98; henceforth referred to as $PcrG^{FL}$) and truncated PcrG (residues 9-76; henceforth referred to as $PcrG^{9-76}$) were PCR amplified from the *P. aeruginosa* pAO1 strain and subcloned into a pET-21a vector at the NdeI and BamHI sites. For PcrG, the expression vector was modified to encode a C-terminal fusion tag consisting of a TEV protease site, the GB1 domain, and a hexahistidine tag. $PcrG^{FL}$ and $PcrG^{9-76}$ were expressed and purified by nickel affinity chromatography as described in section 2.1.1. Cleavage with TEV protease resulted in a C-terminal cloning artifact (GSENLYFQ) in $PcrG^{FL}$ and $PcrG^{9-76}$. $PcrG^{9-76}$ was also expressed and purified as $^{15}N/^{13}C$ double labeled protein.

2.1.4 PcrV construct

P. aeruginosa PcrV residues 25-294 (henceforth referred to as $PcrV^{25-294}$) was subcloned from the *Pseudomonas* pAO1 strain in the same manner as described for the LcrG and LcrV constructs. The N-terminal 24 residues of PcrV were truncated based on sequence similarity to the disordered N-terminal region in the crystal structure of its homologue, LcrV (*5*). Since there

is only one PcrV construct used, $PcrV^{25-294}$ will be referred to as PcrV throughout this dissertation. Recombinant PcrV was expressed and purified by nickel affinity chromatography as described in section 2.1.1.

2.1.5 ^{13}C-ILV labeling of $LcrG^{7-73}$ C34S, $PcrG^{9-76}$ and LcrV

The methyl groups of Ile, Leu and Val were ^{13}C labeled by overexpression of $LcrG^{7-73}$ C34S, $PcrG^{9-76}$ and LcrV in *E. coli* minimal media supplemented with 2-ketobutyric acid-4-^{13}C sodium salt hydrate (Isotec, # 571342) and 2-keto-3-(methyl-^{13}C)-butyric acid-4-^{13}C sodium salt (Isotec # 571334) following published protocols (*6*). The 2-ketobutyric acid-4-^{13}C sodium salt hydrate is the precursor for Ile, and it labels the δ methyl group of Ile. The 2-keto-3-(methyl-^{13}C)-butyric acid-4-^{13}C sodium salt is the precursor for Leu and Val, and it labels the γ1 and γ2 methyl groups of Leu and Val. Cells were grown at 37 °C and supplemented with 100 mgs of the keto acids (sterilized by filtration through 0.2 μm syringe filter after dissolving in sterile water) when A_{600} reached ~0.4-0.5. At A_{600} ~0.6-0.8 or about 45-60 minutes after addition of the keto acids, protein expression was induced with 1 mM IPTG and cell growth was continued overnight in a 15 °C shaker-incubator. Cells were harvested and recombinant proteins were purified by nickel affinity chromatography as described in section 2.1.1. Point mutants of Ile, Leu and Val residues of $LcrG^{7-73}$ C34S, $PcrG^{9-76}$ and LcrV (details of the mutants can be found in chapters 5 and 7) were generated by the Stratagene QuickChange Kit and expressed and purified in the same way as discussed in section 2.1.1.

2.1.6 ^{15}N amino acid specific labeling of LcrG$^{7-73}$ C34S

The backbone amides of Ile and Phe of LcrG$^{7-73}$ C34S were specifically labeled with ^{15}N-Ile and ^{15}N-Phe to generate ^{15}N-Ile-LcrG$^{7-73}$ C34S and ^{15}N-Phe-LcrG$^{7-73}$ C34S respectively. Freshly transformed *E. coli* BL21 (DE3) DNAY cells expressing LcrG$^{7-73}$ C34S were grown overnight in a 1 L LB-broth at 37 °C with shaking. The overnight cell growth was centrifuged and the cell pellet was resuspended in two flasks containing 500 ml M9 minimal media supplemented with 125 mg/L of the specific ^{15}N-labeled amino acid, 450 mg/L of unlabeled Val, Leu (for ^{15}N-Ile) or 450 mg/L of unlabeled Tyr, Trp, Ala, Ser, Gly, Cys (for ^{15}N-Phe) and 300 mg/L of the remaining unlabeled amino acids till an A_{600} ~0.6 was reached. Cells were incubated with shaking at 37 °C for ~20 minutes until the A_{600} reached ~0.8. Protein expression was induced with 1 mM IPTG. Cell growth was continued at 37 °C for ~4 hrs until the A_{600} was ~2.5. Cells were diluted to obtain this A_{600} reading. Cells were harvested by centrifugation and the selectively amino acid labeled recombinant proteins were purified as described in section 2.1.1.

2.2 Circular Dichroism (CD) Spectroscopy and Thermal Denaturation

Typically CD spectra were acquired in triplicate using 1-2 μM of protein samples in buffer (10 mM sodium phosphate pH 7.0, 10 mM NaCl). CD spectra were acquired from 190 to 260 nm at 20 °C with a scan rate of 50 nm/minute using a JASCO J-815 Spectropolarimeter. Thermal denaturation curves were monitored by measuring the molar ellipticity at 222 nm by progressively heating the protein from 20 °C to ~80-100 °C at a temperature ramp rate of 2 °C/minute. CD values in ellipticity (mdeg) were converted to molar ellipticity θ (degcm^2 × dmole^{-1}) by using the formula θ = {mdeg × 100} / {concentration (mM) × 10^5}. The melting

temperature (T_m) of LcrV was determined by using the JASCO software. The CD spectra for the PcrG constructs were acquired by Bryce Nordhues (*7*).

2.3 Nuclear Magnetic Resonance (NMR) Spectroscopy

2.3.1 Two dimensional ^{1}H-^{15}N HSQC spectra of LcrG and PcrG constructs.

NMR data were acquired at 25 °C using a Bruker Avance 800 MHz spectrometer equipped with a cryogenic triple resonance probe. All the NMR samples were dialyzed overnight in NMR buffer (10 mM sodium phosphate pH 7.0, 10 mM NaCl) and NMR samples contained 10% (v/v) D_2O. Initial 2D ^{1}H-^{15}N HSQC spectra (*8*) were acquired using 0.5 - 0.8 mM of protein samples for $LcrG^{FL}$, $LcrG^{7-73}$, $LcrG^{7-73}$ C34S, $LcrG^{7-73}$ C34A, $LcrG^{FL}$ C34S, $PcrG^{9-76}$ and $PcrG^{FL}$. The 2D ^{1}H-^{15}N HSQC spectrum of $LcrG^{FL}$ C34S was acquired using a Bruker Avance 600 MHz spectrometer. Typical NMR acquisition parameters for the LcrG constructs were 16 scans, 23 ppm ^{15}N sweep width centered at 117.5 ppm, 2048 ^{1}H complex points, and 150 ^{15}N complex points. The initial 2D ^{1}H-^{15}N HSQC spectra of PcrG were acquired by Bryce Nordhues (*7*). All NMR data reported were processed with NMRPipe (*9*) and analyzed by NMRView (*10*).

2.3.2 Two dimensional ^{1}H-^{13}C HSQC spectra of LcrG, PcrG and LcrV constructs

NMR data were acquired at 25 °C using a Bruker Avance 600 MHz spectrometer equipped with an inverse triple resonance probe. NMR samples contained 0.3 – 0.5 mM protein ($LcrG^{7-73}$ C34S, $PcrG^{9-76}$, LcrV) and were used to acquire 2D ^{1}H-^{13}C HSQC spectra. For the purpose of assignment of the methyl groups, this experiment was done on several Ile, Leu and Val mutants of the proteins mentioned above (details of the mutants can be found in Chapters 5 and 7).

Typical acquisition parameters used to acquire $^{1}H^{13}C$ HSQC for the LcrG and PcrG constructs were 52 scans, 15 ppm ^{13}C sweep width centered at 16.3 ppm, 1024 ^{1}H complex points, and 200 ^{13}C complex points. For LcrV, the parameters were the same except for 32 scans and 18 ppm ^{13}C sweep width centered at 20 ppm.

2.3.3 Backbone assignments of LcrG$^{7-73}$ C34S, LcrG^{FL} C34S, LcrG$^{7-73}$ C34S-LcrV complex and PcrG$^{9-76}$

To acquire three dimensional (3D) NMR data for backbone assignments, 0.9 mM of $^{15}N/^{13}C$ LcrG$^{7-73}$ C34S, 0.7 mM of $^{15}N/^{13}C$ PcrG$^{9-76}$, 0.8 mM of $^{15}N/^{13}C$ LcrG^{FL} C34S and 0.6 mM of $^{15}N/^{13}C$ LcrG$^{7-73}$ C34S-LcrV complex (1:1.2 ratio) were used for data collection. The 3D NMR datasets HNCA, HNCACB and CBCA(CO)NH were acquired (*11, 12*). Backbone assignments were obtained from 2D ^{1}H-^{15}N HSQC (*8*) and 3D HNCACB datasets. For backbone assignment of LcrG$^{7-73}$ C34S, we also used ^{15}N specific amino acid labeling and mutational approach to assign the backbone resonances of a few amino acids that was difficult to assign from the 3D dataset (details can be found in chapter 4). The secondary structures for LcrG$^{7-73}$ C34S and PcrG$^{9-76}$ were identified from the analysis of the Cα and Cβ chemical shifts (*13, 14*). The random coil chemical shifts are obtained as described in (*13*).

2.3.4 Heteronuclear {^{1}H}- ^{15}N NOE of LcrG$^{7-73}$ C34S and PcrG$^{9-76}$

NMR samples containing 0.7 mM of ^{15}N LcrG$^{7-73}$ C34S or ^{15}N PcrG$^{9-76}$ in NMR buffer (10 mM sodium phosphate pH 7.0, 10 mM NaCl) were used to acquire the heteronuclear {^{1}H}- ^{15}N NOE datasets. The heteronuclear {^{1}H}- ^{15}N NOE datasets were acquired as a pair of 2D datasets

collected in an interleaved manner as previously described (*14*) with 2048 (^{1}H) × 128 (^{15}N) complex points, 60 scans per point and 5 secs recycle delay. The heteronuclear {^{1}H}- ^{15}N NOE was then calculated as the ratio of the intensities of each peak in the two 2D datasets. Error bars were estimated from the standard deviation of the background signal of each spectrum.

2.3.5 T_1 and T_2 relaxation experiment of LcrG$^{7-73}$ C34S and PcrG$^{9-76}$

NMR samples containing 0.7 mM of ^{15}N LcrG$^{7-73}$ C34S or ^{15}N PcrG$^{9-76}$ were used to acquire the T_1 and T_2 backbone amide relaxation datasets. The T_1 and T_2 relaxation were acquired as several separate 2D datasets with varying T_1 (D7) and T_2 (D20) delays as previously (*15*) described. The corresponding R_1 and R_2 values were determined by measuring the intensity decay for each peak as a function of the time delays. The time delays used to determine the rate R_1 were 10, 60, 120, 240, 400, 900 and 1100 ms, and the time delays used to determine the rate R_2 were 20, 40, 50, 60, 70, 90, 100, 120 and 150 ms. Peak intensities were obtained using NMRView (*10*) and fitted using GNUPLOT (*16*), and the deviations from fitting were reported as error bars.

2.3.6 NMR titrations of ^{15}N LcrG$^{7-73}$ C34S with unlabeled LcrV and ^{15}N PcrG$^{9-76}$ with unlabeled PcrV

For all the NMR titrations reported here, the binding partners were dialyzed together in the same NMR buffer. NMR titrations were performed using 0.2 mM ^{15}N LcrG$^{7-73}$ C34S titrated with higher molar ratios (1:0, 1:0.5, 1:1.2, 1:2, 1:3, 1:4 and 1:6.5) of unlabeled LcrV. Two dimensional (2D) ^{1}H-^{15}N HSQC (*8*) spectra were acquired for each titration point and spectra were superimposed to monitor the changes in the HSQC spectra of LcrG$^{7-73}$ C34S upon complex

formation. A 1:1.2 molar ratio for the $^{15}N/^{13}C$ $LcrG^{7-73}$ C34S - LcrV was used to acquire the 3D NMR datasets. This particular molar ratio was chosen, because it yielded the best signal to noise ratio. Typical acquisition parameters used were 56 scans, 23 ppm ^{15}N sweep width centered at 117.5 ppm, 2048 ^{1}H complex points, and 200 ^{15}N complex points. Titration experiments with 0.1 mM of ^{15}N $LcrG^{7-73}$ were also done by addition of LcrV in molar ratios of 1:0 and 1:2 for comparison of the complexes formed by the wild type $LcrG^{7-73}$ and the mutant $LcrG^{7-73}$ C34S with LcrV. The NMR titrations of ^{15}N $PcrG^{9-76}$ with unlabeled PcrV were acquired by Bryce Nordhues (*7*). For NMR chemical shift mapping of the backbone, 2D ^{1}H-^{15}N HSQC spectra were acquired for ^{15}N-$PcrG^{9-76}$ titrated with increasing amounts of unlabeled PcrV. Six samples were prepared in NMR buffer with 0.13 mM ^{15}N-$PcrG^{9-76}$ and varying PcrV concentration in molar ratios of 1:0, 1:0.25, 1:0.5, 1:1, 1:2 and 1:4.

2.3.7 NMR titrations of ^{13}C ILV-$LcrG^{7-73}$ C34S with unlabeled LcrV

NMR data were acquired at 25 °C using Bruker Avance 600 MHz spectrometer. NMR chemical shift mapping of the methyl groups of Ile, Leu and Val of ^{13}C ILV-$LcrG^{7-73}$ C34S were performed by acquiring 2D ^{1}H-^{13}C HSQC spectra at ^{13}C ILV-$LcrG^{7-73}$ C34S: LcrV molar ratios of 1:0, 1:0.25, 1:0.5, 1:1 and 1:2. The concentration of the labeled protein (^{13}C ILV-$LcrG^{7-73}$ C34S) was kept at 0.36 mM. The acquisition parameters used were 52 scans, 15 ppm ^{13}C sweep width centered at 16.3 ppm, 1024 ^{1}H complex points, and 200 ^{13}C complex points.

2.3.8 NMR titrations of ^{13}C ILV-PcrG$^{9-76}$ with unlabeled PcrV

NMR data were acquired at 25 °C using a Bruker Avance 600 MHz spectrometer. NMR samples containing 0.3 mM ^{13}C ILV-PcrG$^{9-76}$ were titrated with unlabeled PcrV at molar ratios of 1:0, 1:0.25, 1:0.5, 1:1, 1:2 and 1:3. The acquisition parameters used were 52 scans, 15 ppm ^{13}C sweep width centered at 16.3 ppm, 1024 ^{1}H complex points, and 200 ^{13}C complex points.

2.3.9 NMR titrations of ^{13}C ILE-LcrV with unlabeled LcrG$^{7-73}$ C34S or LcrG^{FL} C34S

NMR data were acquired at 25 °C using a Bruker Avance 600 MHz spectrometer. NMR samples containing 0.4 mM of LcrV were titrated with unlabeled LcrG$^{7-73}$ C34S at molar ratios of 1:0, 1:0.25, 1:0.5, 1:1, and 1:2. The acquisition parameters used were 36 scans, 20 ppm ^{13}C sweep width centered at 18 ppm, 1024 ^{1}H complex points, and 200 ^{13}C complex points. Similar titrations were done using 0.4 mM of LcrV unlabeled LcrG^{FL} C34S at molar ratios of 1:0, 1:0.25, 1:0.5, 1:1, and 1:2.

2.3.10 NMR titrations of ^{13}C ILE-PcrV with unlabeled PcrG$^{9-76}$ or PcrG^{FL}

^{13}C ILV-PcrV (0.23 mM) was titrated with unlabeled PcrG$^{9-76}$ dissolved in buffer (20 mM sodium phosphate pH 7.0, 20 mM NaCl, 10% D_20). Five molar ratios of ^{13}C ILV-PcrV to PcrG$^{9-76}$ of 1:0, 1:0.5, 1:1, 1:2, and 1:3 were used to acquire the 2D ^{1}H-^{13}C HSQC spectra at 30 °C using a Bruker Avance 600 MHz spectrometer. The acquisition parameters used were 56 scans, 18 ppm ^{13}C sweep width centered at 18 ppm, 1024 ^{1}H complex points, and 200 ^{13}C complex points.

Likewise, 0.13 mM of ^{13}C ILV-PcrV was titrated with $PcrG^{FL}$ at 1:0, 1:0.5, 1:1, 1:2, and 1:3 molar ratios and monitored by 2D ^{1}H-^{13}C HSQC with 80 scans, 18 ppm ^{13}C sweep width centered at 18 ppm, 1024 ^{1}H complex points, and 200 ^{13}C complex points.

2.4 Yersinia Yop secretion assay

This work was done in collaboration with Dr. Gregory V. Plano (University of Miami, Florida). *Y. pestis* KIM5-3001 (parent), the *lcrG* deletion mutant (KIM5-3001.5, Δ39-53) and KIM5-3001.5 carrying pBAD-LcrG or derivatives of this plasmid were cultured overnight at 27 °C in Thoroughly Modified Higuchi's (TMH) medium. Overnight cultures of each strain were used to inoculate 2 ml cultures of TMH alone or TMH containing 2.5 mM $CaCl_2$ to an OD_{620} of 0.2. Protein expression was induced with 0.2% L-(+)- arabinose upon shifting the temperature from 27 ºC to 37 ºC. Fractions were collected after 5 hours incubation at 37 ºC. Around 1 ml of each culture was harvested by centrifugation to separate whole bacterial cells (WC) from secreted proteins. Trichloroacetic acid (TCA) was added to the culture supernatants (10% final concentration), incubated on ice overnight and precipitated proteins were collected by centrifugation. WC and secreted proteins were resuspended in 1X SDS-PAGE solubilization buffer according to the final OD_{620} of the culture, and analyzed by SDS-PAGE and immunoblotting with antisera specific for YopM and LcrG. LcrG C34S, LcrG C34A, and several mutants of the LcrG 52-73 region (deletion mutants Δ52-57, Δ58-62, Δ63-67, Δ68-73, Δ52-73; and point mutants I56N, K57E, K57L, R61E, R61L, I67N, K68E, K68L and L63N) were tested by the Yop secretion assay.

2.5 LcrV crystallization

2.5.1 Crystallization and Data Collection

LcrV was purified and concentrated to 22 mg/ml in 50 mM NaCl, 20 mM Tris-HCl, pH 8.0. Crystallization screenings were conducted at 20 °C in Compact Clover (Emerald Biosystems) sitting drop vapor diffusion plates using 0.5 μL of protein and 0.5 μL of crystallization solution equilibrated against 75 μL of the crystallization solution. LcrV yielded initial crystals, which formed plate clusters **(Figure 3-3A, B),** in approximately 24 hours from the IndexHT screen (Hampton 5 Research) conditions D8 (25% PEG 3350, 100 mM Hepes pH 7.5) and D9 (25% PEG 3350, 100 mM Tris pH 8.5). The crystallization conditions were refined using the pHat buffer screen (Emerald Biosystems), and 25% PEG 3350, 100 mM Bicine pH 7.0 condition yielded prismatic crystals which were used for data collection **(Figure 3-3C)**. Single crystals were transferred to a fresh drop of a cryoprotectant solution containing 80% crystallization solution and 20% PEG 400.

A peptide construct of LcrV's binding partner, LcrG, spanning residues Ser 52 to Arg 73 was also used for crystallization screening of the complex. A 50 mM stock solution of the LcrG peptide was prepared by dissolving 3.3 mg in 24.5 uL of 50 mM NaCl, 20 mM Tris-HCl pH 8.0. 5 uL of the 50 mM LcrG peptide was mixed with 345 uL of the concentrated LcrV to give final concentrations of 0.59 mM and 0.71 mM respectively. In addition, purified LcrV, $LcrG^{7-73}$ C34S and also a size exclusion chromatography (SEC) isolated complex were sent for crystallization. However, the efforts to co-crystallize LcrG and LcrV in complex were not successful.

2.5.2 Structure Solution and Refinement

X-ray diffraction data was collected by Kevin Battaile (Argonne National Laboratory) and the crystal structure was solved by Scott Lovell (Director, Protein structure Laboratory at the University of Kansas). Diffraction data were collected at the Advanced Photon Source beamline 17ID (IMCA-CAT) using a Dectris Pilatus 6M pixel array detector. Diffraction data were integrated and scaled with XDS (*17*) and Scala (*18*) respectively. The Laue class was checked with Pointless (*18*) which indicated that 2/m was correct and the likely space group was *P*21. Structure solution was conducted with Phaser (*19*) via the Phenix (*20*) interface using a previously determined structure of LcrV (PDB: 1R6F) (*5*) as the search model. Following manual model building with Coot (*21*), the structure was improved by automated model building with Arp/warp (*22*). Structure refinement and additional model building were performed with Phenix and Coot respectively. Disordered side chain residues were truncated to the point to which electron density could be observed. Structure validation was conducted with Molprobity (*23*). Crystallographic data are provided in **Table 1**.

2.6 Size Exclusion Chromatography (SEC) of LcrV, LcrG$^{7-73}$ C34S and the complex

After purification, LcrV and LcrG$^{7-73}$ C34S were concentrated to 0.39 mM and 0.851 mM respectively using Amnicon Ultra 3K (Milipore). The proteins were dialyzed overnight in SEC buffer (300 mM NaCl, 20 mM Tris-HCl, pH 8.0), filter sterilized, and applied to a Superdex 75 (column height 51 cm, bed volume ~ 300 ml) analytical size exclusion column (GE Healthcare) equilibrated with 1 CV (column volume) of 300 mM NaCl, 20 mM Tris-HCl, pH 8.0. The buffer was degassed and filtered prior to use. 2 ml volume of 0.3 mM LcrG$^{7-73}$ C34S, 0.1 mM of LcrV

and LcrG$^{7-73}$ C34S-LcrV complex (0.184 mM of LcrG$^{7-73}$ C34S and 0.23 mM LcrV) in a 1:1.2 ratio were loaded separately to the column and three individual runs were carried out. The typical parameters used for the run were: flow rate - 1 ml/min, pressure - 0.3 MPa, elution fraction size - 6 ml and length of elution (CV) - 1.5. Protein standards such as Blue Dextran (200 kDa), Albumin (66 kDa), Carbonic anhydrase (29 kDa), Cytochrome C (12.4 kDa) and Aprotonin (6.5 kDa) were used to calibrate the column and generate a standard curve. Using the equation

$$K_{av} = \frac{V_e - V_0}{V_c - V_0} \qquad \textbf{(2.1)}$$

where V_e = elution volume, V_0 = void volume and V_c = geometric column volume, K_{av} was calculated. By substituting the K_{av} in the equation of the standard curve (y = - 0.4207x + 2.1177, where y = K_{av} and x = molecular weight in dalton) the molecular weights were determined.

2.7 Surface Plasmon Resonance (SPR)

Surface Plasmon Resonance (SPR) was used to measure the binding affinity between LcrG and LcrV using a Biacore 3000 instrument (Biacore, Uppsala, Sweden). The assays were performed at 25° C using freshly prepared and degassed running buffer (10 mM HEPES-NaOH, 150 mM NaCl, 0. 005% (v/v) Surfactant P-20, pH 7. 4). Unlabeled LcrG$^{7-73}$ C34S and LcrG$^{7-73}$ were dialyzed overnight. The experiments were carried out using a CM5 chip and a 1:1 (v/v) mixture of 400 mM 1-ethyl-3- (3-dimethylaminopropyl) carbodiimide (EDC) (Sigma), and 100 mM N-hydroxysuccinimide (NHS) (Sigma) was used to activate the carboxymethylated dextran surface of the chip. LcrG$^{7-73}$ C34S (ligand) was diluted to 15 μg/ml in immobilization buffer (10 mM

sodium acetate, ph 4.5) and injected into the flow cell (flow cell 2/test cell) for direct amine coupling. After ligand injection, blocking buffer (1 M ethanolamine, pH 8.5) (Sigma) was passed over the surface to deactivate the remaining uncoupled surfaces on the CM5 chip. A control flow cell (flow cell 1) was prepared by injecting the EDC/NHS solution, followed by the blocking buffer. These three steps of were performed for 7 mins at a flow rate of 10 µl/min and resulted in the direct coupling of $LcrG^{7-73}$ C34S to the test cell of the CM5 chip. Varying concentrations (12.5 µM, 25 µM, 50 µM and 100 µM) of the analyte, LcrV (dialyzed overnight in running buffer) were then injected into both the flow cells at 40 µl/min. This was followed by surface regeneration using 20 µl pulses of regeneration buffer (10 mM glycine, pH 1.7). Non-specific binding of the analyte to the surface of the chip was determined from flow cell 1, and was substracted from the raw data. The experiment was repeated with $LcrG^{7-73}$ using 50 µM of the analyte concentration.

Apparent dissociation constants (K_d) between $PcrG^{FL}$ or $PcrG^{9-76}$ and PcrV were measured by surface plasmon resonance (SPR) using a Biacore 3000 instrument (Biacore, Uppsala, Sweden). Biacore assays for PcrG were performed by Bryce Nordhues (*7*). A 1:1 (v/v) mixture of 400 mM 1-ethyl-3- (3-dimethylaminopropyl) carbodiimide (EDC) (Sigma) and 100 mM N-hydroxysuccinimide (NHS) (Sigma) was prepared and immediately injected into two flow cells of a CM5 chip to activate the carboxymethylated dextran surface. Lyophilized anti-polyhistidine antibodies (R&D Systems, Inc.) were resuspended to 25 µg/mL in immobilization buffer (10 mM sodium acetate, pH 5.0) and injected into the 2 activated flow cells for amine coupling. The anti-polyhistidine antibodies recognize the C-terminal His_6 tag at the end of the PcrG constructs. The identification of the complex is described in the following paragraph. Remaining uncoupled

surfaces were inactivated by injection of blocking buffer (1 M ethanolamine, pH 8.5) (Sigma). Activation, coupling, and blocking steps were performed for 7 min at a flow rate of 10 µL/min resulting in anti-polyhistidine direct coupling of ~14,000 response units (RUs) in both flow cells.

The assays were carried out at 25° C using freshly prepared and degassed running buffer (10 mM HEPES-NaOH, 150 mM NaCl, 0.005% (v/v) Surfactant P-20, pH 7. 4). Unlabeled $PcrG^{FL}$ or $PcrG^{9-76}$ (fused to C-terminal GB1-His_6 tag) was dialyzed overnight in running buffer and immobilized to the anti-polyhistidine coated surface of flow cell 2 by injection of 6-9 µL of 1 µg/mL protein at 10 µL/min. Varying concentrations (2-32 nM) of the PcrV analyte (TEV cleaved and dialyzed overnight in running buffer) were then injected in both flow cells at 40 µL/min for 3 mins over immobilized $PcrG^{FL}$-GB1-His_6 (200 RU) and $PcrG^{9-76}$-GB1-His_6 (104 RU). Immobilization of the ligand and binding of analyte was repeated for each PcrV concentration followed by surface regeneration using 20 µL pulses of regeneration buffer (10 mM glycine, pH 2.0). Non-specific binding of the analyte to the anti-His_6 antibody coated surface and the bulk effect from the buffer were determined from flow cell 1 and subtracted from the raw data. The K_d values were calculated using BIAevaluation 4.1 software. As an additional control, the above steps were repeated using only the TEV cleaved GB1-His_6 tag as the ligand immobilized (108 RU) to the anti-polyhistidine coated surface to verify that the fusion tag did not contribute to binding. Since we only tested the effect of GB1-His_6 tag, and no other molecule was present, no binding effect was seen.

2.8 Fluorescense polarization (FP)

Fluorescense polarization (FP) was also used to measure the binding affinity between LcrG and LcrV. Purified LcrV and $LcrG^{7-73}$ C34S were dialyzed overnight at room temperature in 1× PBS at pH 7.4. The fluorescent dye fluorescein-5-maleimide (F5M) (4 mgs) was dissolved in 1 ml of DMSO and the microcentrifuge tube was immediately wrapped in aluminium foil. A 10 ml labeling reaction was used for both $LcrG^{7-73}$ and $LcrG^{FL}$ by combining 0.467 μmoles of protein, 4.67 μmoles of TCEP (10 fold excess) and 9.35 μmoles of the dye (20 fold excess), and the rest of the volume was made up with 1× PBS pH 7.4. The protein and TCEP mixture was stirred at room temperature for 20 minutes, after which the dye was slowly added dropwise to the protein while mixing. The labeling reaction was continued for 3 hrs in the dark at room temperature. Excess dye was removed from the reaction mixture by extensive dialysis in buffer (1× PBS pH 7.4). Finally, the F5M-labeled protein was passed several times through an Amnicon Ultra Centrifugation filter until the flow through was colorless. UV-vis spectroscopy was used to determine the extent of labeling in the protein. The FP datasets were then acquired using a Varian Cary Eclipse Fluorescence Spectrophotometer. This method yielded a poor labeling efficiency of the LcrG constructs. A different labeling strategy was tried with GB1-$LcrG^{7-73}$ using 10 μM protein, 10 μM TCEP (allowed to react for 20 mins) and 40 μM dye (allowed to react for 3 hrs). The reaction was then quenched with 1 mM DTT, concentrated to 1 ml using an Amnicon Ultra filter (3K) and desalted twice using Sephadex G50 (Sigma) columns. The data for the FP experiment is not shown in this dissertation, as the LcrG constructs could not be labeled properly. The poor labeling of LcrG, resulted in a linear curve that did not reach saturation.

2.9 References

1. Perry, R. D., Straley, S. C., Fetherston, J. D., Rose, D. J., Gregor, J., and Blattner, F. R. (1998) DNA sequencing and analysis of the low-Ca2+-response plasmid pCD1 of *Yersinia pestis* KIM5, *Infect. Immun. 66*, 4611-4623.
2. Huth, J. R., Bewley, C. A., Jackson, B. M., Hinnebusch, A. G., Clore, G. M., and Gronenborn, A. M. (1997) Design of an expression system for detecting folded protein domains and mapping macromolecular interactions by NMR, *Protein Sci. 6*, 2359-2364.
3. Zhou, P., and Wagner, G. (2010) Overcoming the solubility limit with solubility-enhancement tags: successful applications in biomolecular NMR studies, *J. Biomol. NMR. 46*, 23-31.
4. Geisbrecht, B. V., Bouyain, S., and Pop, M. (2006) An optimized system for expression and purification of secreted bacterial proteins, *Protein Expr. Purif. 46*, 23-32.
5. Derewenda, U., Mateja, A., Devedjiev, Y., Routzahn, K. M., Evdokimov, A. G., Derewenda, Z. S., and Waugh, D. S. (2004) The structure of *Yersinia pestis* V-antigen, an essential virulence factor and mediator of immunity against plague, *Structure 12*, 301-306.
6. Tugarinov, V., Kanelis, V., and Kay, L. E. (2006) Isotope labeling strategies for the study of high-molecular-weight proteins by solution NMR spectroscopy, *Nat Protoc 1*, 749-754.
7. Nordhues, B. A. (2011) NMR Structural Studies of Type III Secretion System Tip Proteins, In *Molecular Biosciences*, p 86, University of Kansas, Lawrence.

8. Grzesiek, S., and Bax, A. (1993) The importance of not saturating H_2O in protein NMR. Application to sensitivity enhancement and NOE measurements., *J. Am. Chem. Soc. 115*, 12593-12594.

9. Delaglio, F., Grzesiek, S., Vuister, G. W., Zhu, G., Pfeifer, J., and Bax, A. (1995) NMRPipe: a multidimensional spectral processing system based on UNIX pipes, *J. Biomol. NMR 6*, 277-293.

10. Johnson, B. A. (2004) Using NMRView to visualize and analyze the NMR spectra of macromolecules, *Methods Mol. Biol. 278*, 313-352.

11. Grzesiek, S., Dobeli, H., Gentz, R., Garotta, G., Labhardt, A. M., and Bax, A. (1992) ^{1}H, ^{13}C, and ^{15}N NMR backbone assignments and secondary structure of human interferon-gamma, *Biochemistry 31*, 8180-8190.

12. Wittekind, M., and Mueller, L. (1993) HNCACB, a high sensitivity 3D NMR experiment to correlate amide proton and nitrogen resonances with the alpha-carbon and beta-carbon resonances in proteins, *J. Magn. Reson. 101B* 201-205.

13. Wishart, D. S., and Nip, A. M. (1998) Protein chemical shift analysis: a practical guide, *Biochem. Cell Biol. 76*, 153-163.

14. Stone, M. J., Fairbrother, W. J., Palmer, A. G., III, Reizer, J., Saier, M. H., Jr., and Wright, P. E. (1992) Backbone dynamics of the Bacillus subtilis glucose permease IIA domain determined from ^{15}N NMR relaxation measurements, *Biochemistry 31*, 4394-4406.

15. Farrow, N. A., Muhandiram, R., Singer, A. U., Pascal, S. M., Kay, C. M., Gish, G., Shoelson, S. E., Pawson, T., Forman-Kay, J. D., and Kay, L. E. (1994) Backbone

dynamics of a free and phosphopeptide-complexed Src homology 2 domain studied by 15N NMR relaxation, *Biochemistry 33*, 5984-6003.

16. Williams, T., and Kelley, C. (2010) Gnuplot 4.4: an interactive plotting program, http://gnuplot.sourceforge.net/.

17. Kabsch, W. (1988) Automatic indexing of rotation diffraction patterns, *J. Appl. Cryst. 21*, 67-72.

18. Evans, P. R. (2006) Scaling and assessment of data quality, *Acta Cryst. D62*, 72-82.

19. McCoy, A. J., Grosse-Kunstleve, R. W., Adams, P. D., Winn, M. D., Storoni, L. C., and Read, R. J. (2007) Phaser crystallographic software, *J. Appl. Cryst. 40*, 658-674.

20. Adams, P. D., Afonine, P. V., Bunkoczi, G., Chen, V. B., Davis, I. W., Echols, N., Headd, J. J., Hung, L. W., Kapral, G. J., Grosse-Kunstleve, R. W., McCoy, A. J., Moriarty, N. W., Oeffner, R., Read, R. J., Richardson, D. C., Richardson, J. S., Terwilliger, T. C., and Zwart, P. H. (2010) PHENIX: a comprehensive Python-based system for macromolecular structure solution, *Acta Crystallogr D Biol Crystallogr 66*, 213-221.

21. Emsley, P., and Cowtan, K. (2004) Coot: model-building tools for molecular graphics, *Acta Crystallogr D Biol Crystallogr 60*, 2126-2132.

22. Langer, G., Cohen, S. X., Lamzin, V. S., and Perrakis, A. (2008) Automated macromolecular model building for X-ray crystallography using ARP/wARP version 7, *Nat Protoc 3*, 1171-1179.

23. Chen, V. B., Arendall, W. B., 3rd, Headd, J. J., Keedy, D. A., Immormino, R. M., Kapral, G. J., Murray, L. W., Richardson, J. S., and Richardson, D. C. (2010) MolProbity: all-

atom structure validation for macromolecular crystallography, *Acta Crystallogr D Biol Crystallogr 66*, 12-21.

CHAPTER 3: Crystal structure of the *Yersinia pestis* type III secretion system tip protein LcrV refined to 1.65 Å

3.1 Introduction

The pathogenesis of *Yersinia pestis*, is strongly dependent on the plasmid encoded type III secretion system (T3SS), which functions by injecting effector Yops (*Yersinia* outer proteins) into the host cell cytosol (*1, 2*). Broadly, the T3SS or injectisome is composed of structural proteins, effector proteins, and chaperones (*3, 4*). The structural component of the *Y. pestis* T3SS (also known as the Ysc-Yop system) is a needle apparatus that comprises a membrane embedded basal complex, an external needle, a tip complex, and a translocon **(Figure 1-1)**. *Y. pestis* responds to host cell contact by assembling the translocon that subsequently creates a pore in the host cell membrane and allows the delivery of effector Yops into the cytosol of targeted host cells. These effector Yops then collectively function by disturbing cytoskeletal dynamics, preventing phagocytosis, and blocking the production of pro-inflammatory cytokines, thereby favoring the survival of *Y. pestis* inside the host (*1, 2*).

In the *Y. pestis* T3SS, the tip complex is formed by several copies of a hydrophilic protein, LcrV (326 residues), that forms a distinct structure at the tip of the needle (*5*). LcrV is a multifunctional protein that plays an essential role in the pathogenicity of *Y. pestis (6-10)*. Firstly, LcrV functions as host cell sensor because of its extracellular localization (*11, 12*). Secondly, LcrV, along with two other hydrophobic proteins (YopB and YopD), is indispensable for the delivery of effector proteins into the host cytosol (*2, 3, 9, 11, 13, 14*). Thirdly, LcrV serves as a platform for the assembly of the translocation pore complex (*10, 13*). Finally, LcrV

forms a complex with its cognate chaperone, LcrG while inside the cytoplasm to regulate the secretion of effectors (*15, 16*).

The closest homolog of LcrV is PcrV, the tip protein of the *Pseudomonas aeruginosa* T3SS. LcrV shares 37% sequence identity and 65% sequence similarity (*17*) with PcrV. LcrV and PcrV can be grouped together in the Ysc family as the V-tip proteins (*3, 17*). The crystal structure of LcrV (residues L24-K326) was determined in 2004 at a resolution of 2.2 Å using a construct containing triple mutations (K40A/D41A/K42A) in a C273S background (PDB # 1R6F) (*18*). The C273S point mutation facilitated protein purification. Since then, crystal structures of other T3SS tip proteins like the *Shigella* IpaD (*19*), the *Salmonella* SipD (*20, 21*), and the *Burkholderia* BipD tip proteins (*19, 22*) have been determined. These crystal structures have revealed structural similarities as well as differences in the T3SS tip proteins. Here, the refined crystal structure of LcrV without the triple mutations but in a C273S background is reported at a resolution of 1.65 Å. The refined structure contains prominent differences in the N-terminal domain of LcrV when compared to the previous crystal structure (1R6F). Notably, the N-terminal domain of LcrV forms the base of the tip complex, playing an important role in the proper assembly of the translocon by allowing for the correct insertion of the translocon protein YopB into the host membrane (*13*). The most notable differences between the refined structure of LcrV and 1R6F are near the site of the triple mutations (K40A/D41A/K42A) in 1R6F. Thus, this refined crystal structure of LcrV represents a more native form of the tip protein and is expected to be functionally more relevant.

3.2 Results

3.2.1 Expression and purification of LcrV

As described in section 2.1.2 the design of LcrV construct was based on the original crystal structure of LcrV (*18*) by truncating the disordered ends with a C273S background mutation. LcrV (residues G28-D322) was expressed in *E. coli* BL21 (DE3) DNAY cells as an N-terminal His_6-GB1 fusion protein. The GB1 tag contained a hexahistidine tag to aid in nickel affinity purification and a TEV protease cleavage site to allow the recovery of purified LcrV after removal of the His_6-GB1 tag. The fusion protein was over-expressed in soluble form in *E. coli*, purified under native conditions, and digested with TEV protease to obtain purified LcrV **(Figure 3-1)**. The purified LcrV yielded millimolar amounts of protein for crystallization studies.

3.2.2 Circular Dichroism and Thermal Denaturation studies of LcrV

Circular Dichroism (CD) spectra of LcrV displayed two characteristic minima at 222 nm and 208 nm, suggesting LcrV has a significant amount of helical structure **(Figure 3-2)**. The thermal denaturation curve of LcrV displayed a single transition at around 80 °C **(Figure 3-2)**. This showed high thermal stability of LcrV, which is in good agreement with the studies of Espina *et al.* (*23*).

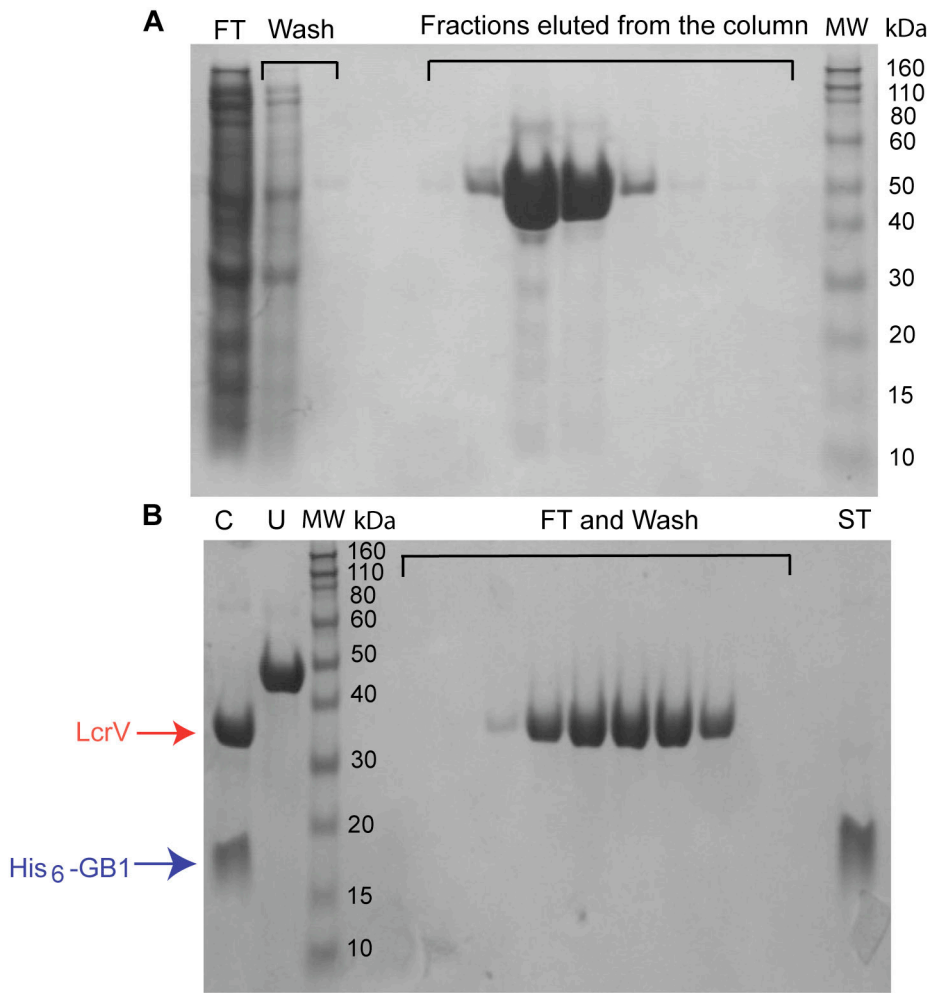

Figure 3-1. SDS-PAGE showing the purification of LcrV by Ni^{+2} affinity chromatography. **(A)** Results of first Ni^{+2} column purification showing flow-through (FT), wash, and fractions eluted from the column. Fractions eluted from the column represent the purified LcrV fused to His_6-GB1 tag. **(B)** Results of TEV digestion of LcrV where "U" (uncut) is the purified LcrV fused to His_6-GB1 tag and "C" (cut) is the TEV protease digested mixture showing both LcrV (red arrow) and the His_6-GB1 tag (blue arrow). FT and wash fractions show the purified LcrV after TEV digestion. "ST" represents the strip fraction, which shows the His_6-GB1 tag after stripping the column with 35 ml of 0.5 M EDTA.

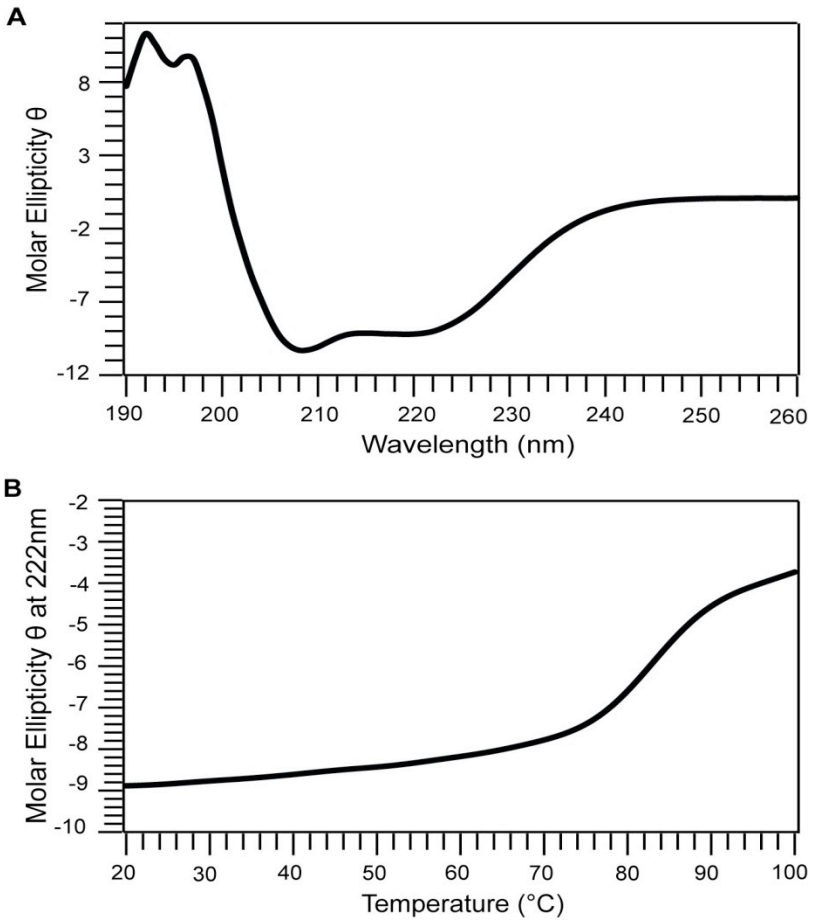

Figure 3-2. CD and thermal denaturation spectra of LcrV. **(A)** CD spectra acquired at 25 °C. **(B)** Thermal denaturation plot of LcrV. (Molar ellipticity θ (deg·cm^2·dmol^{-1}) × 10^{-6}).

3.2.3 Crystal structure of LcrV

LcrV yielded initial crystals in approximately 24 hours from the IndexHT screen conditions D8 (25% PEG 3350, 100 mM Hepes pH 7.5) and D9 (25% PEG 3350, 100 mM Tris-HCl pH 8.5) **(Figure 3-3A, B)**. Following refinement with the pHat buffer screen, LcrV yielded prismatic crystals, which were used for data collection **(Figure 3-3C)**. Crystallographic data are provided in **Table 1**. The final model contained residues G28 to L319, a PEG 400 molecule and 149 water molecules **(Figure 3-4)**. Overall, the refined structure of LcrV was similar to that reported previously (PDB: 1R6F) (*18*) with an RMSD between Cα atoms (244 residues) of 1.62 Å **(Figure 3-5A)** as determined using the secondary structure matching (*24*) routine in Coot (*25*). Residues from K261 to P279 could not be resolved owing to poor electron density due to disorder. The overall shape of the protein structure can be described as a "dumbbell-shaped" made up of a central coiled coil region connecting two domains (*18*). Like 1R6F (*18*), the present three-dimensional structure of LcrV also showed that it is highly α-helical with 55% of residues present in twelve α-helices (α1- α12) while, 7% of the residues form six β-strands (β1- β6) and the remaining 32% of the residues are in random coils. The N-terminal globular domain is formed by six helices (α1-α6) that packs on one end of a long central coiled coil formed by helix α7 and helix α12, and two anti-parallel beta strands (β1 and β2). The central coiled coil connects to the C-terminal globular domain formed by a mix of alpha helices and beta strands. The bulk of this mixed α/β domain is unstructured, as compared to the N-terminal globular domain, and is composed of coils and turns connecting short helices and beta strands. It contains four short helices (α8-α11) and four anti-parallel beta strands (β3- β6).

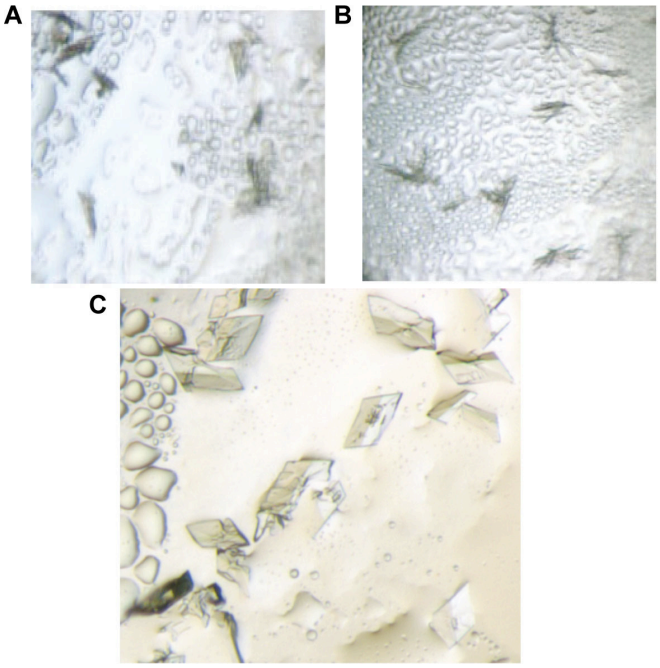

Figure 3-3. Crystals of LcrV obtained from **(A)** Hampton Index D8 **(B)** Hampton Index D9 and **(C)** following refinement with the pHat buffer screen.

Table 1. Crystallographic data for LcrV (G28-D322, C273S) refined to 1.65 Å resolution.

	LcrV (G28-D322, C273S)
Data Collection	
Unit-cell parameters (Å, °)	a=39.51, b=51.44, c=65.18, β=92.00
Space group	$P2_1$
Resolution (Å)[1]	51.44-1.65 (1.74-1.65)
Wavelength (Å)	1.0000
Temperature (K)	100
Observed reflections	103,407
Unique reflections	31,392
Mean $<I/\sigma(I)>$[1]	18.0 (2.2)
Completeness (%)[1]	99.3 (99.8)
Multiplicity[1]	3.3 (3.3)
R_{merge} (%)[1, 2]	3.4 (50.5)
R_{meas}[4]	4.0 (60.3)
R_{pim}[4]	2.2 (32.6)
Refinement	
Resolution (Å)	34.33-1.65
Reflections (working/test)	29,790 / 1582
R_{factor} / R_{free} (%)[3]	18.0 / 22.3
No. of atoms (protein / PEG 400 / water)	2,219 / 10 / 153
Model Quality	
R.m.s deviations	
Bond lengths (Å)	0.015
Bond angles (°)	1.436
Average B factor (Å^2)	
All Atoms	28.8
Protein	28.3
PEG 400	43.8
Water	35.6
Coordinate error based on maximum likelihood (Å)	0.46
Ramachandran Plot	
Most favored (%)	98.9
Additionally allowed (%)	1.1

1) Values in parenthesis are for the highest resolution shell.
2) $R_{merge} = \Sigma_{hkl}\Sigma_i |I_i(hkl) - <I(hkl)>| / \Sigma_{hkl}\Sigma_i I_i(hkl)$, where $I_i(hkl)$ is the intensity measured for the ith reflection and $<I(hkl)>$ is the average intensity of all reflections with indices hkl.
3) $R_{factor} = \Sigma_{hkl} ||F_{obs}(hkl)| - |F_{calc}(hkl)|| / \Sigma_{hkl} |F_{obs}(hkl)|$; Rfree is calculated in an identical manner using 5% of randomly selected reflections that were not included in the refinement.
4) R_{meas} = redundancy-independent (multiplicity-weighted) R (*26*). R_{pim} = precision-indicating (multiplicity-weighted) R (*27, 28*).

There are significant differences between the earlier structure of LcrV (1R6F) and the refined structure presented herein. At the N-terminal domain, there are differences in residues G28-N43, I46-V63 and Y77-Q95 **(Figure 3-5B)**. In 1R6F, helix α1 starts at G28 (residues G23-H27 could not be modeled in 1R6F). However in the current structure, residues G28-S30 formed a random coil with helix α1 starting only at residue V31. Further, the relative orientation of helix α1 is shifted as compared to the helix α1 of 1R6F. In the current structure, residues I46-V63 formed an ordered loop that packs at the C-terminal end of one of the helices (helix α12) of the central coiled coil. In 1R6F, residues K49-V63 lacked electron density and were not visible. Most of the notable differences between the structures of 1R6F and the refined structure are close to the site of the triple mutations present in 1R6F. Another difference is that while the residue Y90 is not visible in 1R6F, it could be resolved in the current refined structure. Additionally, the helical turn spanning residues Y77-Q95 are oriented differently in the two structures. In 1R6F the residues N260-D275 could not be modeled. Similarly in our model the residues K261 to P279 could not be modeled due to disorder.

3.3 Discussion

3.3.1 Comparison of the type III secretion system tip protein structures

The T3SSs of *Yersinia pestis, Pseudomonas aeruginosa,* and *Aeromonas salmonicida* belong to the Ysc family of injectisome, while the T3SSs of *Salmonella typhimurium*, and *Shigella flexneri* belong to the Inv-Mxi-Spa family of injectisomes (*3, 11, 17*). Though there is a low level of sequence identity (< 20 %) among the different families of tip proteins, the sequence conservation is high (~ 30-50 % sequence identity) within the tip proteins of the same family.

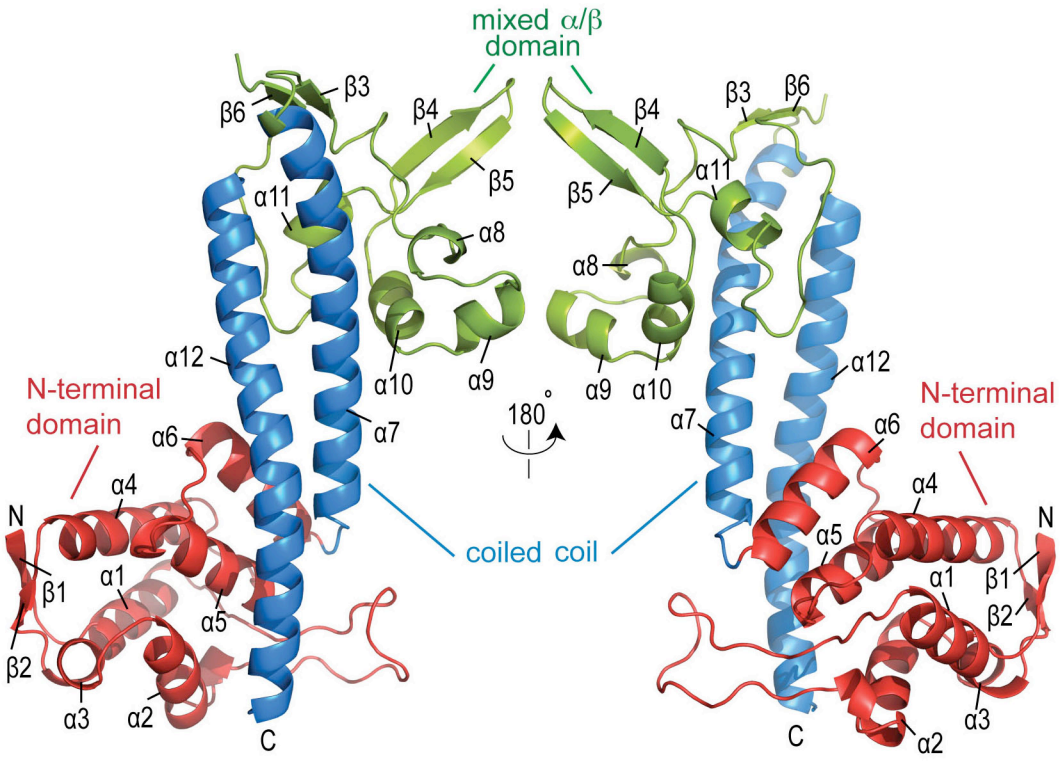

Figure 3-4. Crystal structure of LcrV refined to 1.65 Å resolution. The LcrV structure can be divided into three domains: N-terminal domain (red), the less structured domain of mixed α-helices and β-strands (green) and the coiled coil domain (blue).

The tip protein LcrV is more closely related to PcrV from *Pseudomonas* as compared to SipD, IpaD and BipD. Despite the low level of sequence conservation among the different families of tip proteins, they share a common topology consisting of the central coiled coil connected by two domains **(Figure 3-6)**. The central coiled coil is highly conserved among the T3SS tip proteins (*12*), suggesting it plays an important role in type III secretion (*12, 29*). Recently, others have shown that the central coiled coil of SipD is the site of protein-protein interactions with the PrgI needle protein and the SipD-PrgI interaction plays a critical role in the assembly of the needle apparatus (*21, 30*).

There are however significant differences between LcrV and the tip proteins IpaD, BipD and SipD with respect to the N-terminal domain (*12, 20*). In IpaD, BipD, and SipD the N-terminal region **(**pink in **Figure 3-6)** forms an α-helical hairpin, which functions as a self-chaperone for these tip proteins (*12, 19, 22*). Howevre, this α-helical hairpin domain is absent in LcrV. Another T3SS protein, LcrG, acts as a chaperone for LcrV by forming an LcrG-LcrV complex (*12, 15, 16, 31, 32*). Another difference between LcrV and the self-chaperoned tip proteins (IpaD, BipD, and SipD), is that the C-terminal helix of LcrV is bent and has a kink, whereas in the other tip proteins the equivalent helix is straight (*12*) **(Figure 3-6).** These structural differences suggest that the needle tip assembly process may vary between different T3SS families.

3.3.2 Significance of the N-terminal globular domain in LcrV

Results from scanning transmission electron microscopy (STEM) revealed that LcrV formed the tip complex on the *Yersinia enterocolitica* needle and consists of three distinct parts with a head,

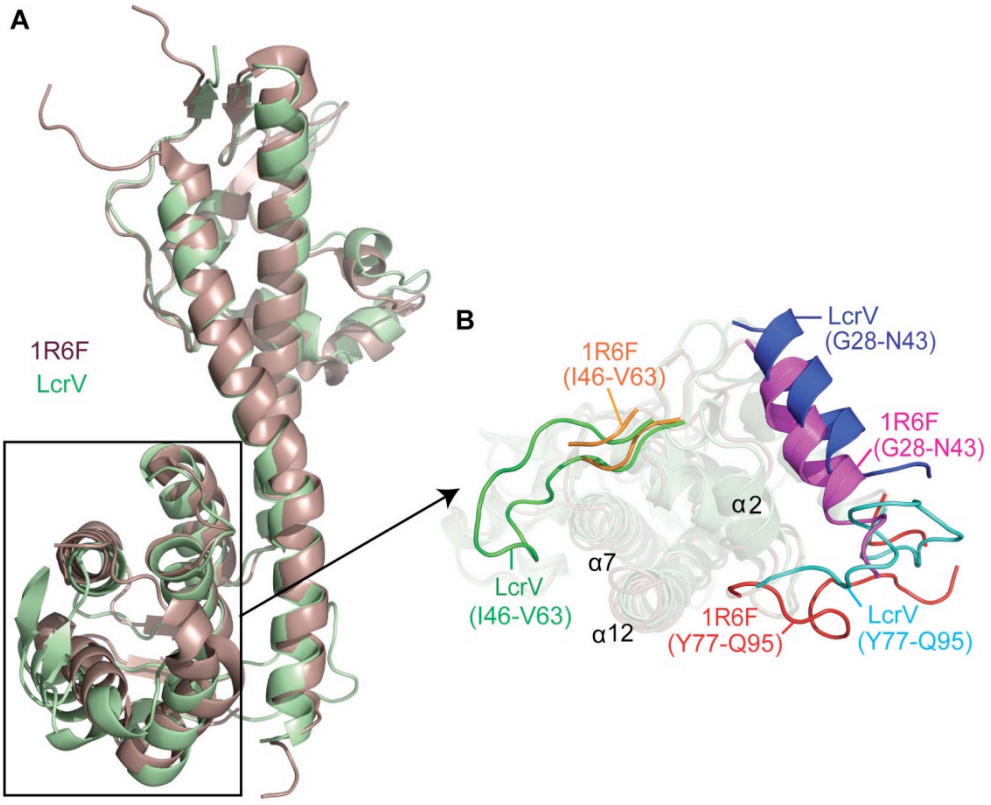

Figure 3-5. Comparison of the refined crystal structure of LcrV with 1R6F. **(A)** Alignment of the refined crystal structure of LcrV and 1R6F. The boxed area shows the N-terminal globular domain of LcrV. **(B)** Comparison of the differences in the N-terminal globular domain of the refined structure of LcrV with that of 1R6F.

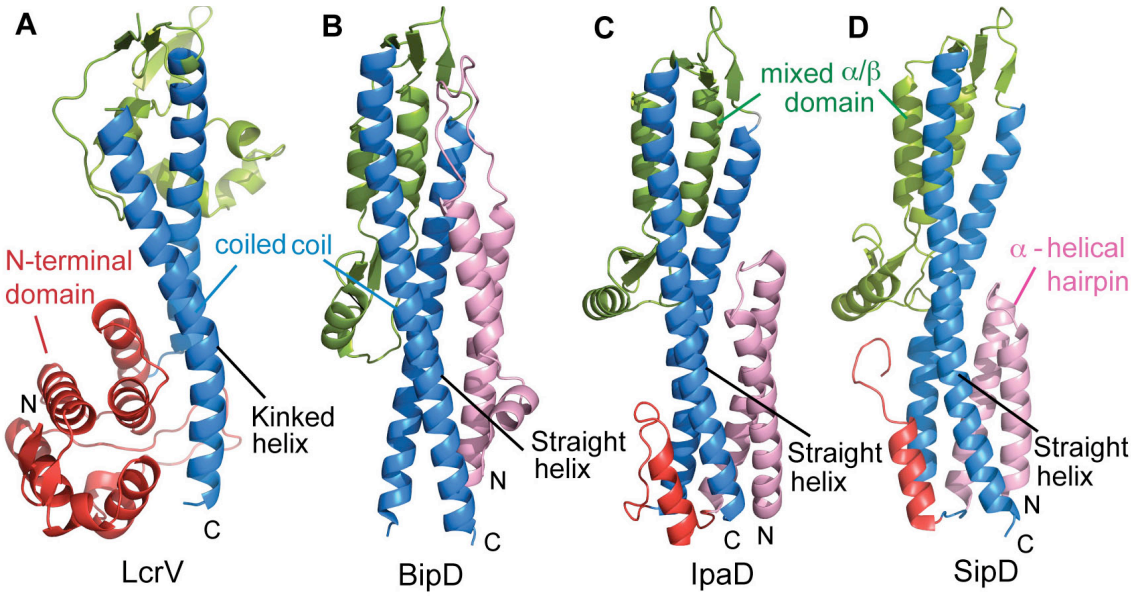

Figure 3-6. Comparison of the tip proteins from different bacterial species: **(A)** LcrV from *Yersinia pestis*, **(B)** BipD from *Burkholderia pseudomallei*, **(C)** IpaD from *Shigella flexneri*, and **(D)** SipD from *Salmonella typhimurium*. The central coiled coil is colored blue and the mixed α/β domain is colored green. The N-terminal domain of BipD, IpaD and SipD adopt an α-helical hairpin (pink), followed by short α-helices (red). The N-terminal α-helical hairpin domain is absent in LcrV. Instead, the LcrV N-terminal region forms a globular domain (red). The kinked helix in LcrV and the straight helices in BipD, IpaD, and SipD are labeled.

a neck and a base (*5*). The importance of the N-terminal globular domain of LcrV was demonstrated by Broz *et al. (13)* by forming hybrid proteins. Taking advantage of the fact that *Aeromonas* AcrV and *Pseudomonas* PcrV can form tip complexes on *Y. enteroclolitica* needle (*5*), Broz *et al.* (*13*) constructed chimeric hybrid proteins with the N-terminal domain from one protein while the coiled coil and the C-terminal globular domain from another protein. All these hybrid proteins could complement an *lcrV* deletion strain. The AcrV hybrids (LcrV-AcrV and AcrV-LcrV) were capable of forming functional tip complexes, which was assessed based on as the ability of these proteins to form functional pores in red blood cells (RBC). However, PcrV and PcrV-LcrV hybrid could not form functional pores and was unable to insert the YopB translocon protein efficiently into the RBC membranes. Interestingly enough, the PcrV hybrid consisting of the LcrV N-terminal domain (LcrV-PcrV) could successfully form functional pores. This highlighted the importance of the N-terminal domain of LcrV as a platform for the assembly of the translocation pore complex by allowing the efficient insertion of YopB into the host cell membrane (*13*).

STEM results on the hybrid tip complexes performed by Broz *et al.* (*5, 13*) showed that the size of the head and base domains differs among the chimeric hybrid proteins due to the different sizes of the globular domains in AcrV, PcrV, and LcrV. These differences suggested that the N-terminal domain of LcrV forms the base of the tip complex.

The refined structure of LcrV reported herein using wild type residues in the N-terminal domain would thus be important in studies of LcrV-translocon interactions.

3.4 References

1. Cornelis, G. R. (2002) *Yersinia* type III secretion: send in the effectors, *J. Cell Biol. 158*, 401-408.
2. Cornelis, G. R. (2002) The *Yersinia* Ysc-Yop 'type III' weaponry, *Nat Rev Mol Cell Biol 3*, 742-752.
3. Cornelis, G. R. (2006) The type III secretion injectisome, *Nat. Rev. Microbiol. 4*, 811-825.
4. Hauser, A. R. (2009) The type III secretion system of Pseudomonas aeruginosa: infection by injection, *Nat. Rev. Microbiol. 7*, 654-665.
5. Mueller, C. A., Broz, P., Muller, S. A., Ringler, P., Erne-Brand, F., Sorg, I., Kuhn, M., Engel, A., and Cornelis, G. R. (2005) The V-antigen of *Yersinia* forms a distinct structure at the tip of injectisome needles, *Science 310*, 674-676.
6. Carter, P. B., Zahorchak, R. J., and Brubaker, R. R. (1980) Plague virulence antigens from Yersinia enterocolitica, *Infect Immun 28*, 638-640.
7. Price, S. B., Cowan, C., Perry, R. D., and Straley, S. C. (1991) The Yersinia pestis V antigen is a regulatory protein necessary for Ca2(+)-dependent growth and maximal expression of low-Ca2+ response virulence genes, *J Bacteriol 173*, 2649-2657.
8. Skrzypek, E., and Straley, S. C. (1995) Differential effects of deletions in lcrV on secretion of V antigen, regulation of the low-Ca2+ response, and virulence of Yersinia pestis, *J Bacteriol 177*, 2530-2542.
9. Pettersson, J., Holmstrom, A., Hill, J., Leary, S., Frithz-Lindsten, E., von Euler-Matell, A., Carlsson, E., Titball, R., Forsberg, A., and Wolf-Watz, H. (1999) The V-antigen of

Yersinia is surface exposed before target cell contact and involved in virulence protein translocation, *Mol Microbiol 32*, 961-976.

10. Goure, J., Broz, P., Attree, O., Cornelis, G. R., and Attree, I. (2005) Protective anti-V antibodies inhibit Pseudomonas and Yersinia translocon assembly within host membranes, *J.Infect.Dis. 192*, 218-225.

11. Mueller, C. A., Broz, P., and Cornelis, G. R. (2008) The type III secretion system tip complex and translocon, *Mol. Microbiol. 68*, 1085-1095.

12. Blocker, A. J., Deane, J. E., Veenendaal, A. K., Roversi, P., Hodgkinson, J. L., Johnson, S., and Lea, S. M. (2008) What's the point of the type III secretion system needle?, *Proc. Natl. Acad. Sci. U.S.A. 105*, 6507-6513.

13. Broz, P., Mueller, C. A., Muller, S. A., Philippsen, A., Sorg, I., Engel, A., and Cornelis, G. R. (2007) Function and molecular architecture of the Yersinia injectisome tip complex, *Mol. Microbiol. 65*, 1311-1320.

14. Galan, J. E., and Wolf-Watz, H. (2006) Protein delivery into eukaryotic cells by type III secretion machines, *Nature 444*, 567-573.

15. Hamad, M. A., and Nilles, M. L. (2007) Roles of YopN, LcrG and LcrV in controlling Yops secretion by *Yersinia pestis*, *Adv. Exp. Med. Biol. 603*, 225-234.

16. Matson, J. S., and Nilles, M. L. (2001) LcrG-LcrV interaction is required for control of Yops secretion in *Yersinia pestis*, *J. Bacteriol. 183*, 5082-5091.

17. Sato, H., and Frank, D. W. (2011) Multi-Functional Characteristics of the *Pseudomonas aeruginosa* Type III Needle-Tip Protein, PcrV; Comparison to Orthologs in other Gram-negative Bacteria, *Front. Microbiol. 2*, 142.

18. Derewenda, U., Mateja, A., Devedjiev, Y., Routzahn, K. M., Evdokimov, A. G., Derewenda, Z. S., and Waugh, D. S. (2004) The structure of *Yersinia pestis* V-antigen, an essential virulence factor and mediator of immunity against plague, *Structure 12*, 301-306.

19. Johnson, S., Roversi, P., Espina, M., Olive, A., Deane, J. E., Birket, S., Field, T., Picking, W. D., Blocker, A. J., Galyov, E. E., Picking, W. L., and Lea, S. M. (2007) Self-chaperoning of the type III secretion system needle tip proteins IpaD and BipD, *J. Biol. Chem. 282*, 4035-4044.

20. Chatterjee, S., Zhong, D., Nordhues, B. A., Battaile, K. P., Lovell, S. W., and De Guzman, R. N. (2011) The Crystal Structure of the Salmonella Type III Secretion System Tip Protein SipD in Complex with Deoxycholate and Chenodeoxycholate, *Protein Sci. 20*, 75-86.

21. Lunelli, M., Hurwitz, R., Lambers, J., and Kolbe, M. (2011) Crystal structure of PrgI-SipD: insight into a secretion competent state of the type three secretion system needle tip and its interaction with host ligands, *PLoS Pathog. 7*, e1002163.

22. Erskine, P. T., Knight, M. J., Ruaux, A., Mikolajek, H., Wong Fat Sang, N., Withers, J., Gill, R., Wood, S. P., Wood, M., Fox, G. C., and Cooper, J. B. (2006) High Resolution Structure of BipD: An Invasion Protein Associated with the Type III Secretion System of *Burkholderia pseudomallei*, *J. Mol. Biol. 363*, 125-136.

23. Espina, M., Ausar, S. F., Middaugh, C. R., Baxter, M. A., Picking, W. D., and Picking, W. L. (2007) Conformational stability and differential structural analysis of LcrV, PcrV, BipD, and SipD from type III secretion systems, *Protein Sci. 16*, 704-714.

24. Krissinel, E., and Henrick, K. (2004) Secondary-structure matching (SSM), a new tool for fast protein structure alignment in three dimensions, *Acta Crystallogr D Biol Crystallogr 60*, 2256-2268.

25. Emsley, P., Lohkamp, B., Scott, W. G., and Cowtan, K. (2010) Features and development of Coot, *Acta Crystallogr D Biol Crystallogr 66*, 486-501.

26. Evans, P. (2006) Scaling and assessment of data quality, *Acta Crystallogr D Biol Crystallogr 62*, 72-82.

27. Diederichs, K., and Karplus, P. A. (1997) Improved R-factors for diffraction data analysis in macromolecular crystallography, *Nat Struct Biol 4*, 269-275.

28. Weiss, M. S. (2001) Global indicators of X-ray data quality, *Journal of Applied Crystallography 34*, 130-135.

29. Deane, J. E., Roversi, P., Cordes, F. S., Johnson, S., Kenjale, R., Daniell, S., Booy, F., Picking, W. D., Picking, W. L., Blocker, A. J., and Lea, S. M. (2006) Molecular model of a type III secretion system needle: Implications for host-cell sensing, *Proc. Natl. Acad. Sci. U.S.A. 103*, 12529-12533.

30. Rathinavelan, T., Tang, C., and De Guzman, R. N. (2011) Characterization of the Interaction between the *Salmonella* Type III Secretion System Tip Protein SipD and the Needle Protein PrgI by Paramagnetic Relaxation Enhancement, *J. Biol. Chem. 286*, 4922-4930.

31. Hamad, M. A., and Nilles, M. L. (2007) Structure-function analysis of the C-terminal domain of LcrV from *Yersinia pestis*, *J. Bacteriol. 189*, 6734-6739.

32. Matson, J. S., and Nilles, M. L. (2002) Interaction of the *Yersinia pestis* type III regulatory proteins LcrG and LcrV occurs at a hydrophobic interface, *BMC Microbiol. 2*, 16.

CHAPTER 4: Structural characterization of the *Yersinia pestis* tip protein chaperone LcrG

4.1 Introduction

An important determinant of pathogenicity of *Yersinia pestis* is its ability to assemble a protein export machinery, the type III secretion system (T3SS) (*1, 2*). The needle apparatus of the T3SS is assembled from structural proteins that form the base, an external needle, a tip complex, and a translocon (*3*). In addition to structural proteins, effectors and chaperones are also required for the proper function of the T3SS (*3*). In *Yersinia*, the tip complex is formed by several copies of LcrV (326 residues) (*4*) and while inside the bacterial cytosol, LcrV is chaperoned by a smaller protein, LcrG (95 residues) (*5, 6*). LcrG functions as a chaperone of the LcrV tip protein by facilitating its secretion (*6, 7*).

The secretion of Yops by the *Y. pestis* T3SS is a highly regulated process, and Yops are secreted only upon contact with the host cells (*8*). *In vitro*, the concentration of Ca^{+2} plays an important role in regulation of Yop secretion. The presence of millimolar amounts of Ca^{+2} prevents Yop secretion, while removal of Ca^{+2} from the growth medium results in Yop secretion (*9, 10*). Several proteins are involved in regulating Yop secretion, among which, LcrG and LcrV play important roles in this regulation process. LcrG acts as a negative regulator of Yop secretion, i.e. increased levels of LcrG result in blockage of Yop secretion (*10, 11*). Deletion of the gene encoding LcrG results in the loss of regulation of Yop secretion leading to constitutive expression and secretion of Yops regardless of Ca^{+2} concentration (*6, 11-13*).

LcrG is functionally versatile and has multiple roles in type III secretion. It is involved in regulating the secretion of Yops, and it facilitates the targeting of Yop effectors into the host

cells (*7, 10, 11*). Additionally, it serves as a chaperone to the tip protein, LcrV (*6, 7*). Unlike chaperones of effectors, translocators and needle proteins (*14-16*), much less is known about the atomic structures of the chaperones of tip proteins. The tip proteins from *Salmonella typhimurium* (SipD), *Shigella flexneri* (IpaD) and *Burkholderia pseudomallei* (BipD) have an N-terminal α-helical hairpin domain that acts as a self-chaperone for these proteins (*17-20*). However, the tip protein of *Yersinia pestis* (LcrV) lacks this self-chaperoning domain. Hence, it has been suggested by others that LcrG, which serves as a chaperone for LcrV adopts a similar coiled coil structure analogous to the self-chaperoning domains of the other tip proteins (*17, 18, 20*) **(Figure 4-1)**. However, the atomic structures of the LcrG family of chaperone proteins remain unknown.

A goal of this research was to determine the structure of LcrG by using NMR spectroscopy and other biophysical methods. In contrast to the hypothesis that LcrG forms a coiled coil structure, data from NMR and CD spectroscopy show that LcrG is a flexible protein with an α-helical secondary structure, and the protein lacks a tertiary fold. This knowledge about the structure of LcrG is important in elucidating the mechanism by which it achieves its functional versatility.

4.2 Results

4.2.1 Expression and purification of LcrG

The LcrG constructs were expressed in *E. coli* as N-terminal His_6-GB1 fusion proteins. The His_6 tag aided in the nickel affinity purification. The TEV protease cleavage site was used to obtain the purified proteins after digestion by TEV protease to remove the His_6-GB1 tag.

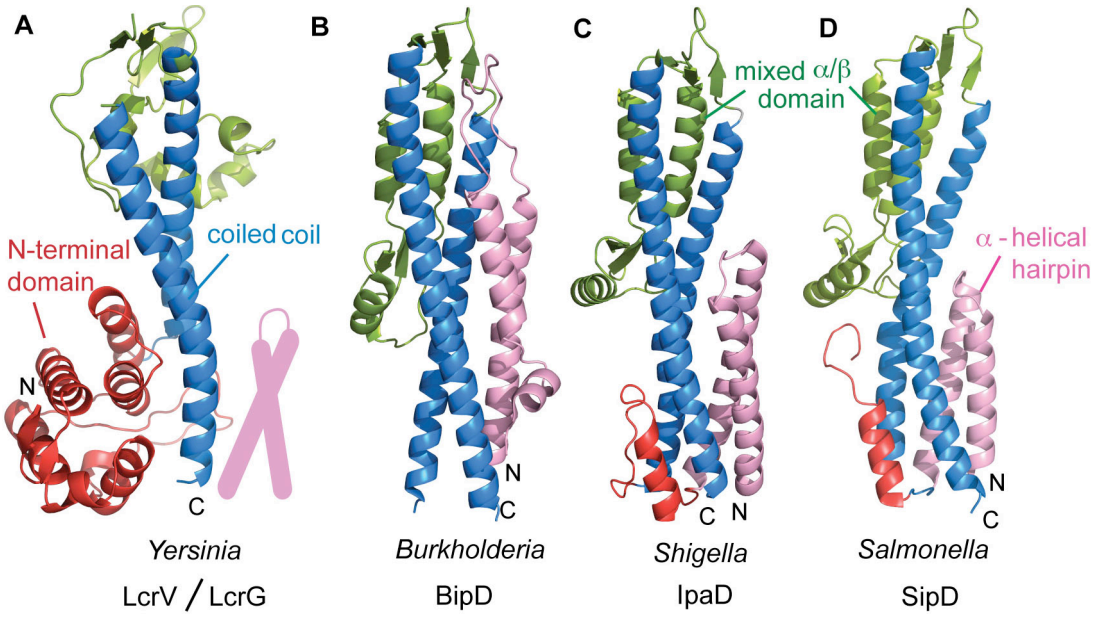

Figure 4-1. Comparison of crystal structures of T3SS tip proteins: **(A)** LcrV from *Yersinia pestis,* **(B)** BipD from *Burkholderia pseudomallei,* **(C)** IpaD from *Shigella flexneri,* and **(D)** SipD from *Salmonella typhimurium.* The central coiled coil is colored blue and the mixed α/β domain is colored green. The N-terminal domain of BipD, IpaD and SipD adopt an α-helical hairpin (pink), which are proposed to function as self-chaperones for the respective tip proteins. Instead, the LcrV N-terminal region forms a globular domain (red). Since the N-terminal α-helical hairpin is absent in LcrV, the chaperone LcrG has been modeled based on the N-terminal domain of IpaD (*20*).

The fusion proteins were expressed in soluble forms in *E. coli* and purified under native conditions followed by TEV protease digestion. All the constructs described in this chapter produced high yields of protein that facilitated NMR studies.

4.2.2 Designing an ideal LcrG construct for NMR studies

Multiple sequence alignment of LcrG (95 amino acids) showed conservation with other members of the LcrG family of chaperone proteins **(Figure 4-2)**. Full-length LcrG ($LcrG^{FL}$) showed a poor quality two-dimensional (2D) ^{1}H-^{15}N HSQC NMR spectrum where the amide peaks were barely resolved and the numbers of peaks were much less than expected from a 95-residue protein **(Figure 4-3A)**. Based on the secondary structure prediction by PSIPRED (*21*) **(Figure 4-2B)**, the disordered tails of LcrG were truncated, while maintaining the hydrophilic terminal residues to generate the truncated construct spanning residues Asp-7 to Arg-73 ($LcrG^{7-73}$). Using $LcrG^{7-73}$ somewhat improved the 2D ^{1}H-^{15}N HSQC spectrum as compared to $LcrG^{FL}$, but $LcrG^{7-73}$ did not yield an ideal NMR spectrum either. Only 58% of the residues in the protein were represented in the 2D ^{1}H-^{15}N HSQC spectrum of $LcrG^{7-73}$ and the peaks were broadened and poorly resolved **(Figure 4-3B)**. It was reasoned that this non-ideal NMR spectrum of $LcrG^{7-73}$ could be due to the presence of a native cysteine at position 34 (C34) (shown by an arrow in **Figure 4-2A**), and this C34 might be responsible for forming disulphide linkage and contribute to the aggregation of the protein. Hence, the native cysteine (C34) was mutated into serine and alanine thereby creating the constructs $LcrG^{7-73}$ C34S and $LcrG^{7-73}$ C34A. $LcrG^{7-73}$ C34S yielded a better quality ^{1}H-^{15}N HSQC spectrum with sharp and well-resolved peaks **(Figure 4-3C)** compared to $LcrG^{7-73}$ C34A **(Figure 4-4)**. Since NMR is sensitive to the amount of DTT, it could not be used at the sufficient concentration.

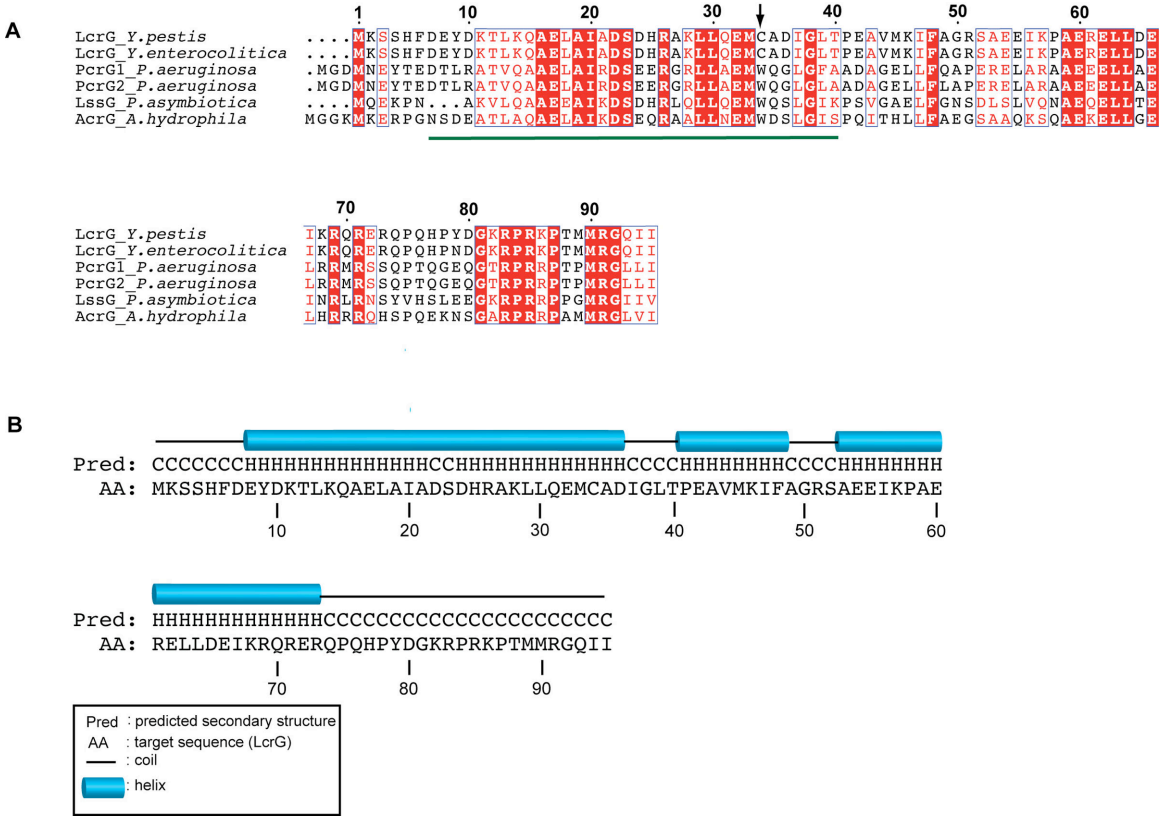

Figure 4-2. Multiple sequence alignment (MSA) of LcrG family of tip chaperones and secondary structure prediction for LcrG. **(A)** MSA of LcrG family of proteins using CLUSTALW (*22*). The homologous proteins were obtained from BLAST and denoted as follows: LcrG (from *Yersinia pestis*), LcrG (from *Yersinia enterocolitica*), PcrG 1 and 2 (from two different strains of *Pseudomonas aeruginosa*), LssG (from *Photorhabdus asymbiotica*) and AcrG (from *Aeromonas hydrophila*). The green line denotes the region Asp-7 to Thr-40 in LcrG that is suggested to bind to LcrV using yeast two-hybrid assays (*23*). The black arrow points to the cysteine at position 34. **(B)** Result of secondary structure prediction for LcrG from PSIPRED (*21*). Residues in random coil or helical regions are denoted by "C" or "H", respectively. A cartoon representation is also provided where the helices and random coils are represented as blue cylinders and black lines respectively.

To verify that the truncation of the flexible tails were essential to achieving the well-resolved NMR spectrum, $LcrG^{FL}$ C34S protein was expressed. While the 2D ^{1}H-^{15}N HSQC spectrum of $LcrG^{FL}$ C34S was better than $LcrG^{FL}$, it was poor compared to the 2D ^{1}H-^{15}N HSQC spectrum of $LcrG^{7-73}$ C34S **(Figure 4-4)**. $LcrG^{FL}$ C34S showed a significant number of overlapping peaks and exhibited conformational heterogeneity **(Figure 4-4)**, which possibly arose from the cis-trans isomerization of the prolines present at the flexible C-terminus of LcrG. However, both $LcrG^{FL}$ C34S and $LcrG^{7-73}$ C34S had similar biophysical characteristics as seen from the CD and thermal denaturation curves **(Figure 4-6)**. Additionally, both the $LcrG^{FL}$ C34S and $LcrG^{7-73}$ C34S bind similarly to LcrV **(Figure 5-10** in chapter 5**)**. The same set of LcrV residues were affected in the same manner when titrated with either $LcrG^{FL}$ C34S or $LcrG^{7-73}$ C34S **(Figure 5-10** in chapter 5). Therefore, I used $LcrG^{7-73}$ C34S for NMR studies.

4.2.3 Circular Dichroism and Thermal Denaturation

Circular Dichroism (CD) spectra of $LcrG^{FL}$, $LcrG^{7-73}$, $LcrG^{7-73}$ C34S, and $LcrG^{FL}$ C34S **(Figure 4-6)** showed that the LcrG constructs are primarily α-helical in secondary structure as demonstrated by the characteristic minima at 222 and 208 nm. The 222/208 nm ratios of $LcrG^{FL}$, $LcrG^{7-73}$ and $LcrG^{FL}$ C34S were ~0.8. The 222/208 nm ratio of the $LcrG^{7-73}$ C34S was ~0.7. The slight difference in the θ_{222} reading at 25 °C between the CD and thermal denaturation of the $LcrG^{FL}$ C34S, was due to the difference among the three thermal denaturation readings that was averaged. Thermal denaturation curves of $LcrG^{FL}$, $LcrG^{7-73}$, $LcrG^{FL}$ C34S and $LcrG^{7-73}$ C34S showed that they unfolded in a non-cooperative manner without displaying a clear inflection point **(Figure 4-6)**.

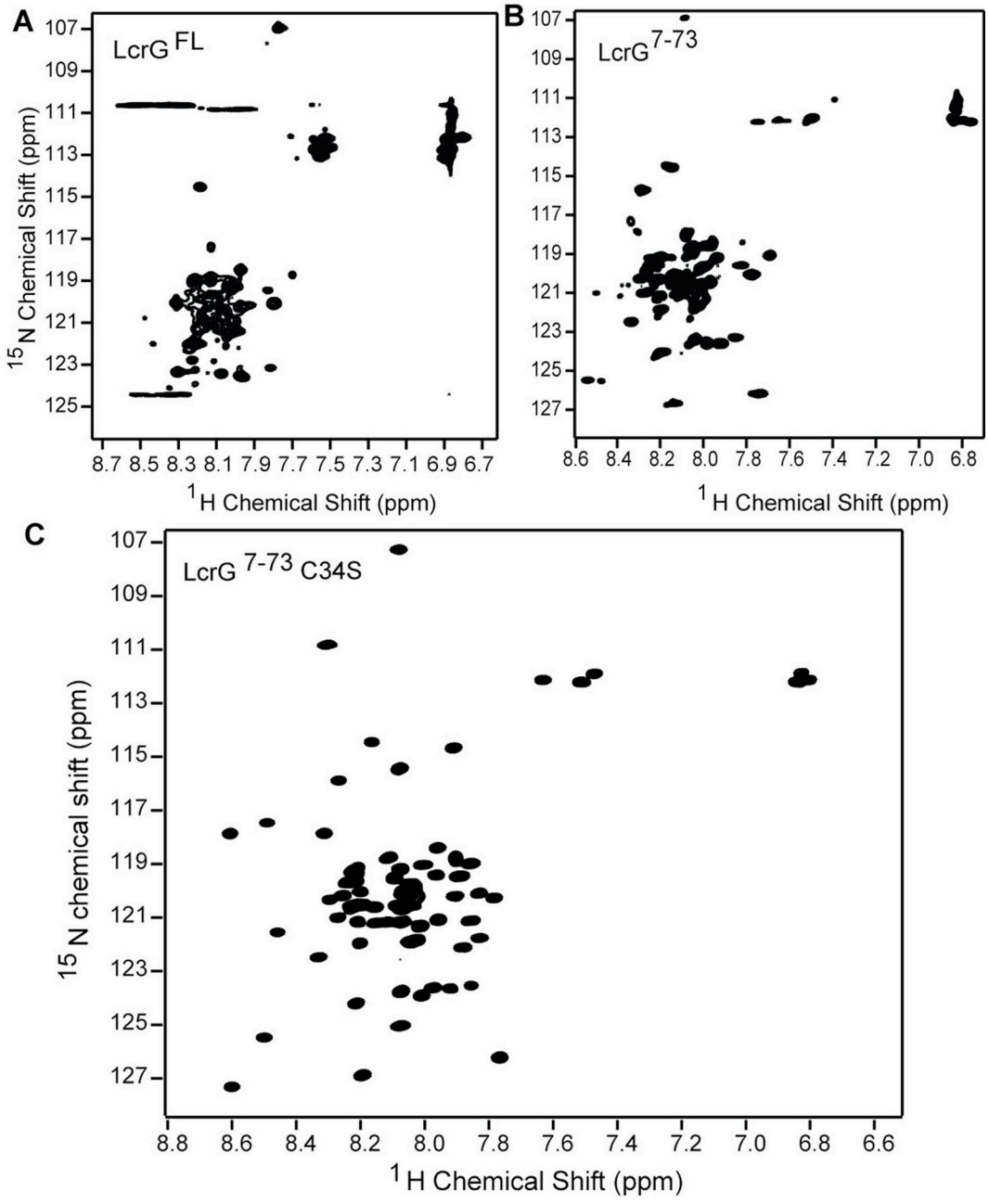

Figure 4-3. 2D ^{1}H-^{15}N HSQC spectra of **(A)** LcrG^{FL} **(B)** LcrG$^{7-73}$ and **(C)** LcrG$^{7-73}$ C34S.

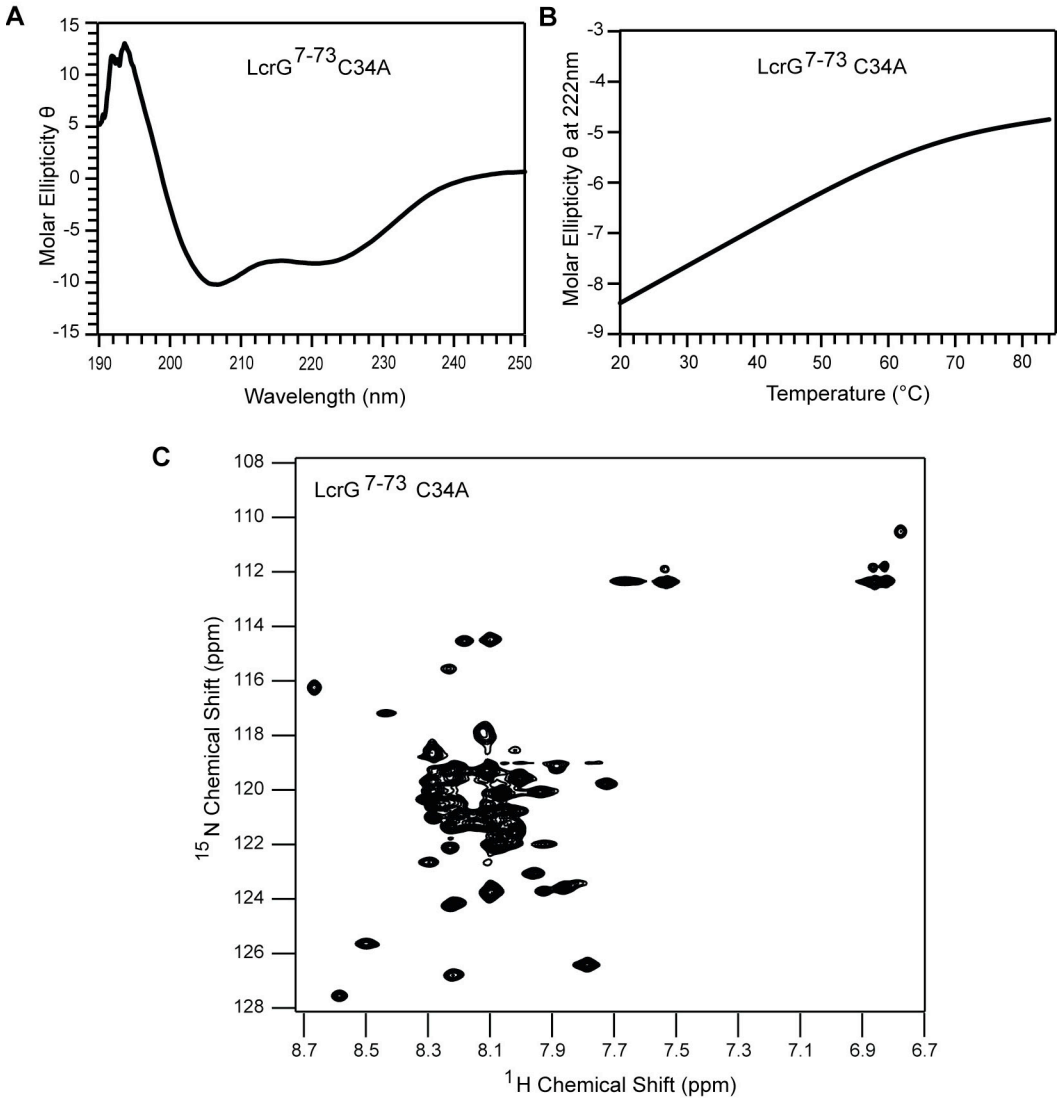

Figure 4-4. CD **(A)**, thermal denaturation **(B)**, and 2D ^{1}H-^{15}N HSQC spectrum **(C)** of LcrG$^{7-73}$ C34A.

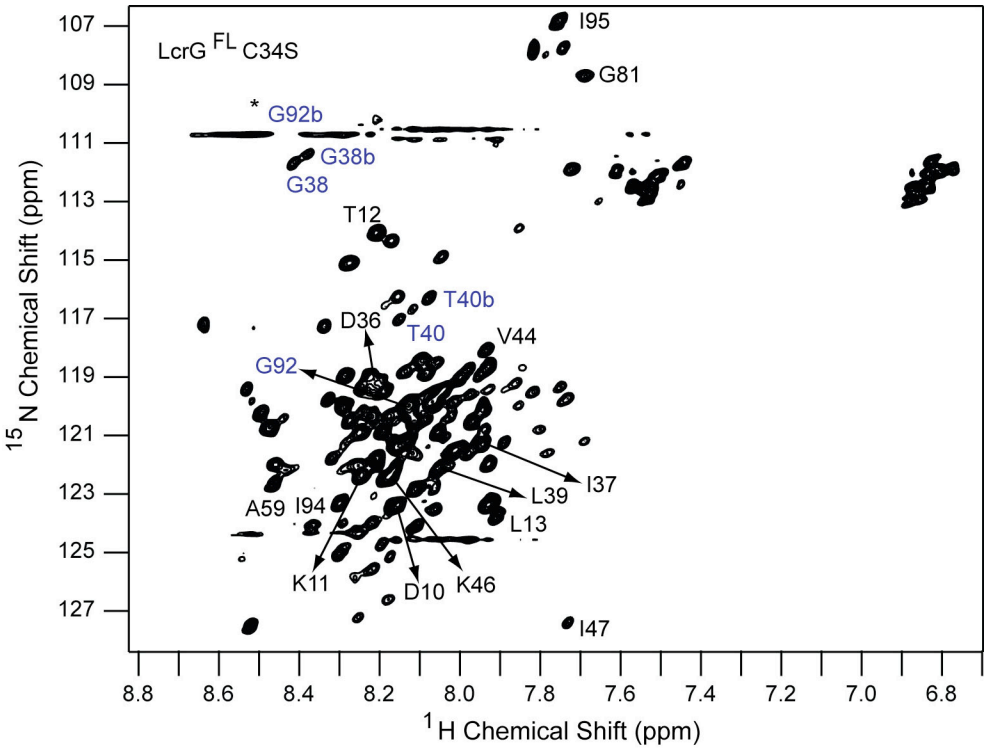

Figure 4-5. 2D ^{1}H-^{15}N HSQC spectrum of LcrG^{FL} C34S shown with partial backbone assignments. The residues in blue display conformational heterogeneity. The intensity of the G92b peak is low, and hence not shown. The position of G92b is indicated with black asterisk.

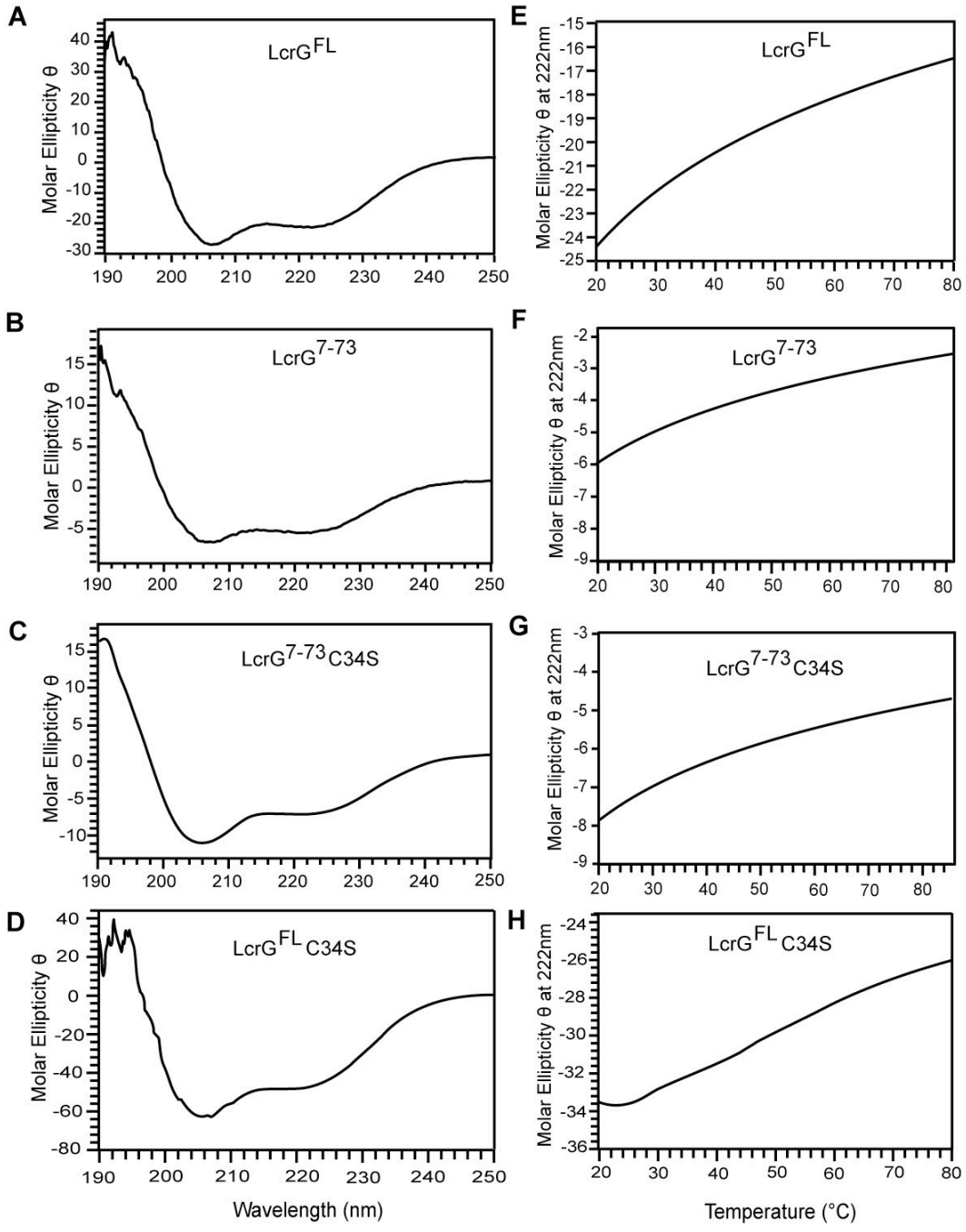

Figure 4-6. CD and thermal denaturation spectra of the various LcrG constructs. CD spectra were acquired at 25° C for **(A)** $LcrG^{FL}$, **(B)** $LcrG^{7-73}$, **(C)** $LcrG^{7-73}$ C34S, and **(D)** $LcrG^{FL}$ C34S. Thermal denaturation plots of **(E)** $LcrG^{FL}$, **(F)** $LcrG^{7-73}$, **(G)** $LcrG^{7-73}$ C34S and **(H)** $LcrG^{FL}$ C34S, (Molar ellipticity $\theta = (deg \cdot cm^2 \cdot dmol^{-1}) \times 10^{-5}$).

4.2.4 Functional characterization of LcrG C34S mutant in Yersinia pestis

A Yop secretion assay was used to evaluate the functional significance of mutations on LcrG. The mutant protein (LcrG C34S) was expressed from a pBAD18 vector and tested with regards to Yop secretion in *Y. pestis.* LcrG C34S mutant successfully complemented a Δ*lcrG* mutation, restoring Ca^{+2} regulated secretion of YopM proteins **(Figure 4-7)**. In other words, LcrG C34S secreted YopM only in the absence of Ca^{+2} and not in its presence, which is similar to behavior of wild type LcrG. On the other hand, the null LcrG mutant constitutively secreted YopM both in the presence and absence of Ca^{+2}. The expression of YopM and LcrG proteins in whole cells was confirmed by immunoblotting with their respective antibodies. Another construct, LcrGC34A was functional **(Figure 4-7)**, and had similar secondary structure composition, compared to wild type LcrG **(Figure 4-4)**. However, further NMR studies were performed using the LcrGC34S construct because it gave better NMR data.

4.2.5 LcrG backbone assignments

The construct $LcrG^{7-73}$ C34S was soluble at high concentrations and afforded millimolar amounts of purified protein. Three-dimensional NMR datasets were acquired using $^{15}N/^{13}C$ $LcrG^{7-73}$ C34S for backbone resonance assignments. Of the 67 backbone amides of $LcrG^{7-73}$ C34S, 62 were assigned **(Figure 4-8)**. However, the backbone amides of His-25, Arg-26, Glu-32, Lys-46 and Met-45 were either in rapid exchange with the solvent or overlapped with other peaks, and hence could not be assigned. The other overlapping peaks in the assigned $LcrG^{7-73}$ C34S spectrum are indicated in **Figure 4-8** with asterisks. The backbone resonances of Ile-37, Ile-47 and Phe-48 were assigned by ^{15}N amino acid specific labeling of $LcrG^{7-73}$ C34S as described in section 2.1.6 **(Figure 4-8)**.

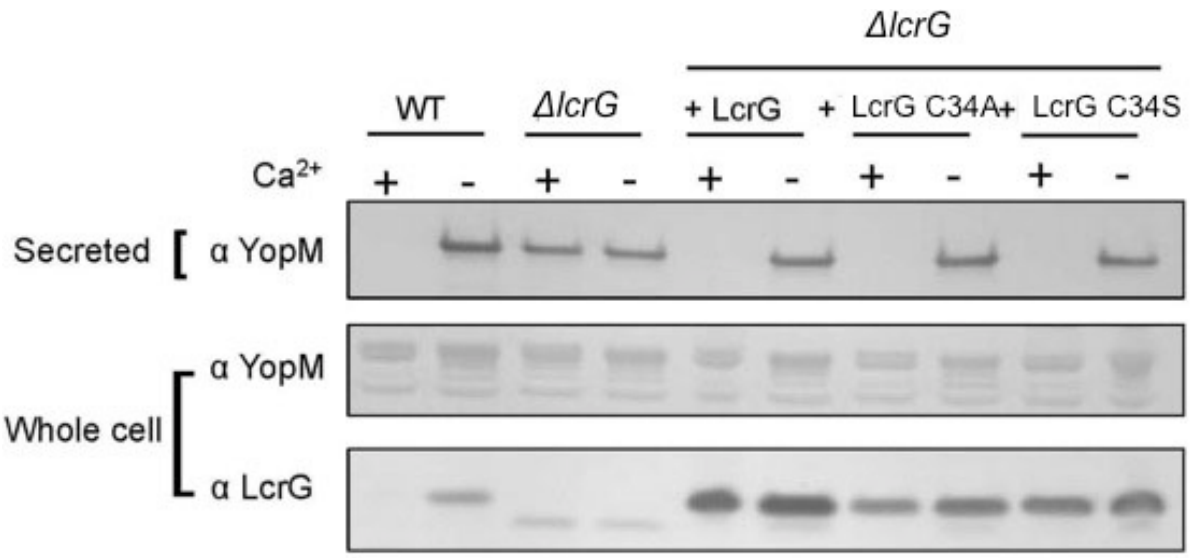

Figure 4-7. Functional characterization of LcrG substitution mutants in *Yersinia pestis*. Both mutants LcrG C34S and LcrG C34A are capable of complementing a Δ*lcrG* mutation, restoring Ca^{+2} regulated secretion of YopM proteins. The Δ*lcrG* represents a non-functional deletion mutant of LcrG (Δ39-54), and hence the lower bands are seen in the whole cell blot of Δ*lcrG*.

Since there were two isoleucines (Ile-37 and Ile-47) that could not be assigned by the 3D datasets, a 2D ^{1}H-^{15}N HSQC of the point mutant I37A in addition to the ^{15}N amino acid (Ile) specific labeling **(Figure 4-9)** was used to confirm the assignment of the two isoleucines. Overlay of the two HSQC spectra, ^{15}N LcrG$^{7-73}$ C34S (black) and ^{15}N Ile LcrG$^{7-73}$ C34S (blue), showed the backbone amide peak positions of the five isoleucines (blue) **(Figure 4-9A)**. Of the five isoleucines, three (Ile-20, Ile-56 and Ile-67) were already assigned by using the 3D datasets. **Figure 4-9B** showed that upon superposition of the two HSQC spectra, ^{15}N LcrG$^{7-73}$ C34S (black) and ^{15}N LcrG$^{7-73}$ C34S I37A (red), there was absence of a red peak in one position for the backbone amide of I37A, thus identifying that peak as I37. A similar ^{15}N amino acid selective labeling approach was used to assign the backbone resonance of Phe-48 **(Figure 4-9C)**. Since there is only one Phe in LcrG, it could be assigned based simply on the selective labeling with ^{15}N-phenylalanine. Examples of the carbon backbone connectivity of some of the representative LcrG residues are illustrated in **Figure 4-10**.

Analysis of the secondary Cα and Cβ chemical shifts suggested the presence of three α-helices from residues Asp-7 to Gly-38, Glu-42 to Gly-50 and Ala-59 to Arg-73 **(Figure 4-11)**. If the Cα chemical shifts are consistently positive, it is denoted as a α-helix. The random coil chemical shifts are determined as described in Chapter 2 (section 2.3.3). However, the first α-helix (Asp-7 to Gly-38) displayed low helicity compared to the other two helices. These helices are separated by a very short three-residue linker between helix α1 and helix α2, and an eight-residue linker between helix α2 and helix α3.

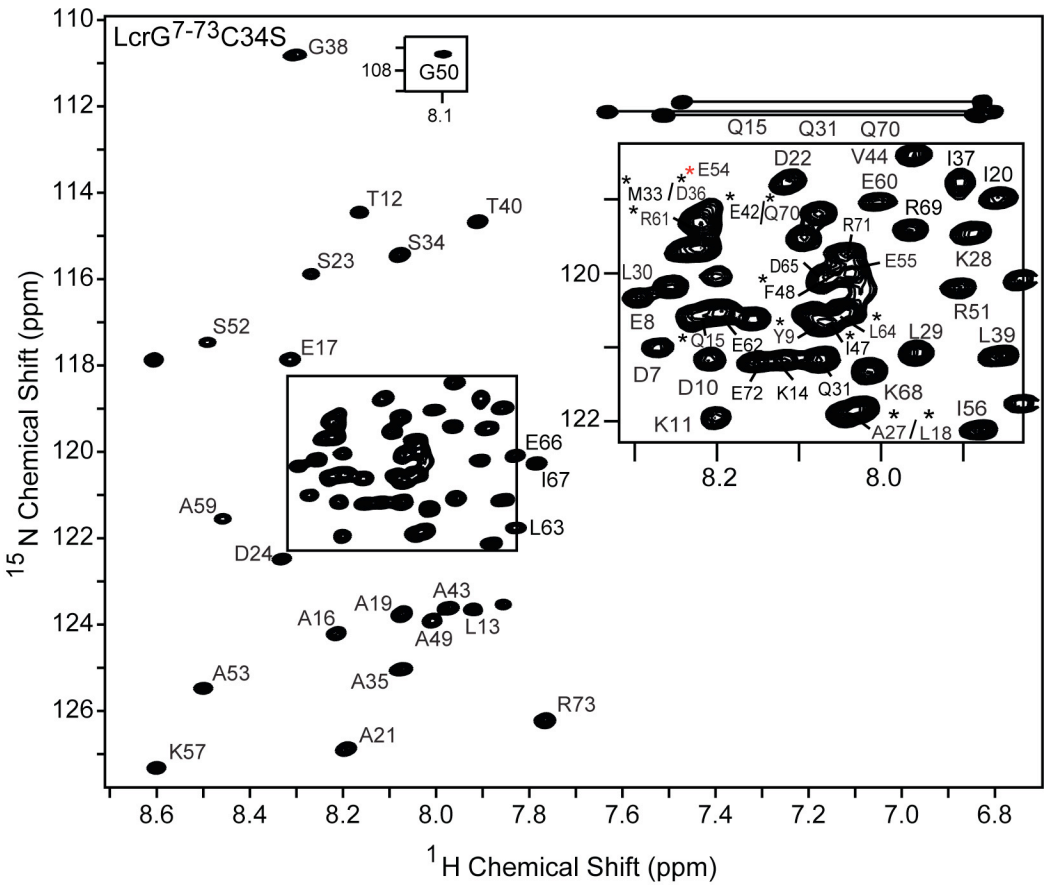

Figure 4-8. Assigned 2D ^{1}H-^{15}N HSQC spectrum of LcrG$^{7-73}$ C34S. Residue names are labeled next to their corresponding peaks. Overlapped peaks are indicated with asterisk (A27* is overlapped with L18*; Y9*, I47* and L64* are all overlapped; E42* is overlapped with Q70*; M33* is overlapped with D36*. Q15*, R61* and F48* were not resolved. The intensity of the E54 peak is low and not shown. The position of E54 is indicated with red asterisk.

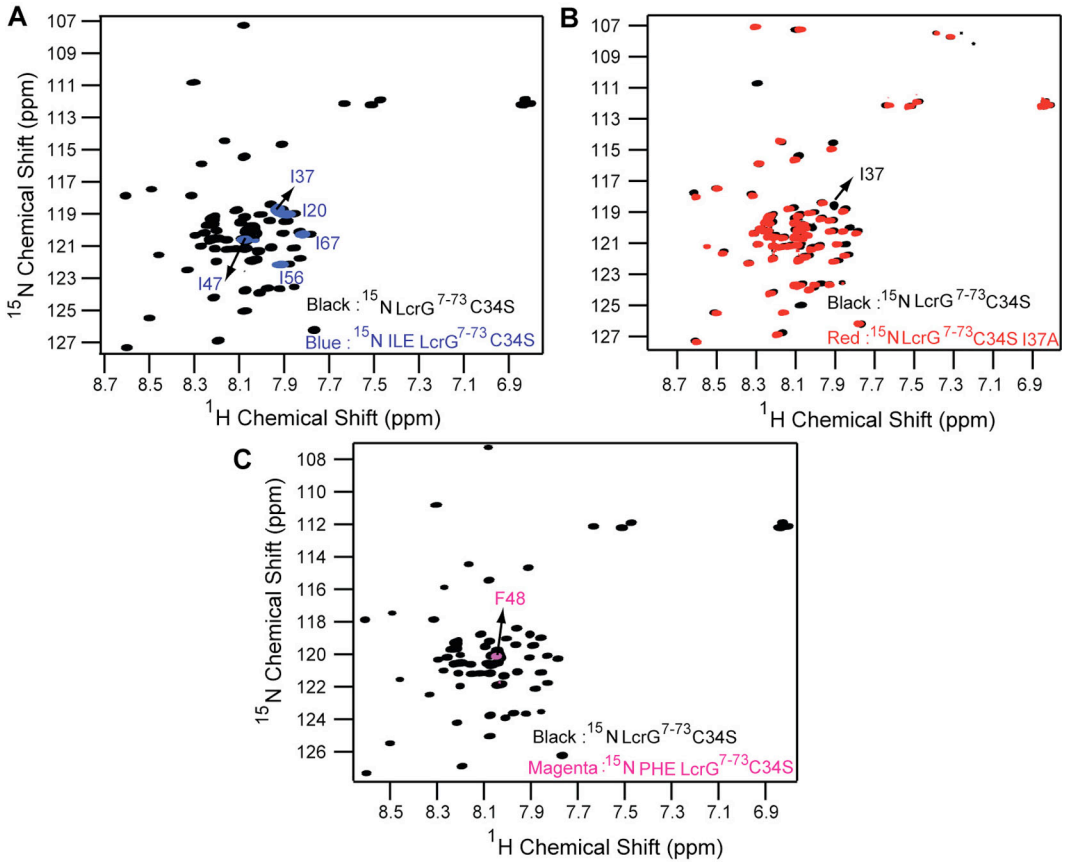

Figure 4-9. Overlay of 2D ^{1}H-^{15}N HSQC spectrum of LcrG$^{7-73}$ C34S (black) with **(A)** 2D ^{1}H-^{15}N Ile HSQC spectrum of LcrG$^{7-73}$ C34S (blue). The five isoleucines are marked next to their corresponding peak positions. Arrows show the backbone resonances of Ile-37 and Ile-47, assigned by selective labeling and mutagenesis. **(B)** 2D ^{1}H-^{15}N HSQC spectrum of LcrG$^{7-73}$ C34S I37A (red). The arrow shows the assignment of the backbone resonance of Ile-37. Overlay of 2D ^{1}H-^{15}N HSQC spectrum of LcrG$^{7-73}$ C34S (black) with **(C)** 2D ^{1}H-^{15}N Phe HSQC spectrum of LcrG$^{7-73}$ C34S (magenta). The arrow shows the assignment of the backbone resonance of Phe-48.

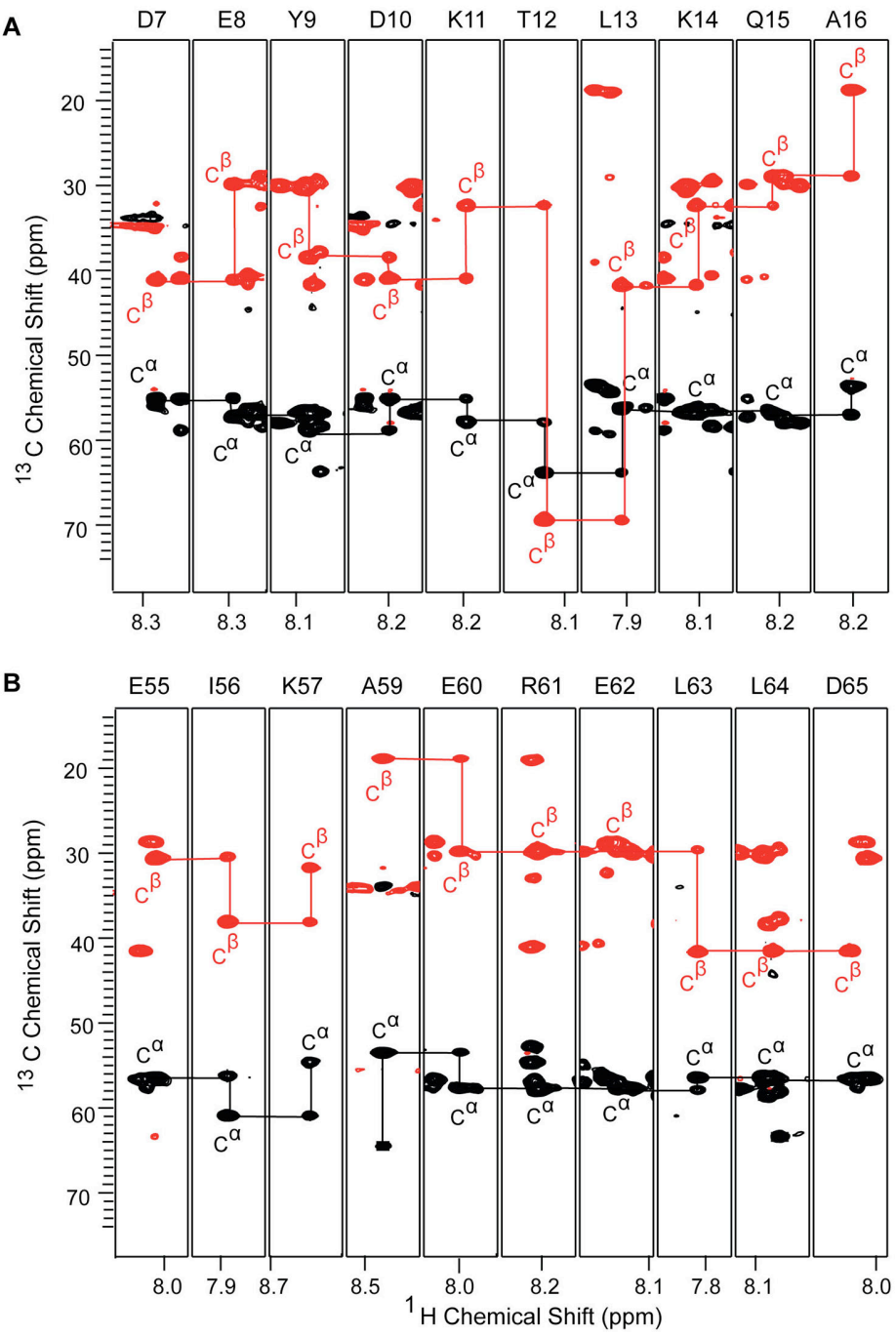

Figure 4-10. Representative strips of the 3D HNCACB spectrum of $^{15}N/^{13}C$ LcrG$^{7-73}$ C34S spanning residues D7 to A16 (top) and E55 to D65 (bottom) to illustrate the backbone connectivity identified for LcrG$^{7-73}$ C34S assignment.

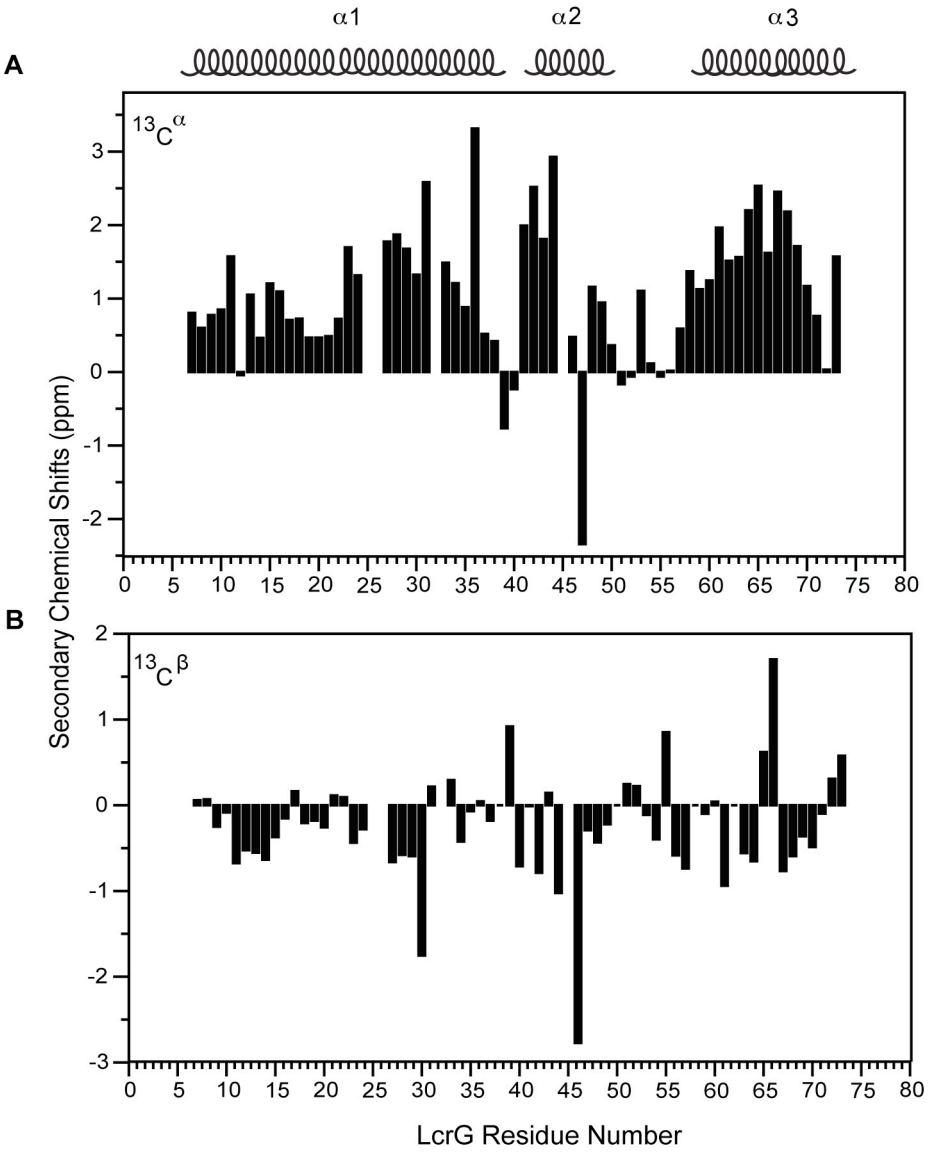

Figure 4-11. (A) Cα and **(B)** Cβ Secondary chemical shifts of LcrG$^{7-73}$ C34S suggest the presence of three α-helical regions. If the Cα chemical shifts are consistently positive, it is denoted as an α-helix. The positions of the helices are indicated. The random coil chemical shifts are determined as described in Chapter 2 (section 2.3.3).

4.2.6 LcrG backbone dynamics

The steady state heteronuclear $\{^1H\}$-^{15}N NOE and ^{15}N backbone relaxation rates (R_1 and R_2) were acquired on $LcrG^{7-73}$ C34S to assess the backbone dynamics of the protein. The heteronuclear $\{^1H\}$-^{15}N NOEs provide a read out of fast protein backbone dynamics at the picosecond to nanosecond time scales. Residues with $\{^1H\}$-^{15}N NOEs above 0.6 generally indicate that they form well-structured regions and can be qualitatively described as being rigid. Whereas residues with $\{^1H\}$-^{15}N NOEs between 0.4-0.6 suggest semi-rigid flexibility, and the residues with $\{^1H\}$-^{15}N NOEs below 0.2 indicate these residues are random coil. The extreme terminal residues of $LcrG^{7-73}$ C34S (Asp-7 and Arg-73) were in random coil flexibility as seen from their $\{^1H\}$-^{15}N NOE values of below 0.2 **(Figure 4-12A)**. Most of the residues in the α-helices have semi-rigid flexibility as shown by their $\{^1H\}$-^{15}N NOEs that range between 0.4-0.6 **(Figure 4-12A)**. There were a few residues in the beginning of α-helix 1 (Glu-8, Asp-10, Lys-11, Lys-14, Ala-19) and one in the extreme end of α-helix 3 (Glu-72) that displayed higher flexibility, as indicated by their $\{^1H\}$-^{15}N NOE values of below 0.4 **(Figure 4-12A)**. Interestingly, there were residues in all the three α-helices (Lys-28, Leu-29, Ala-43, Glu-66 and Arg-69) with $\{^1H\}$-^{15}N NOE values of above 0.6. Additionally, residues outside the α-helices displayed $\{^1H\}$-^{15}N NOE values above 0.4, suggesting these regions have flexibility approaching that of a well-structured state.

The ^{15}N backbone relaxation rates (R_1 and R_2) indicated that the α-helices behaved with nearly similar backbone amide dynamics with respect to each other. There is no appreciable difference in the relaxation rates from the beginning to the end of the protein **(Figure 4-12B, C)**. Residues (Arg-51 to Glu-55) in the linker region between α-helix 2 and α-helix 3 showed a uniform

decrease in R_2 and increase in R_1 **(Figures 4-12B, C)**. Interestingly, the penultimate residue of α-helix 1, Ile-37 and the linker residue Lys-57, showed increased R_2 without a corresponding increase in R_1. This suggested chemical exchange on the μs-ms timescale for Ile-37 and Lys-57 **(Figure 4-12B, C)**. Chemical exchange means that these residues can exist in multiple conformations. Excluding these two residues, the relaxation rates remained almost uniform throughout the protein. The gaps in all the datasets refer to the unassigned and overlapping peaks that have been omitted from the analyses.

4.3 Discussion

Despite the critical importance of the role of LcrG in the regulation of Yop secretion (*7, 10, 11*) no atomic structure is available for this small 95 amino acid protein. It has been hypothesized, based on the structure of the self-chaperonin domain of tip proteins IpaD, BipD and SipD, that LcrG forms a coiled coil (*17-20*). However, no experimental studies to validate this hypothesis were carried out. Thus, NMR spectroscopy was used to obtain insight into the three-dimensional structure of LcrG.

4.3.1 LcrG is a partially folded protein

The initial attempt to use full-length LcrG for NMR characterization was not successful because of the non-ideal 2D ^{1}H-^{15}N HSQC spectrum of $LcrG^{FL}$ **(Figure 4-3A)**. This was reasoned to be due to the disordered regions in LcrG. By truncating the flexible tails of LcrG and mutating the single cysteine to serine, the construct $LcrG^{7-73}$ C34S was generated that gave an ideal 2D ^{1}H-^{15}N HSQC spectrum for the NMR studies **(Figure 4-3C)**. This truncated LcrG from residues Asp-7

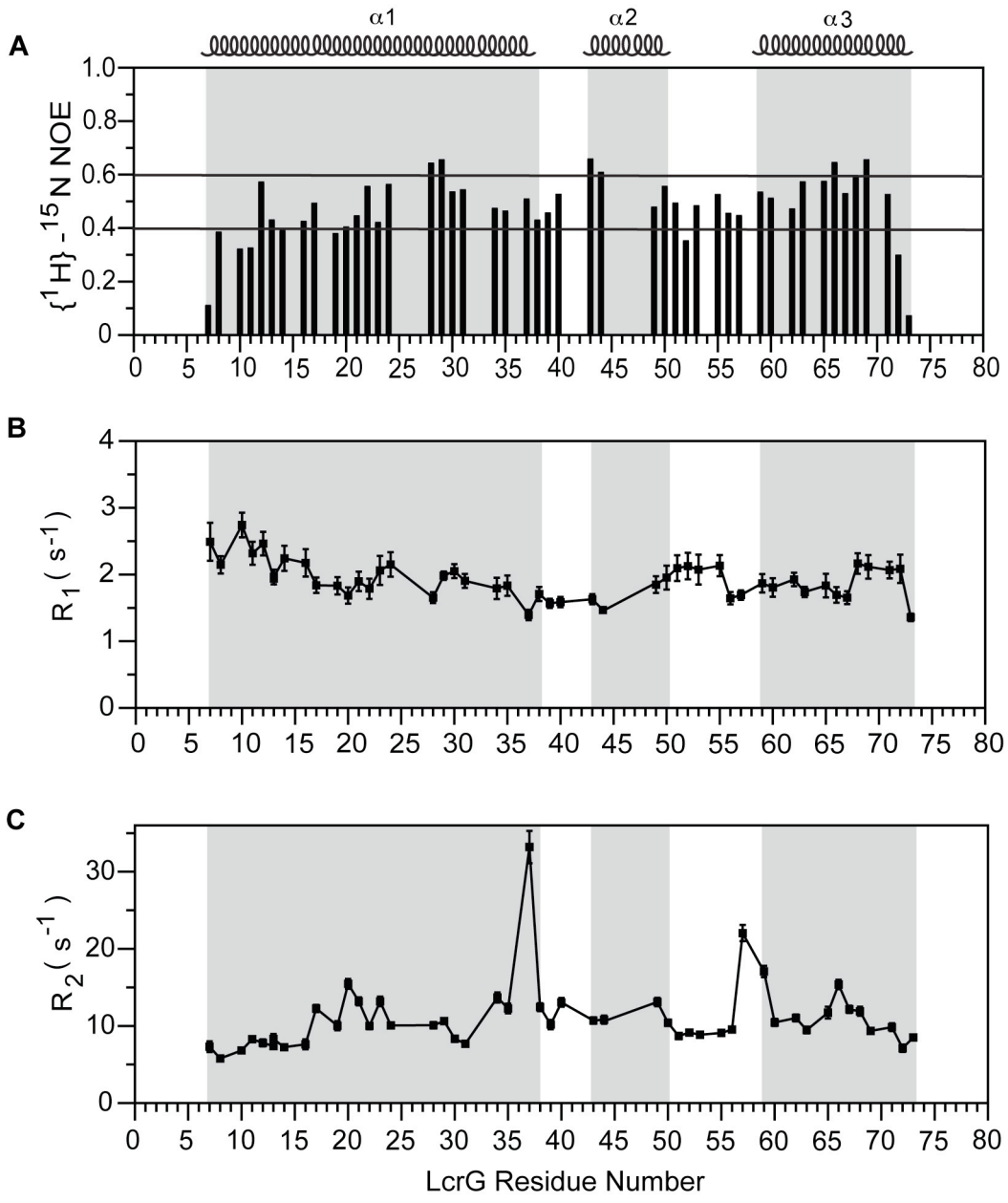

Figure 4-12. **(A)** Heteronuclear $\{^1H\}$-^{15}N NOEs, **(B)** R_1 and **(C)** R_2 relaxation data for $LcrG^{7\text{-}73}$ C34. The helical regions are shaded.

to Arg-73 included the minimum LcrG region (Asp-7 to Thr-40) required for interaction with LcrV (shown in **Figure 4-2A** with a green line) (*23*). Along with CD spectroscopy and thermal denaturation, it was shown that all the four LcrG constructs ($LcrG^{FL}$, $LcrG^{7-73}$, $LcrG^{7-73}$ C34S and $LcrG^{FL}$ C34S) have similar secondary structures and are primarily α-helical **(Figure 4-6)**.

NMR titrations using ^{13}C ILE-LcrV showed that both $LcrG^{FL}$ C34S and $LcrG^{7-73}$ C34S bind to the same surface of LcrV, as the same set of isoleucine residues in LcrV were perturbed on binding to either of the LcrG constructs (Chapter 5, **Figure 5-10**). Thus the truncated LcrG behaved similarly to the full-length LcrG with respect to binding to LcrV. Through a collaboration with Dr. Gregory V. Plano (University of Miami), the use of the C34S mutation was validated by showing that the C34S mutant can function as the wild type LcrG in *Y. pestis* by restoring Ca^{+2} dependent regulation of effector Yop (YopM) **(Figure 4-7)**. Although this single cysteine (shown by an arrow in **Figure 4-2A**) is conserved in the *Yersinia* species, it is not conserved in homologous proteins from other bacterial species **(Figure 4-2A)**. Rather, it is replaced by a tryptophan in the other species **(Figure 4-2A)**. The cysteine is possibly not important in function and hence, mutating it to a similar amino acid like serine helped retain the function of LcrG while preventing the non-specific oligomerization mediated by disulfide bonds.

Based on the observation that $LcrG^{7-73}$ C34S retained wild type secondary structure and the fact that it produced an ideal 2D ^{1}H-^{15}N HSQC spectrum with sharp and well-resolved peaks, we used $LcrG^{7-73}$ C34S for further NMR characterization. The secondary chemical shift mapping (Cα and Cβ) derived from the backbone resonance assignments of $LcrG^{7-73}$ C34S suggested that the secondary structure of LcrG is dominated by three α-helices **(Figure 4-11)**. Characterization of LcrG backbone dynamics by heteronuclear $\{^{1}H\}$-^{15}N NOE suggested that the α-helices

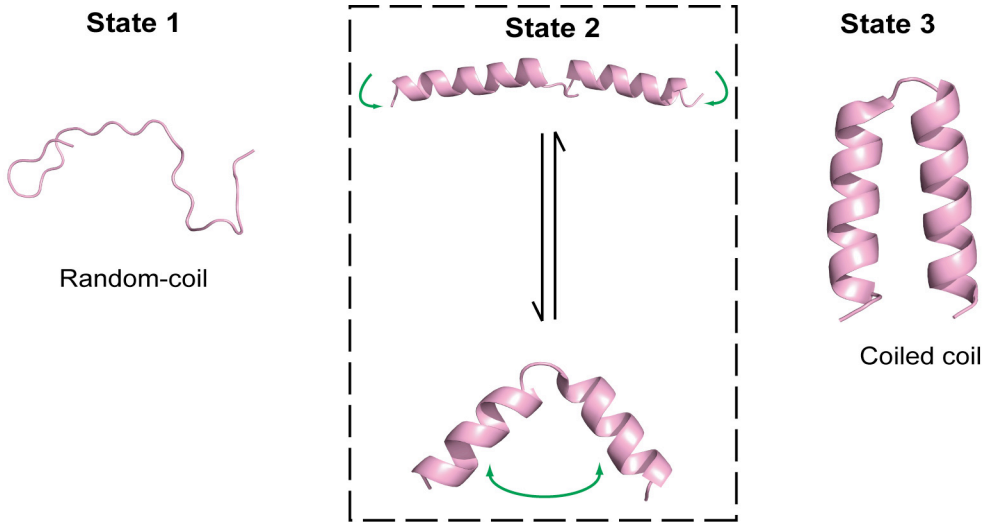

Figure 4-13. A proposed model for the dynamic behavior of LcrG structure. A protein can exist in any of the three states shown above. State 1 is a representation of a random coil conformation, while state 3 represents a typical well-structured 3D conformation adapted by α-helical proteins. LcrG, however most likely is in state 2, i.e. it is a highly α-helical protein but it does not adapt a well-folded tertiary structure like state 3.

display semi-rigid flexibility and do not form well-structured regions. However, there are residues in all the three α-helices with $\{^1H\}$-^{15}N NOE values of above 0.6 **(Figure 4-12A)**, which implies that, although LcrG lacks a well-structured three-dimensional fold, it is not completely disordered and there are residues whose flexibility approach a more stable conformation. The ^{15}N backbone relaxation rates (R_1 and R_2) **(Figure 4-12B, C)** suggested that the α-helices behave with nearly similar backbone amide dynamics and LcrG tumbles as a single unit in solution.

Surprisingly though and contrary to the earlier hypothesis of LcrG being a coiled coil, LcrG was shown to lack a compact tertiary structure. A number of data were used to corroborate this conclusion. First, the 2D ^1H-^{15}N HSQC spectra of the LcrG constructs **(Figure 4-3A, B and C)** displayed a narrow proton chemical shift range (<1 ppm), which suggests that the protein is either highly α-helical or unstructured. Secondly, CD spectroscopy and thermal denaturation showed the absence of a distinct melting temperature, which indicates the lack of a closely packed tertiary fold **(Figure 4-6)**. Thirdly, data indicating a loosely packed helical protein can also be found from the molar ellipticity $\theta_{222/208}$ ratio of 0.7-0.8 (a $\theta_{222/208}$ ratio of 1.0 indicates a well folded helical protein) obtained from the CD spectra. Finally as discussed above, the NMR backbone dynamics data suggested that the helices in LcrG lack a well-structured 3D state, and LcrG tumbles as a single unit in solution.

Thus, our NMR and CD data point towards LcrG being a highly α-helical, yet intrinsically flexible protein lacking a compact tertiary fold **(Figure 4-13)**.

4.3.2 Significance of LcrG as a partially folded protein

The conformational dynamics of LcrG perhaps contribute to its functional versatility, which is a characteristic signature of many flexible proteins (*24, 25*). The conformationally interchangeable nature of intrinsically flexible structures like LcrG ensures easier adaptation of distinct states required for carrying out multiple non-concurrent roles within the cellular environment. Such intrinsically disordered proteins have also been observed among both effectors and structural proteins of the T3SS (*16, 26*).

4.4 References

1. Cornelis, G. R. (2002) The *Yersinia* Ysc-Yop 'type III' weaponry, *Nat Rev Mol Cell Biol 3*, 742-752.
2. Cornelis, G. R. (2002) *Yersinia* type III secretion: send in the effectors, *J. Cell Biol. 158*, 401-408.
3. Cornelis, G. R. (2006) The type III secretion injectisome, *Nat. Rev. Microbiol. 4*, 811-825.
4. Mueller, C. A., Broz, P., Muller, S. A., Ringler, P., Erne-Brand, F., Sorg, I., Kuhn, M., Engel, A., and Cornelis, G. R. (2005) The V-antigen of *Yersinia* forms a distinct structure at the tip of injectisome needles, *Science 310*, 674-676.
5. DeBord, K. L., Lee, V. T., and Schneewind, O. (2001) Roles of LcrG and LcrV during type III targeting of effector Yops by *Yersinia enterocolitica*, *J. Bacteriol. 183*, 4588-4598.
6. Matson, J. S., and Nilles, M. L. (2001) LcrG-LcrV interaction is required for control of Yops secretion in *Yersinia pestis*, *J. Bacteriol. 183*, 5082-5091.

7. Fields, K. A., Nilles, M. L., Cowan, C., and Straley, S. C. (1999) Virulence role of V antigen of Yersinia pestis at the bacterial surface, *Infect.Immun. 67*, 5395-5408.

8. Pettersson, J., Nordfelth, R., Dubinina, E., Bergman, T., Gustafsson, M., Magnusson, K. E., and Wolf-Watz, H. (1996) Modulation of virulence factor expression by pathogen target cell contact, *Science 273*, 1231-1233.

9. Perry, R. D., and Fetherston, J. D. (1997) Yersinia pestis--etiologic agent of plague, *Clin Microbiol Rev 10*, 35-66.

10. Straley, S. C., Plano, G. V., Skrzypek, E., Haddix, P. L., and Fields, K. A. (1993) Regulation by Ca2+ in the Yersinia low-Ca2+ response, *Mol Microbiol 8*, 1005-1010.

11. Skrzypek, E., and Straley, S. C. (1993) LcrG, a secreted protein involved in negative regulation of the low-calcium response in *Yersinia pestis*, *J. Bact. 175*, 3520-3528.

12. Hamad, M. A., and Nilles, M. L. (2007) Roles of YopN, LcrG and LcrV in controlling Yops secretion by *Yersinia pestis*, *Adv. Exp. Med. Biol. 603*, 225-234.

13. Lee, P. C., Stopford, C. M., Svenson, A. G., and Rietsch, A. (2010) Control of effector export by the Pseudomonas aeruginosa type III secretion proteins PcrG and PcrV, *Mol. Microbiol. 75*, 924-941.

14. Sun, P., Tropea, J. E., Austin, B. P., Cherry, S., and Waugh, D. S. (2008) Structural Characterization of the Yersinia pestis Type III Secretion System Needle Protein YscF in Complex with Its Heterodimeric Chaperone YscE/YscG, *J. Mol. Biol. 377*, 819-830.

15. Schreiner, M., and Niemann, H. H. (2012) Crystal structure of the Yersinia enterocolitica type III secretion chaperone SycD in complex with a peptide of the minor translocator YopD, *BMC Struct Biol 12*, 13.

16. Rodgers, L., Gamez, A., Riek, R., and Ghosh, P. (2008) The type III secretion chaperone SycE promotes a localized disorder-to-order transition in the natively unfolded effector YopE, *J. Biol. Chem. 283*, 20857-20863.

17. Johnson, S., Roversi, P., Espina, M., Olive, A., Deane, J. E., Birket, S., Field, T., Picking, W. D., Blocker, A. J., Galyov, E. E., Picking, W. L., and Lea, S. M. (2007) Self-chaperoning of the type III secretion system needle tip proteins IpaD and BipD, *J. Biol. Chem. 282*, 4035-4044.

18. Chatterjee, S., Zhong, D., Nordhues, B. A., Battaile, K. P., Lovell, S. W., and De Guzman, R. N. (2011) The Crystal Structure of the Salmonella Type III Secretion System Tip Protein SipD in Complex with Deoxycholate and Chenodeoxycholate, *Protein Sci. 20*, 75-86.

19. Erskine, P. T., Knight, M. J., Ruaux, A., Mikolajek, H., Wong Fat Sang, N., Withers, J., Gill, R., Wood, S. P., Wood, M., Fox, G. C., and Cooper, J. B. (2006) High Resolution Structure of BipD: An Invasion Protein Associated with the Type III Secretion System of *Burkholderia pseudomallei*, *J. Mol. Biol. 363*, 125-136.

20. Blocker, A. J., Deane, J. E., Veenendaal, A. K., Roversi, P., Hodgkinson, J. L., Johnson, S., and Lea, S. M. (2008) What's the point of the type III secretion system needle?, *Proc. Natl. Acad. Sci. U.S.A. 105*, 6507-6513.

21. McGuffin, L. J., Bryson, K., and Jones, D. T. (2000) The PSIPRED protein structure prediction server, *Bioinformatics 16*, 404-405.

22. Thompson, J. D., Higgins, D. G., and Gibson, T. J. (1994) CLUSTAL W: improving the sensitivity of progressive multiple sequence alignment through sequence weighting,

position-specific gap penalties and weight matrix choice, *Nucleic Acids Res 22*, 4673-4680.

23. Matson, J. S., and Nilles, M. L. (2002) Interaction of the *Yersinia pestis* type III regulatory proteins LcrG and LcrV occurs at a hydrophobic interface, *BMC Microbiol. 2*, 16.

24. Babu, M. M., van der Lee, R., de Groot, N. S., and Gsponer, J. (2011) Intrinsically disordered proteins: regulation and disease, *Curr Opin Struct Biol 21*, 432-440.

25. Wright, P. E., and Dyson, H. J. (2009) Linking folding and binding, *Curr Opin Struct Biol 19*, 31-38.

26. Zhong, D., Lefebre, M., Kaur, K., McDowell, M. A., Gdowski, C., Jo, S., Wang, Y., Benedict, S. H., Lea, S. M., Galan, J. E., and De Guzman, R. N. (2012) The *Salmonella* Type III Secretion System Inner Rod Protein PrgJ Is Partially Folded, *J. Biol. Chem. 287*, 25303-25311.

CHAPTER 5: Characterization of the interaction between *Yersinia pestis* tip protein LcrV and the chaperone LcrG

5.1 Introduction

The LcrV tip protein of the *Yersinia pestis* type III secretion system (T3SS) forms a stable complex with the chaperone LcrG (*1-6*). This LcrG-LcrV complex plays an important role in the regulation of Yop secretion (*1-3, 7*). The current model that explains the regulation of Yop secretion by LcrG and LcrV is the "Titration" model **(Figure 1-3** in chapter 1) proposed by Nilles and coworkers (*1-3*). According to this model, in the absence of host cell contact or in the presence of Ca^{+2}, LcrG plugs the T3SS from the cytoplasmic face and prevents the secretion of Yops. Upon host cell contact or in the absence of Ca^{+2}, there is an upregulation of the expression of LcrV, which then titrates away LcrG by forming a stable LcrG-LcrV complex. This relieves the negative block thereby allowing the secretion of Yops. Thus, if LcrG-LcrV interaction is blocked, LcrG cannot be titrated away from the T3SS. This would result in a constitutive blockage of secretion of Yops regardless of host cell contact or Ca^{+2} concentration.

Direct binding between LcrG and LcrV has been demonstrated previously (*1-6*), and the results of yeast two-hybrid assays indicate that the N-terminus of LcrG is involved in the interaction with LcrV (*3*). Lawton *et al.* (*4*) further demonstrated that LcrG and LcrV form a tight complex as indicated by their nanomolar binding affinity (K_d = 140 nM by SPR). The coiled coil domain of LcrV has been shown to be the site of protein-protein interaction with LcrG (*4, 5*). However, the atomic detail of this interaction is not well understood. Since the LcrG-LcrV complex was not amenable to crystallization (Chapter 2), a primary objective of this research was to use NMR

spectroscopy to elucidate the details of the protein-protein interaction of the LcrG-LcrV complex.

Here, the direct interaction between LcrG and LcrV was confirmed by size exclusion chromatography (SEC). Further, the results of NMR experiments suggested that protein-protein interaction between LcrG and LcrV caused a global effect on the structure of LcrG and spans almost its entire length as opposed to local perturbations in the N-terminal region only. The C-terminus of LcrG (Ser-52 to Ile-67) was identified to be important in blocking the secretion of Yop effectors. It has also been confirmed by NMR Spectroscopy that the coiled coil domain of LcrV is perturbed on binding to LcrG.

5.2 Results

5.2.1 Size exclusion chromatography of the LcrG$^{7-73}$ C34S-LcrV complex

Purified LcrV, LcrG$^{7-73}$ C34S, and the LcrG$^{7-73}$ C34S- LcrV complex (formed by mixing the two proteins in a 1:1.2 molar ratio) were separately loaded and run through a Superdex 75 size exclusion column (SEC) column (described in section 2.6). Purified LcrV eluted from the SEC at 140 ml. Purified LcrG$^{7-73}$ C34S eluted at 164 ml. The eluted LcrV corresponded to an approximate molecular weight of 43 kDa (the actual molecular weight of LcrV is 34kDa), based on the marker proteins used for calibration of the SEC column. LcrG$^{7-73}$ C34S corresponded to an approximate molecular weight of 22 kDa. Notably, the molecular weight of LcrG$^{7-73}$ C34S is 8 kDa, which is consistent with its migration in SDS-PAGE **(Figure 5-1B)**. This is approximately one-third the molecular weight (22 kDa) at which it eluted from the SEC column. The LcrG$^{7-73}$ C34S and LcrV complex co-eluted from the size exclusion column at 136 ml **(Figure 5-1)**. This corresponded to an approximate molecular weight of 47.8 kDa for the

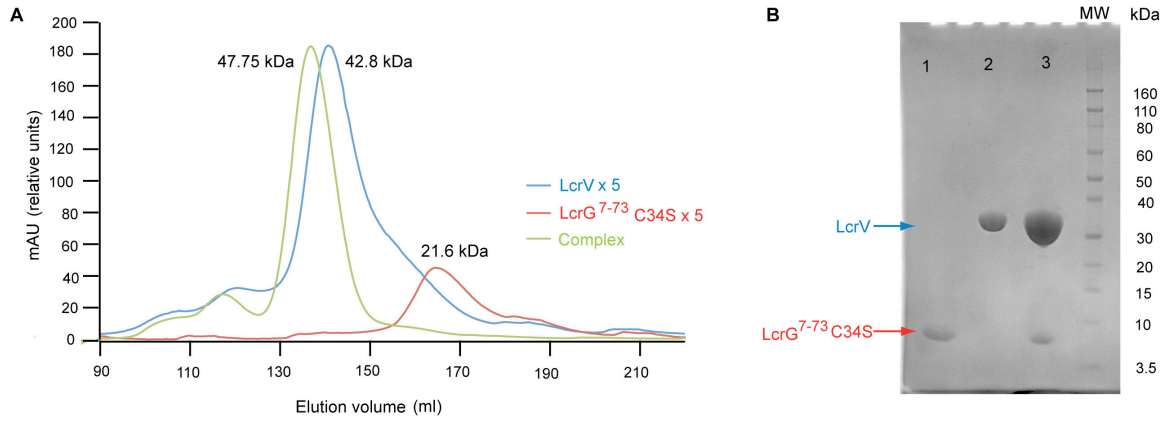

Figure 5-1. Size exclusion chromatography (SEC) showing **(A)** the elution profiles of LcrV in blue, LcrG$^{7-73}$ C34S in red and the complex (LcrG$^{7-73}$ C34S- LcrV mixed in a 1:1.2 molar ratio) in green. The mAU readings for LcrV and LcrG$^{7-73}$ C34S were multiplied five times to adjust the scale. **(B)** The migration pattern of the peak fractions from SEC were analyzed by SDS-PAGE. Lane 1 corresponds to LcrG$^{7-73}$ C34S (red arrow), lane 2 corresponds to LcrV (blue arrow), and lane 3 corresponds to the complex. The trimeric nature of LcrG$^{7-73}$ C34S seen in the SEC column (run at 4 °C) is not evident in the denaturing gel (SDS-PAGE), but a Native-PAGE would possibly have resolved this.

complex, which is roughly equal to the molecular weight of an LcrG-LcrV heterodimer (the predicted molecular weight of the heterodimer is 43 kDa). **Figure 5-1** shows the migration of peak fractions in SEC of LcrV, $LcrG^{7-73}$ C34S, and the $LcrG^{7-73}$ C34S- LcrV complex as well as the SDS-PAGE gel of the proteins.

5.2.2 NMR titrations using ^{15}N $LcrG^{7-73}$ C34S

NMR chemical shift mapping was used to characterize the interaction between LcrV and LcrG. ^{15}N $LcrG^{7-73}$ C34S was titrated with unlabeled LcrV at molar ratios of 0.0, 0.5, 1.2, 2, 3, 4 and 6.5. Two-dimensional ^{1}H-^{15}N HSQC (*8*) spectra were acquired for each titration point and they were overlayed to monitor the changes in the HSQC spectra of ^{15}N $LcrG^{7-73}$ C34S upon binding to LcrV **(Figure 5-2)**. Majority of the residues of LcrG showed significant reduction in peak intensities with increasing molar ratios of LcrV **(Figure 5-2)**. The progressive reduction in peak intensities upon complex formation is the intermediate exchange time scale. Additionally, some of the residues of LcrG appeared as new peaks (marked with asterisks in **Figure 5-2**) in the 2D ^{1}H-^{15}N HSQC spectrum of ^{15}N $LcrG^{7-73}$ C34S upon complex formation. The appearance of new peaks in the LcrG spectrum upon complex formation indicated that the interaction is in the slow exchange NMR time scale. Slow exchange means tight binding and intermediate exchange means weaker binding.

In order to identify the residues of LcrG that appeared as new peaks, three-dimensional NMR datasets were acquired on the $^{15}N/^{13}C$ $LcrG^{7-73}$ C34S-LcrV complex in a 1:1.2 molar ratio. Residues Ser-52 to Arg-73 (except Arg-61) of LcrG appeared as new peaks upon complex formation and the rest of the protein (Asp-7 to Arg-51) showed significant reduction in peak

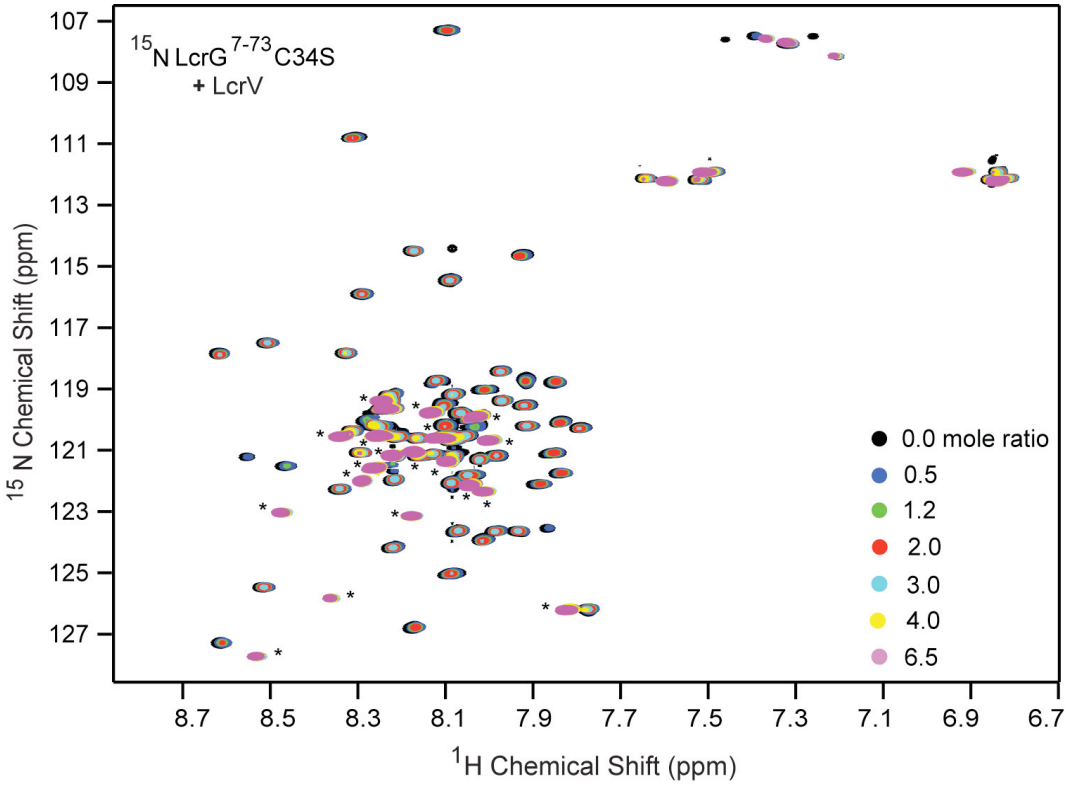

Figure 5-2. Seven overlaid 2D ^{1}H-^{15}N HSQC spectra of LcrG$^{7-73}$ C34S with increasing molar ratios of LcrV. Backbone amide peaks that appeared in new positions on complex formation are marked with asterisks. The rest of the backbone amide peaks showed significant reduction in peak intensities.

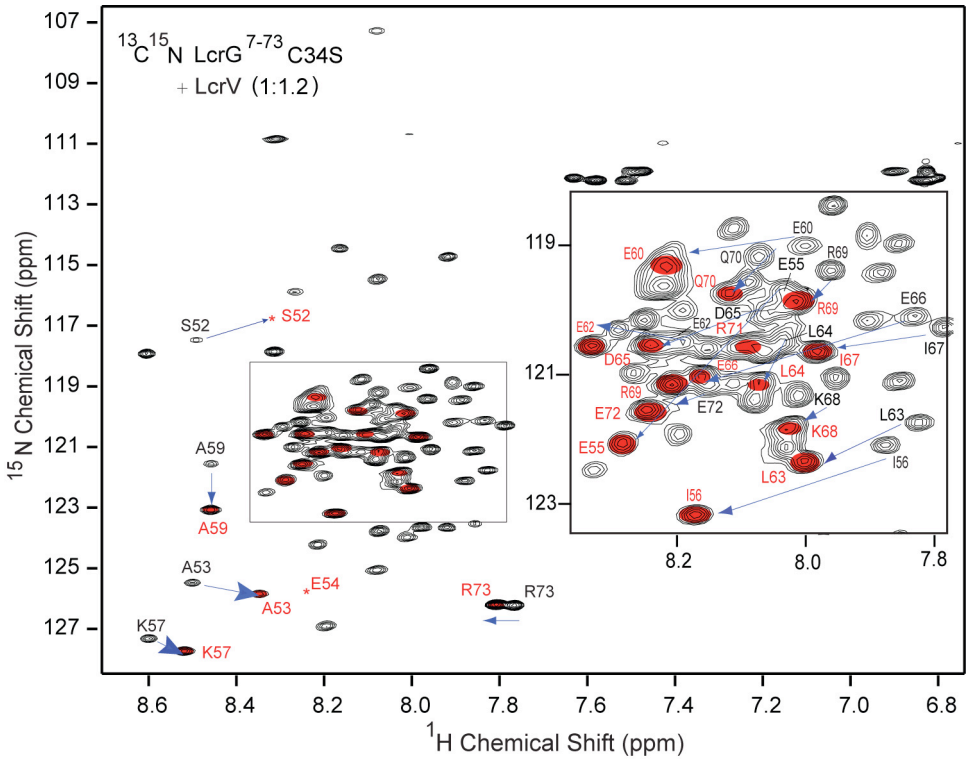

Figure 5-3. Assigned 2D ^{1}H-^{15}N HSQC spectrum of the $LcrG^{7-73}$ C34S- LcrV complex. Backbone amide peaks of residues Ser-52 to Arg-73 appeared in new positions upon complex formation. The original peak positions of these residues are indicated. Blue arrows point to the new peak positions (shown in red), whose names are also indicated. The red asterisks indicate the new complex peaks (S52 and E54) whose intensities were low, and do not appear on the contour level of the spectrum shown.

intensities. The assigned 2D ^{1}H-^{15}N HSQC spectrum of the complex **(Figure 5-3)** shows the assignments of the backbone resonances of the residues of LcrG that appeared in new positions. For R73 was the original position and R73 (colored red) was the new position of the residue Arg-73. A blue arrow is used to indicate the change in position of the peaks. The residue Arg-69 appeared in two new positions indicated in red as Arg-69. The rest of the residues of LcrG are not marked in this figure as they remained in the same position as the free protein shown in **Figure 4-7** (Chapter 4).

To test if the flexible tails of LcrG would be important in binding to LcrV, ^{15}N $LcrG^{FL}$ C34S was titrated with increasing amounts of unlabeled LcrV in molar ratios of 0.0, 0.25, 0.5, 1.0 and 2. Several peaks of $LcrG^{FL}$ C34S showed a significant reduction in peak intensities on complex formation with LcrV **(**indicated with arrows in **Figure 5-4)**. But this data was not consistent with the titration data using the truncated construct, ^{15}N $LcrG^{7-73}$ C34S. The attempt to assign the backbone resonances of $LcrG^{FL}$ C34S was not successful as seen in Chapter 4 **(Figure 4-5)**. This hindered any further work with the labeled $LcrG^{FL}$ C34S construct. It was reasoned that owing to the flexibility of the tails and the conformational heterogeneity **(Figure 4-5)** arising from the cis-trans isomerization of the prolines present at the C-terminal end of LcrG, led to the inconsistent results.

5.2.3 NMR titrations using ^{13}C ILV-$LcrG^{7-73}$ C34S

In addition to the traditional ^{15}N backbone labeling, ^{13}C methyl labeling of the side chains of isoleucines, leucine, and valine (ILV) of $LcrG^{7-73}$ C34S were also used. The advantages of ^{13}C methyl labeling of ILV are threefold. Firstly, this reduces the complexity of the spectra making

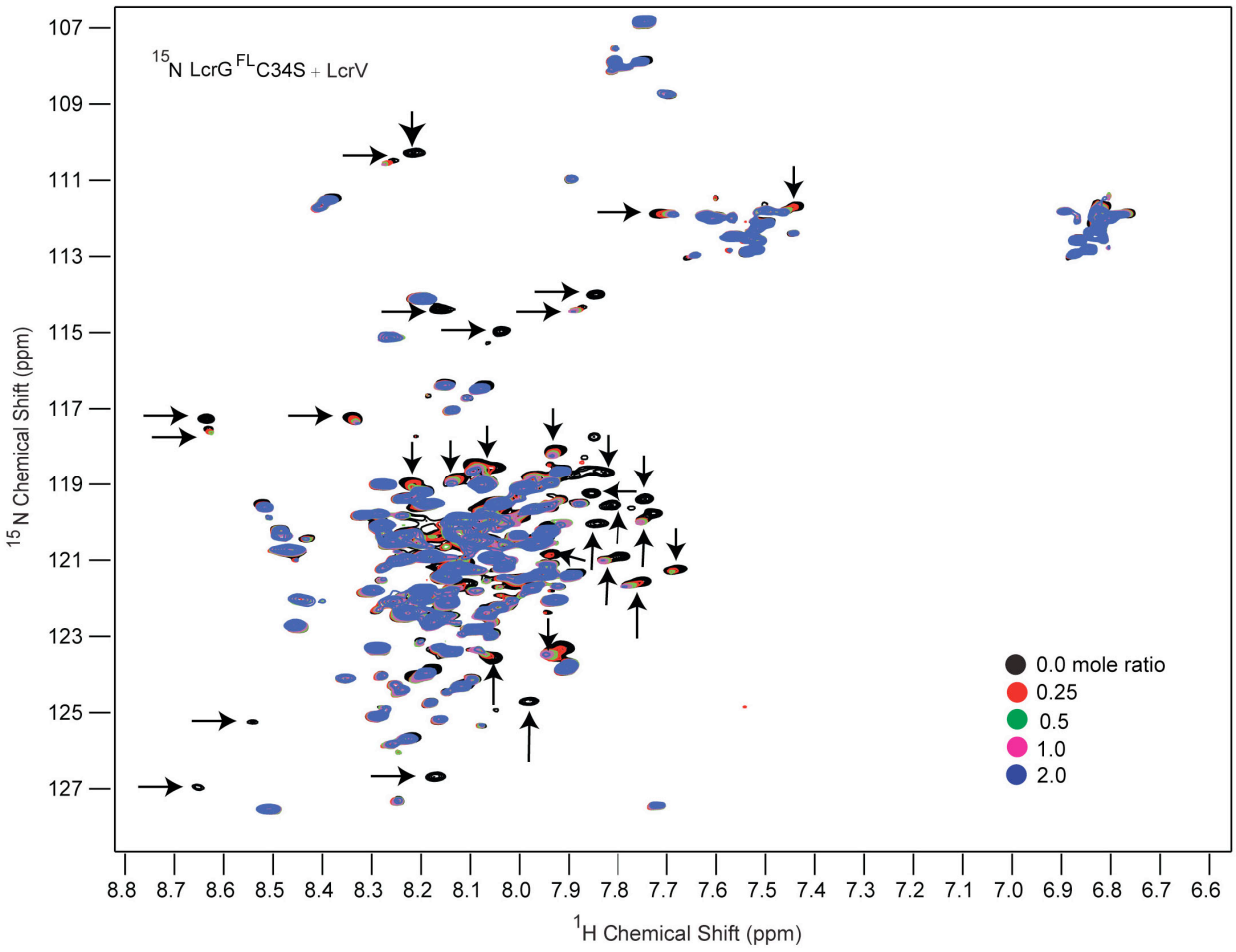

Figure 5-4. Five overlaid 2D ^{1}H-^{15}N HSQC spectra of $LcrG^{FL}$ C34S with increasing molar ratios of LcrV. Backbone amide peaks that showed significant reduction in peak intensities are marked with arrows.

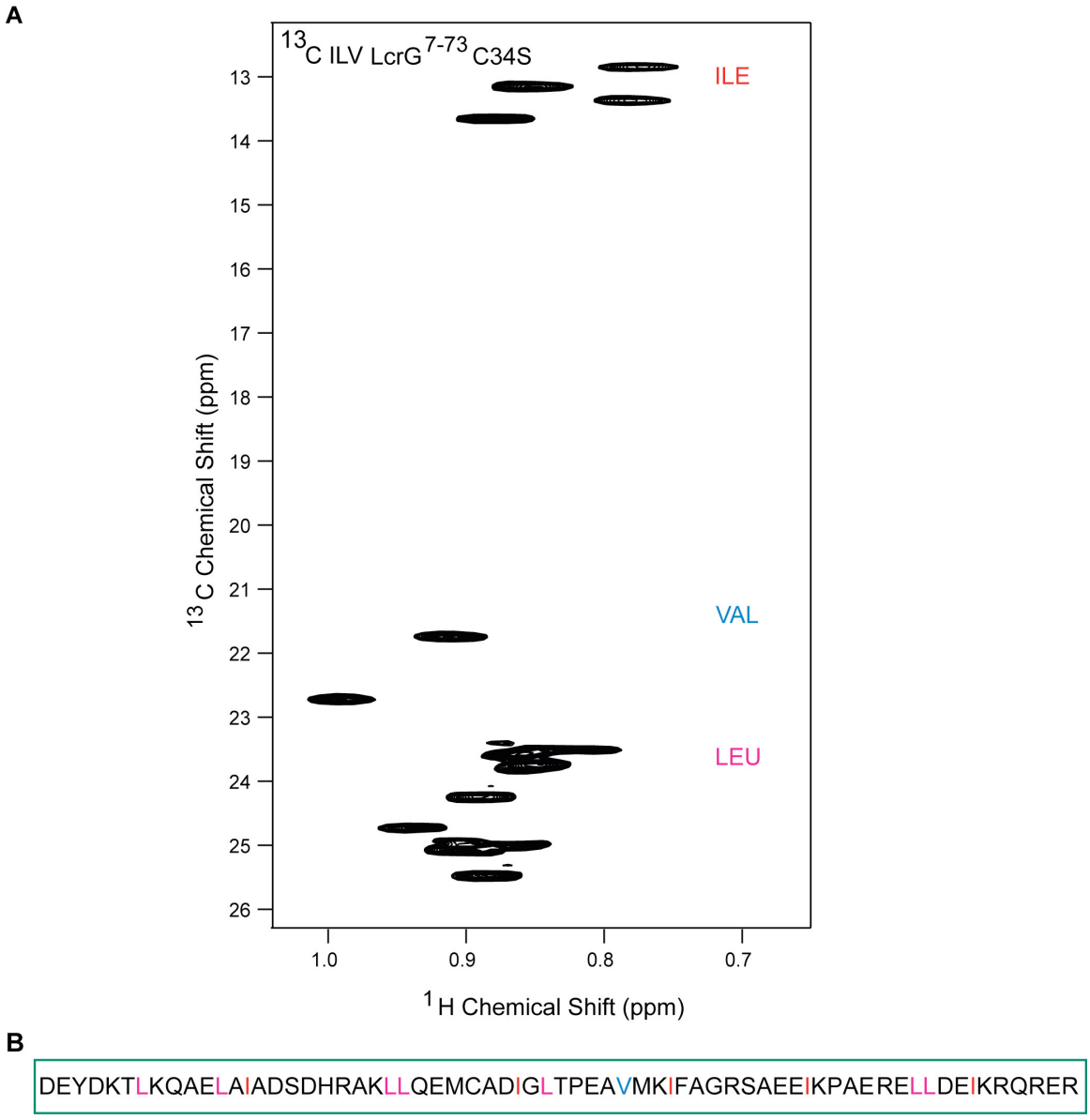

Figure 5-5. **(A)** 2D ^{1}H-^{13}C HSQC spectrum of ^{13}C ILV-LcrG$^{7-73}$ C34S where the positions of the ^{13}C methyl groups of Ile, Leu and Val are indicated. **(B)** Amino acid sequence of LcrG$^{7-73}$ C34S showing the distribution of Ile (red), Leu (pink), and Val (blue).

analysis more amenable. Secondly, the ^{13}C methyl specific probes are more sensitive, as there are three protons in CH_3 as opposed to one proton in NH. Thirdly, the ILVs are well distributed along LcrG **(Figure 5-5B)**, and since hydrophobic interaction is an important component of protein-protein interactions, mapping the effects on ^{13}C-methyl labeled ILV will identify the binding interface. The methyl resonances of Ile, Leu, and Val of $LcrG^{7-73}$ C34S are indicated in the 2D ^{1}H-^{13}C HSQC spectrum of ^{13}C ILV-$LcrG^{7-73}$ C34S **(Figure 5-5A)**. The ^{13}C methyl resonances of Ile and Val of ^{13}C ILV-$LcrG^{7-73}$ C34S were assigned by mutagenesis. The isoleucines (Ile-20, Ile-37, Ile-47, Ile-56 and Ile-67) and valine (Val-44) of LcrG were serially mutated to alanine, and 2D ^{1}H-^{13}C HSQC spectra were acquired for each mutant. The 2D ^{1}H-^{13}C HSQC spectrum of each mutant was superimposed with the spectrum of the wild type protein to identify the peak that had disappeared **(Figure 5-6)**. For example in **Figure 5-6A**, it can be clearly seen that a peak disappeared (shown by an arrow) upon superimposition of the two HSQC spectra (^{13}C ILE-$LcrG^{7-73}$ C34S in black and ^{13}C ILE-$LcrG^{7-73}$ C34S I37A in red) thus identifying that peak as belonging to Ile-37. With this approach, the ^{13}C methyl side chains of all five isoleucines and one valine residue were assigned **(Figure 5-6)**. The methyl side chains of Ile-20 and Ile-67 were overlapped **(Figure 5-6)**. However, this approach of mutagenesis is not amenable for assigning the methyl resonances of leucine because of the significant number of overlapping peaks. Nevertheless, Ile and Val assignments were used to identify the residues of LcrG that were perturbed upon binding to LcrV.

NMR titrations were performed using purified ^{13}C ILV-$LcrG^{7-73}$ C34S mixed with increasing amounts of unlabeled LcrV. Two-dimensional ^{1}H-^{13}C HSQC spectra were acquired at each LcrG:LcrV molar ratios (0.0, 0.25, 0.5, 1.0 and 2.0) and the spectra were overlayed **(Figure 5-7)** to monitor the changes in the HSQC spectra of ^{13}C ILV-$LcrG^{7-73}$ C34S upon binding to LcrV.

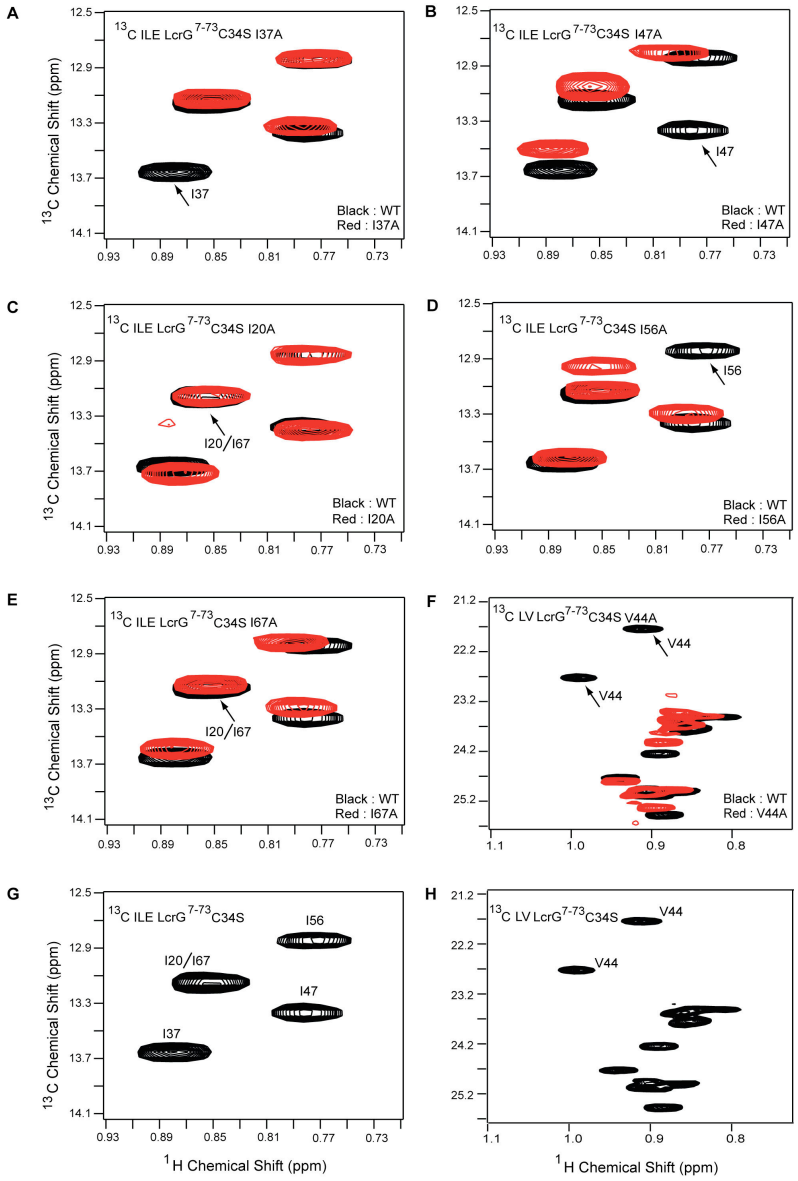

Figure 5-6. Overlaid 2D ^{1}H-^{13}C HSQC spectra of ^{13}C ILE-LcrG$^{7-73}$ C34S (WT) in black with **(A)** I37A in red **(B)** I47A in red **(C)** I20A in red **(D)** I56A in red **(E)** I67A in red. Overlaid 2D spectrum of ^{13}C LV (leucine and valine) LcrG$^{7-73}$ C34S (WT) in black with **(F)** V44A in red. **(G)** 2D ^{1}H-^{13}C HSQC spectrum of ^{13}C ILE-LcrG$^{7-73}$ C34S showing all the assigned isoleucines, with the residue names next to the corresponding peaks. **(H)** 2D ^{1}H-^{13}C HSQC spectrum of ^{13}C LV-LcrG$^{7-73}$ C34S showing the assigned valine residue.

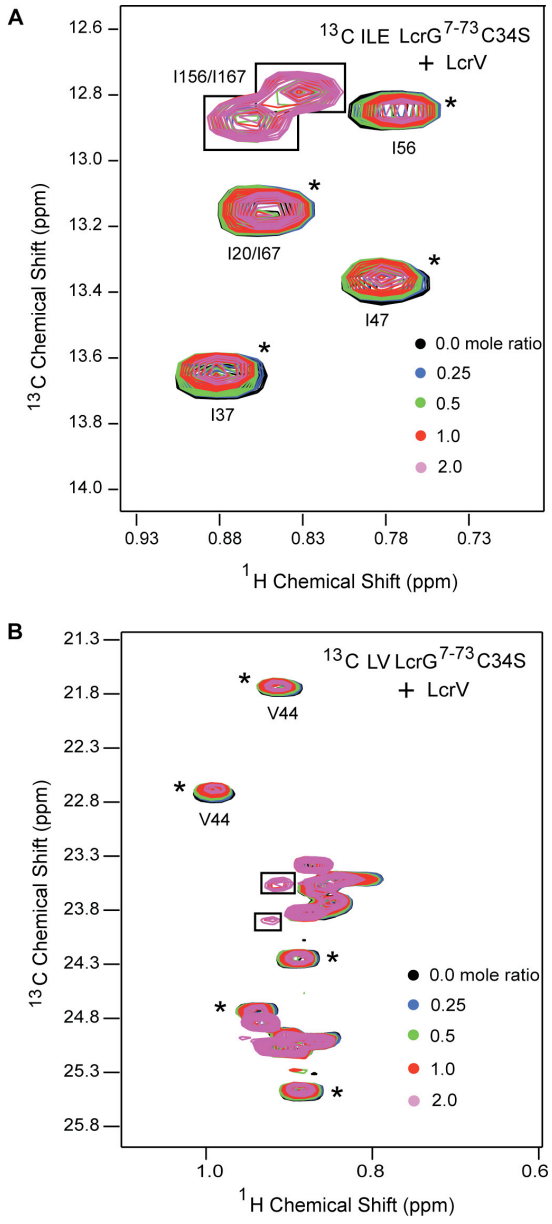

Figure 5-7. Five overlaid 2D ^{1}H-^{13}C HSQC spectra of **(A)** ^{13}C ILE-LcrG$^{7-73}$ C34S (isoleucine spectrum) and **(B)** ^{13}C LV-LcrG$^{7-73}$ C34S (leucine and valine spectrum) with increasing molar ratios of LcrV. Residues that showed reduction in peak intensities are indicated with asterisks. Peaks that appeared in new positions on complex formation are shown in boxes. The names of the isoleucines and valine residues are indicated next to their corresponding peaks.

All the five isoleucines (Ile-20, Ile-37, Ile-47, Ile-56 and Ile-67) and one valine (Val-44) showed reduction in peak intensities **(Figure 5-7)** upon complex formation with LcrV. Additionally, new peaks appeared in the Ile methyl region which, according to the ^{15}N titration data (discussed in section 5.2.2), was expected to lie in the region of residues Ser-52 to Arg-73. Two isoleucine residues, Ile-56 and Ile-67, were present in this region. Therefore, the two new peaks that appeared upon complex formation in the ^{13}C ILE-LcrG$^{7-73}$ C34S spectrum may possibly belong to Ile-56 and Ile-67. The complex peaks are labeled as Ile-156/Ile-167 in **Figure 5-7A**.

5.2.4 Mutational analysis of the Ser-52 to Arg-73 region of LcrG in Yersinia pestis

Based on the observation from the NMR titration experiments that residues from Ser-52 to Arg-73 of LcrG were perturbed upon complex formation with LcrV, a "Yop secretion assay" was used to evaluate the functional significance of this region in *Y. pestis*. This work was done in collaboration with Dr. Gregory V. Plano (University of Miami). Several point mutants and deletion mutants of LcrG were constructed in this region. These mutants were introduced in the pBAD vector in LcrG C34S background and expressed in *Y. pestis*. The ability of these mutants to control secretion of the effector protein YopM was tested by the *Yersinia* Yop secretion assay described in section 2.4. Four mini deletion mutants (Δ52-57, Δ58-62, Δ63-67 and Δ68-73) and a mutant with a deletion of the entire region (Δ52-73) were constructed. In addition to these deletion mutants, nine point mutants (I56N, K57E, K57L, R61E, R61L, I67N, K68E, K68L and L63N) were also constructed. The details of the mutants can be found in **Table 2**.

Based on the helical nature of the C-terminus of LcrG from the NMR secondary chemical shifts (**Figure 4-10** in Chapter 4), a helical wheel of the region Ser-52 to Arg-73 was done. The helical wheel of Ser-52 to Arg-73 **(Figure 5-8)** showed that residues Ile-56, Leu-63 and Ile-67 of LcrG

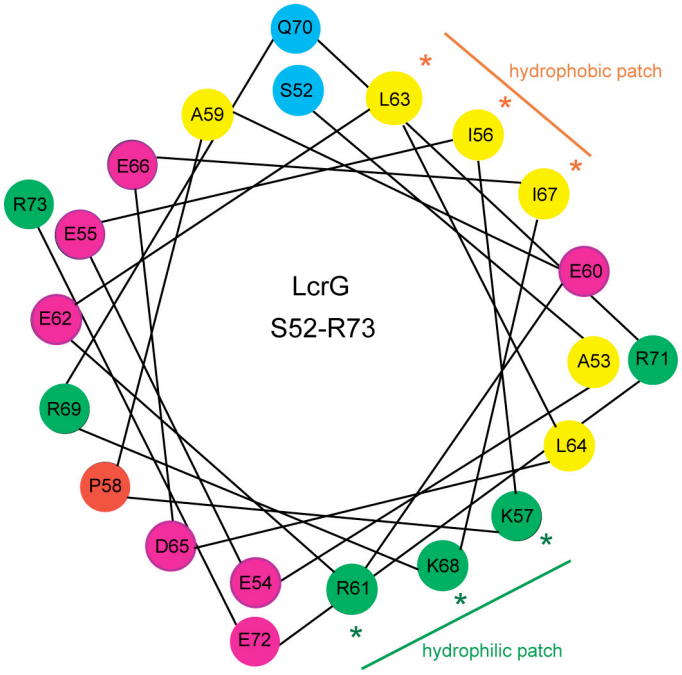

Figure 5-8. Helical wheel projection of the region Ser-52 to Arg-73 in LcrG. The hydrophobic residues are in yellow, the uncharged polar residues are in blue, the positively and the negatively charged polar residues are in green and pink respectively, and proline is in red. The orange asterisks indicate a hydrophobic patch and the green asterisks indicate a polar patch. These residues indicated with asterisks were chosen for mutation

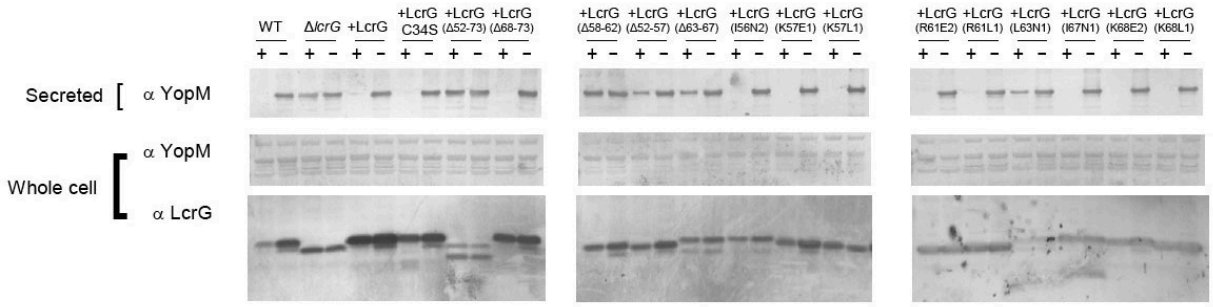

Figure 5-9. Mutational analysis of the Ser-52 to Arg-73 region of LcrG in *Y. pestis.* All the point mutants (except LcrG L63N) and one deletion mutant Δ68-73 behaved as wild type LcrG. The point mutant LcrG L63N and the deletion mutants Δ52-73, Δ52-57, Δ58-62 and Δ63-67 were defective in secretion blocking activity of LcrG and hence constitutively secreted YopM both in the presence and absence of Ca^{+2}. The Δ*lcrG* represents a non-functional deletion mutant of LcrG (Δ39-54), and hence the lower bands are seen in the whole cell blot of Δ*lcrG*. All the mutants, except Δ52-73 and L63N showed normal expression of LcrG.

Table 2. List of the point mutants and the deletion mutants of the region Ser-52 to Arg-73 in LcrG, along with the rationale for creating them. Results of the Yop secretion assay are also shown.

Point Mutants	Rationale	Effect on secretion of the effector YopM
1. L63N	Non-polar to polar	Defective. Constitutively secreted YopM in presence and absence of Ca^{+2}.
2. I56N	Non-polar to polar	Behaved as wild type. Secretion of YopM only in the absence of Ca^{+2}.
3. I67N	Non-polar to polar	Behaved as wild type. Secretion of YopM only in the absence of Ca^{+2}.
4. K57E	Charge reversal	Behaved as wild type. Secretion of YopM only in the absence of Ca^{+2}.
5. K57L	Polar to non-polar	Behaved as wild type. Secretion of YopM only in the absence of Ca^{+2}.
6. K68E	Charge reversal	Behaved as wild type. Secretion of YopM only in the absence of Ca^{+2}.
7. K68L	Polar to non-polar	Behaved as wild type. Secretion of YopM only in the absence of Ca^{+2}.
8. R61E	Charge reversal	Behaved as wild type. Secretion of YopM only in the absence of Ca^{+2}.
9. R61L	Polar to non-polar	Behaved as wild type. Secretion of YopM only in the absence of Ca^{+2}.
Deletion mutants		
Δ52-73		Defective. Constitutively secreted YopM in presence and absence of Ca^{+2}.
Δ52-57		Defective. Constitutively secreted YopM in presence and absence of Ca^{+2}.
Δ58-62		Defective. Constitutively secreted YopM in presence and absence of Ca^{+2}.
Δ63-67		Defective. Constitutively secreted YopM in presence and absence of Ca^{+2}.
Δ68-73		Behaved as wild type. Secretion of YopM only in the absence of Ca^{+2}.

formed a hydrophobic patch, and residues Lys-57, Arg-61 and Lys-68 formed a hydrophilic patch. The hydrophobic and the charged nature of these residues were conserved among all the homologous species **(Figure 4-2A** in Chapter 4**)**. The mutations were designed to alter a hydrophobic amino acid to a polar amino acid, a charged amino acid to its opposite charge, and to a hydrophobic amino acid **(Table 2)**. Results of the Yop secretion assay show that the deletion mutants, Δ52-73, Δ52-57, Δ58-62, and Δ63-67 were all defective in LcrG dependent regulation of YopM secretion, and hence they constitutively secreted YopM both in the presence and absence of Ca^{+2} **(Figure 5-9)**. However, the deletion mutant, Δ68-73 behaved as wild type and secreted YopM only in the absence of Ca^{+2} **(Figure 5-9)**. Similarly, all the point mutants except L63N behaved as wild type. The mutant L63N showed a defect in LcrG dependent regulation of YopM secretion, and hence constitutively secreted YopM **(Figure 5-9)**. The results of the Yop secretion assay are summarized in **Table 2**. The levels of YopM and LcrG in the whole cells were analyzed in all the constructs by blotting with antibodies. Except for the LcrG Δ52-73 and L63N mutants, all the mutants showed normal expression of LcrG.

5.2.5 NMR Titration using ^{13}C ILE-LcrV

To confirm whether the coiled coil domain of LcrV was involved in the interaction with LcrG, NMR titrations were carried out using labeled tip protein, LcrV combined with increasing amounts of unlabeled chaperone, $LcrG^{7-73}$ C34S. The positions of the methyl groups of Ile, Leu and Val of LcrV are indicated in the 2D ^{1}H-^{13}C HSQC spectrum of ^{13}C ILV-LcrV **(Figure 5-10A)**. The Ile, Leu, and Val are very well distributed along the structure of LcrV **(Figure 5-10B)**. Since the methyl groups of Ile (shown as red spheres in **Figure 5-10B**) are also well distributed along the structure of LcrV, ^{13}C ILE-LcrV was used for the NMR titrations. 2D ^{1}H-^{13}C HSQC spectra were acquired for each LcrV:LcrG molar ratio (0.0, 0.25, 0.5, 1.0 and 2.0) and

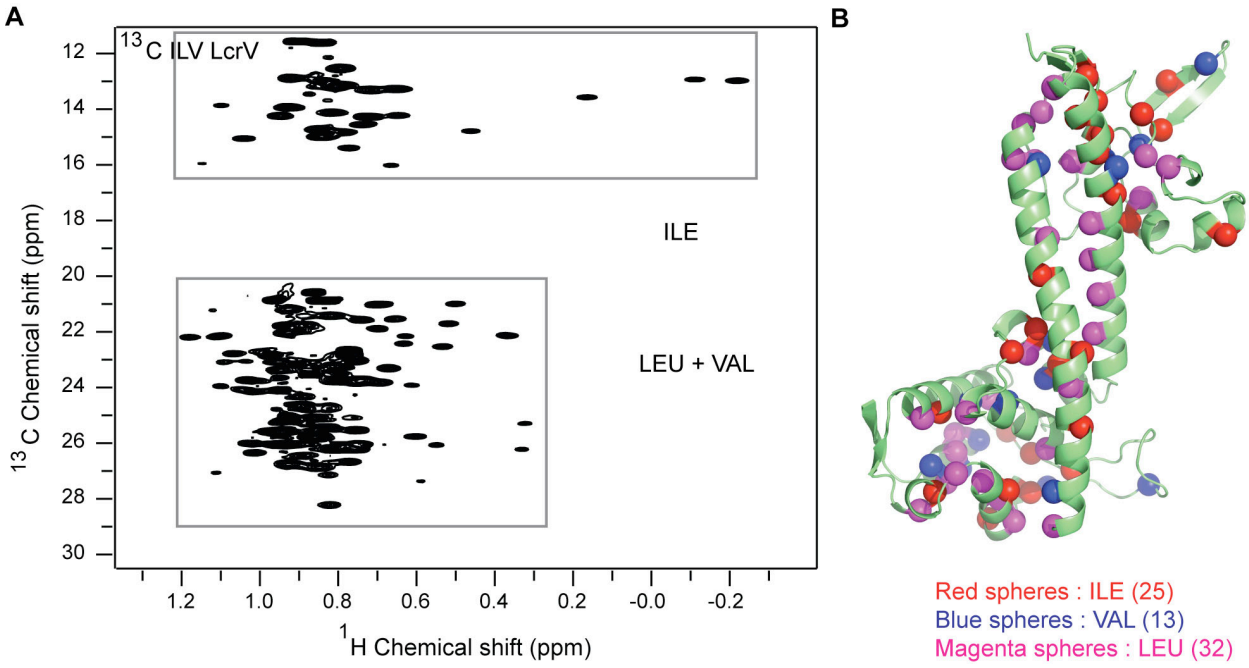

Figure 5-10. **(A)** Two-dimensional ^{1}H-^{13}C HSQC spectrum of LcrV where the positions of the ^{13}C methyl groups of Ile, Leu and Val are boxed. **(B)** Structure of LcrV showing the distribution of Ile (red), Val (blue) and Leu (Magenta). The number of ILVs in the structure are indicated.

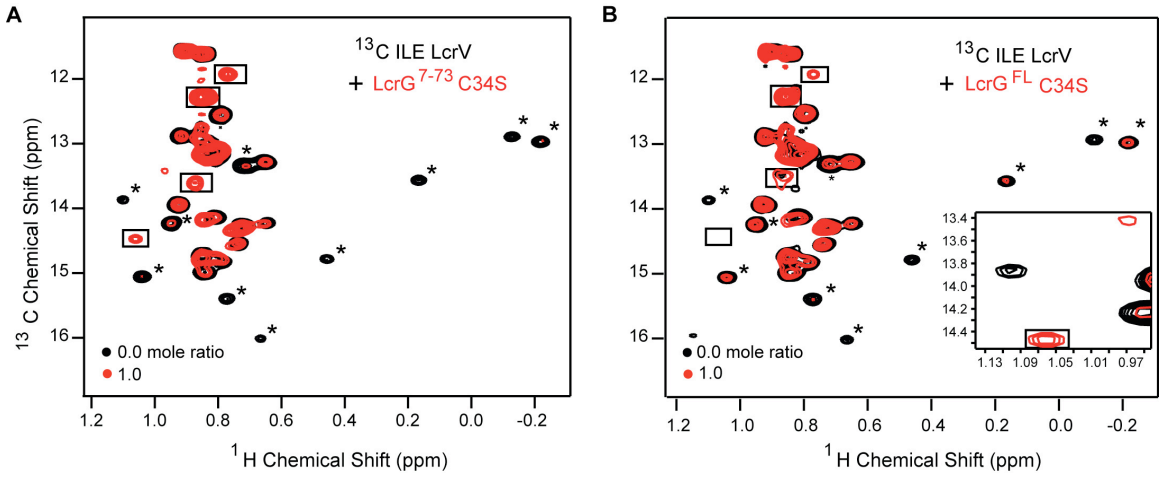

Figure 5-11. Two overlaid 2D ^{1}H-^{13}C HSQC spectra of ^{13}C ILE-LcrV in complex with **(A)** LcrG$^{7-73}$ C34S and **(B)** LcrG^{FL} C34S in a 1:1 molar ratio. New peaks and the peaks which decreased in intensity on complex formation, are indicated with boxes and asterisks, respectively. The inset in **B** represents an expanded view of the blank box to show the presence of the complex peak that is present at a lower contour level compared to the rest of the peaks.

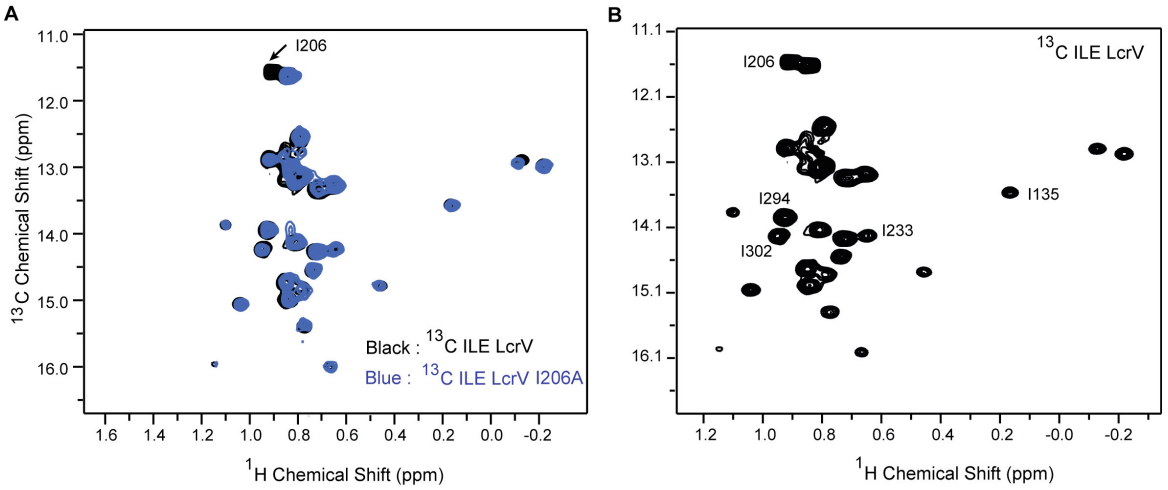

Figure 5-12. **(A)** Two overlaid 2D ^{1}H-^{13}C HSQC spectra of ^{13}C ILE-LcrV (black) with ^{13}C ILE-LcrV I206A (blue). The arrow shows the assignment of I206. **(B)** Two-dimensional ^{1}H-^{13}C HSQC spectrum of ^{13}C ILE-LcrV showing the assignments for the isoleucines. Residue names are labeled next to their corresponding peaks.

the spectra were overlayed. Similar titrations were repeated using ^{13}C ILE-LcrV combined with increasing amounts of unlabeled $LcrG^{FL}$ C34S. For comparison of the two sets of titrations, only the spectra acquired with the complex at molar ratios of 0.0 and 1.0 are shown for clarity **(Figure 5-11)**. The same set of Ile residues of LcrV were perturbed on binding to both $LcrG^{7-73}$ C34S and $LcrG^{FL}$ C34S. In both cases, there were four peaks that appeared in new positions (boxed in **Figure 5-11**), and same peaks that underwent significant reduction in intensities (marked with asterisks) **(Figure 5-11)**. Thus, we could conclude that both truncated LcrG ($LcrG^{7-73}$ C34S) and the full-length LcrG ($LcrG^{FL}$ C34S) bind similarly to LcrV.

To assign the ^{13}C methyl resonances of isoleucines in LcrV, a similar mutational approach as described in section 5.2.2 was followed. The ^{13}C methyl side chains of the five isoleucines (Ile-206, Ile-294, Ile-302, Ile-233 and Ile-135) of LcrV were assigned **(Figure 5-12B)**. An example of the mutagenesis method used in assigning LcrV Ile-206 is shown in **Figure 5-12A**. Upon mapping the NMR titration data to the crystal structure of LcrV (Chapter 3), it was seen that Ile-302 and Ile-294 which were perturbed on binding to LcrG, both lie in the coiled coil domain of LcrV **(Figure 5-13)**. Ile-135 of LcrV, which also showed significant decrease in peak intensity upon complex formation, is located in helix α-6, which makes a close contact with helix α-12 of the coiled coil. The residue Ile-206, which lies in the mixed α/β domain of LcrV, was not perturbed upon binding to LcrG. However, Ile-233 that is present in a loop in the mixed α/β domain of LcrV was perturbed to some extent upon titration of LcrG.

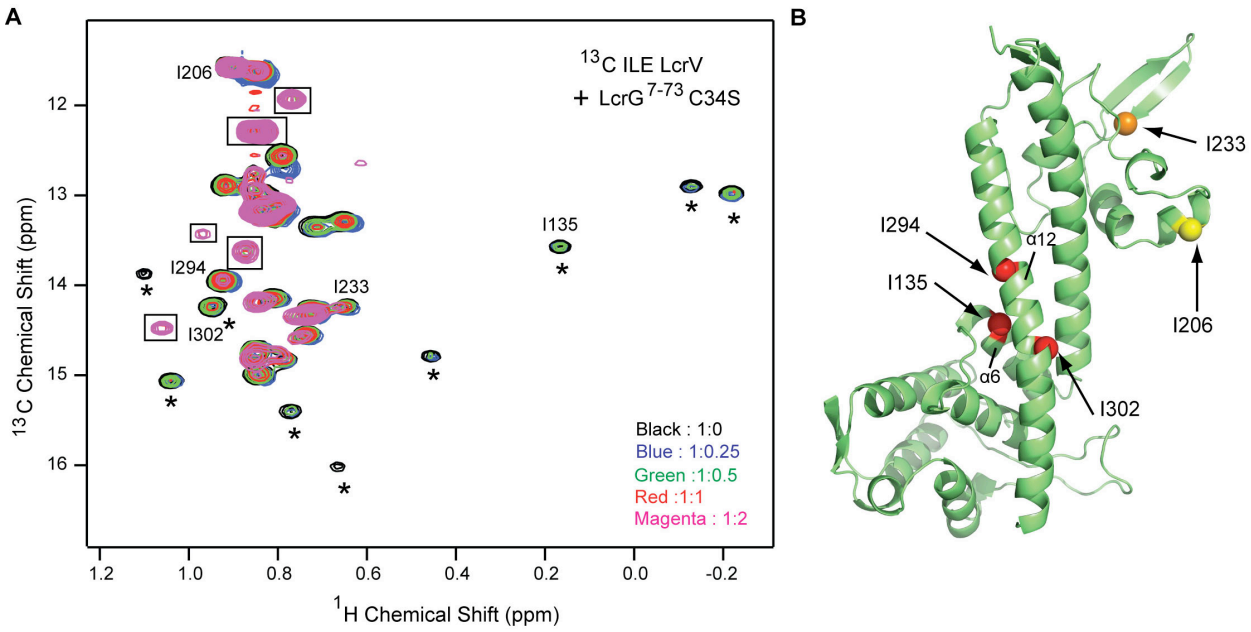

Figure 5-13. **(A)** Five overlaid 2D ^{1}H-^{13}C HSQC spectra of ^{13}C ILE-LcrV titrated with increasing molar ratios of LcrG$^{7-73}$ C34S. Peaks that showed reduction in intensities are indicated with asterisks. Peaks that appeared in new positions upon complex formation are boxed. The assignments of isoleucine residues are indicated. **(B)** Crystal structure of LcrV (obtained as described in Chapter 3) shown with the positions of the assigned isoleucines. The isoleucines that were highly perturbed on binding are shown as red spheres, the one slightly perturbed is shown as an orange sphere, and the one that remains unpertubed is shown as a yellow sphere.

5.3 Discussion

5.3.1 LcrG and LcrV form a tight complex

$LcrG^{7-73}$ C34S eluted at the position of a trimer (22 kDa) through the SEC column **(Figure 5-1)**. The low temperature (4° C) at which the SEC column was run probably contributed to LcrG aggregation. It is possible that the aggregated form of LcrG is physiologically relevant, and may be required for its stabilization. The observed SEC peak corresponding to the complex however, roughly equals the molecular weight of an LcrG-LcrV heterodimer. This suggested that in the presence of LcrV, the LcrG trimer dissociates to form an LcrG-LcrV heterodimer. Since, LcrG and LcrV co-migrated in gel filtration **(Figure 5-1)**, this suggested that they form a high-affinity complex. Additionally, the interaction between LcrG and LcrV was in the slow exchange NMR time scale, indicating a tight binding interaction **(Figures 5-2, 5-3 and 5-7)**. This is in agreement with the nanomolar binding affinity of the LcrG-LcrV complex as reported by Lawton *et al.* (*4*).

Unfortunately, attempts to obtain a K_d to quantify the binding were not successful using either surface plasmon resonance (SPR) or florescence polarization (FP) which were carried out according to the protocols described in sections 2.7 and 2.8. For SPR, a clear binding response curve was not observed, and this is possibly due to the degradation of LcrG upon immobilization on the CM5 chip used in SPR. On the other hand, the poor labeling efficiency of LcrG with the fluorescent dye (F5M) impeded FP experiments. Due to the dynamic nature of LcrG, the solvent accessibility of the native cysteine residue could not be ascertained, and this probably contributed to the poor labeling efficiency.

5.3.2 LcrG is perturbed along the entire length upon binding to LcrV

NMR titrations using ^{15}N LcrG$^{7-73}$ C34S indicated that LcrV induced a global change in the structure of LcrG upon binding. LcrG residues Asp-7 to Arg-51 showed significant reduction in peak intensities (intermediate exchange), whereas the residues Ser-52 to Arg-73 appeared as peaks in new positions (slow exchange) upon complex formation **(Figure 5-2 and Figure 5-3)**. This meant that LcrG is perturbed along the entire length upon binding to LcrV. This observation is further supported by NMR titrations using ^{13}C ILV-LcrG$^{7-73}$ C34S **(Figure 5-7)**. On one hand, our data agrees with the published results that showed that the N-terminus of LcrG is the binding site for LcrV (*2, 3*). On the other hand, NMR titrations shown here also indicated that the C-terminus of LcrG is perturbed upon binding. Thus, it is possible that the sheer difference in size between the two binding partners (37 kDa for LcrV and 8 kDa for LcrG) entails that almost the full length of the smaller protein (LcrG) is needed to form a stable binding interface. Since LcrG is partially folded and intrinsically flexible, it is highly likely that LcrG wraps around LcrV. This is not uncommon since many flexible proteins present a larger surface area for interaction as compared to globular proteins (*9*). The data presented here does not indicate that the interhelical contacts within LcrG become tighter on complex formation, as that would result in an increase in the backbone amide proton chemical shift range of the ^{15}N LcrG$^{7-73}$ C34S HSQC spectrum upon binding to LcrV.

5.3.3 Ser-52 to Ile-67 of LcrG is important for blocking the Y. pestis T3SS

The N-terminal region of LcrG has been shown to interact with LcrV by yeast two-hybrid assays (*3*). Mutational analysis of the N-terminus of LcrG identified a mutant, A16R that could block the secretion of Yop effectors (*2, 3*). Results of NMR titrations shown here indicated that both

the N and the C-termini of LcrG were affected upon binding to LcrV. Through collaboration with Dr. Gregory V. Plano (University of Miami), the biological significance of the C-terminal region (Ser-52 to Arg-73) of LcrG was evaluated by a Yop secretion assay in *Y. pestis*. Several LcrG point and deletion mutants were constructed and the ability of these mutants to control the secretion of Yop effector (YopM) was tested **(Figure 5-9)**. Interestingly, all the deletion mutants (Δ52-57, Δ58-62, Δ63-67, and Δ52-73) and the one point mutant, L63N, showed defects in the secretion blocking activity of LcrG **(Figure 5-9)**. The rest of the point mutants and one deletion mutant, Δ68-73, behaved as wild type LcrG. Since all the mutants showed expression of LcrG, it was concluded that the secretion blocking activity is not an artifact of the LcrG protein level, which was observed with Δ52-73 and L63N. NMR results plus the results of the Yop secretion assay suggested that the region Ser-52 to Ile-67 in LcrG plays an important role in blocking the secretion of Yops. Preliminary results of Matson and coworkers (*3*) suggested that the C-terminus of LcrG, in particular residue Phe-48, is involved in blocking the secretion of Yops. The NMR and the results of the Yop secretion assay shown here are further corroborated by results on the homolog, PcrG, which also implicated that the C-terminus is important in blocking the secretion of effector proteins (*10*). Thus, to connect the NMR titration data with the results from the Yop secretion assay; the C-terminus of LcrG (52-73) was suggested to be the site of tight binding as indicated by the slow exchange peaks, and the region 52-67 in LcrG was shown to be important in blocking the secretion of Yops. Hence it is highly likely, that the LcrV binding and secretion blocking regions in LcrG overlap, and so none of the mutants could block secretion of YopM.

5.3.4 The coiled coil domain of LcrV is perturbed upon binding to LcrG

Since LcrV is a rather large protein (326 residues), assigning each backbone amide peak for uniformly labeled ^{15}N LcrV to identify the residues perturbed upon complex formation is time consuming. However, the presence of a number of isoleucines in the primary amino acid sequence of LcrV, which are well distributed throughout its length offered an amenable way in mapping the binding region. Thus, NMR titrations using ^{13}C ILE-LcrV and unlabeled LcrG$^{7-73}$ C34S were carried out, and the results indicated that the coiled coil domain of LcrV is perturbed upon binding to LcrG. The isoleucine residues of LcrV, Ile-294, Ile-302, and Ile -135 that were perturbed on binding to LcrG lie on the same surface of LcrV **(Figure 5-13)**. The residues Ile-294 and Ile-302 lie in the longer helix α-12 that forms part of the coiled coil in LcrV. The residue Ile-135 lies in the helix α-6 of LcrV that is in close contact with the coiled coil **(Figure 5-13B)**. However, the perturbation observed in the LcrV residue Ile-233 (located in a loop of the mixed α/β domain) on binding to LcrG could be an indirect effect of the interaction. Overall, these data suggest that the coiled coil region of LcrV is perturbed on binding to LcrG, in agreement with previous reports (*4, 5*).

In summary, it is shown by NMR spectroscopy that LcrV induced a global change in the structure of LcrG upon complex formation, and the LcrV coiled coil domain is important in binding to LcrG. The results of the Yop secretion assay indicated LcrG Ser-52 to Ile-67 plays an important role in blocking the *Yersinia pestis* T3SS.

5.4 References

1. Nilles, M. L., Williams, A. W., Skrzypek, E., and Straley, S. C. (1997) Yersinia pestis LcrV forms a stable complex with LcrG and may have a secretion-related regulatory role in the low-Ca2+ response, *J Bacteriol 179*, 1307-1316.
2. Matson, J. S., and Nilles, M. L. (2001) LcrG-LcrV interaction is required for control of Yops secretion in *Yersinia pestis*, *J. Bacteriol. 183*, 5082-5091.
3. Matson, J. S., and Nilles, M. L. (2002) Interaction of the *Yersinia pestis* type III regulatory proteins LcrG and LcrV occurs at a hydrophobic interface, *BMC Microbiol. 2*, 16.
4. Lawton, D. G., Longstaff, C., Wallace, B. A., Hill, J., Leary, S. E., Titball, R. W., and Brown, K. A. (2002) Interactions of the type III secretion pathway proteins LcrV and LcrG from *Yersinia* pestis are mediated by coiled-coil domains, *J. Biol. Chem. 277*, 38714-38722.
5. Hamad, M. A., and Nilles, M. L. (2007) Structure-function analysis of the C-terminal domain of LcrV from *Yersinia pestis*, *J. Bacteriol. 189*, 6734-6739.
6. DeBord, K. L., Lee, V. T., and Schneewind, O. (2001) Roles of LcrG and LcrV during type III targeting of effector Yops by *Yersinia enterocolitica*, *J. Bacteriol. 183*, 4588-4598.
7. Nilles, M. L., Fields, K. A., and Straley, S. C. (1998) The V antigen of Yersinia pestis regulates Yop vectorial targeting as well as Yop secretion through effects on YopB and LcrG, *J Bacteriol 180*, 3410-3420.

8. Grzesiek, S., and Bax, A. (1993) The importance of not saturating H_2O in protein NMR. Application to sensitivity enhancement and NOE measurements., *J. Am. Chem. Soc. 115*, 12593-12594.

9. Babu, M. M., van der Lee, R., de Groot, N. S., and Gsponer, J. (2011) Intrinsically disordered proteins: regulation and disease, *Curr Opin Struct Biol 21*, 432-440.

10. Lee, P. C., Stopford, C. M., Svenson, A. G., and Rietsch, A. (2010) Control of effector export by the Pseudomonas aeruginosa type III secretion proteins PcrG and PcrV, *Mol. Microbiol. 75*, 924-941.

CHAPTER 6: Structural studies on PcrG and PcrG-PcrV interaction from the type III secretion system of *Pseudomonas aeruginosa*

6.1 Introduction

Pseudomonas aeruginosa is an opportunistic Gram-negative pathogen that is most frequently associated with nosocomial infections in patients with cystic fibrosis, pneumonia, AIDS, cancer, or other ailments that compromise the immune system (*1*). Despite treatment with potent antibiotics, the mortality rate is approximately 40% in case of incidences of acute infection (*2*). To initiate infection, the bacterium deploys the type III secretion system (T3SS) to inject effector proteins into host cells (*3*) in order to modulate host cell biology for the benefit and survival of the bacterium (*4, 5*). The two proteins that play critical roles in the assembly and regulation of type III secretion in *P. aeruginosa* are the tip protein, PcrV (*6*) and its chaperone, PcrG (*7, 8*).

Secretion of effector proteins by the T3SS in *P. aeruginosa* is tightly regulated and is triggered by either host cell contact or depletion of Ca^{+2} (*5*). Deletion of genes encoding either PcrG or PcrV results in the loss of regulation of effector secretion leading to constitutive secretion of effectors (*8*). Multiple results confirm that PcrG and PcrV interact directly (*8-10*). Remarkably, control of effector secretion was seen to be maintained in the case of a point mutation, V16R, which disrupts PcrG-PcrV binding (*8*). However, this mode of secretion regulation is different from its homolog, LcrG of *Yersinia pestis (11, 12)*. PcrG helps to facilitate PcrV secretion (*8*). PcrG also helps in directing the translocation of effector proteins into the host cell (*7*).

Following the investigations on the *Yersinia* tip protein chaperone LcrG reported in chapters 4 and 5, another question remains unanswered: whether the structural disorder that was observed

for LcrG is a hallmark of members of the V-tip chaperone family, or whether it is typical of LcrG alone. Accordingly PcrG, which shares sequence and functional homology to LcrG was chosen for a similar NMR-based structural characterization. Results of NMR and CD spectroscopy show that PcrG, like LcrG, adopts a partially folded α-helical structure instead of forming a tightly packed coiled coil. Additionally, PcrG and PcrV were shown to bind tightly with a nanomolar binding affinity, confirming the results of Nanao *et al. (9)*. NMR characterization of the PcrG-PcrV binding was in agreement with the LcrG-LcrV binding interaction, showing PcrV induced a global change on PcrG structure upon complex formation.

6.2 Results

6.2.1 Defining a PcrG construct for NMR characterization

NMR data using ^{15}N-labeled full-length PcrG (PcrG^{FL}, 98 amino acids) yielded an NMR spectrum **(Figure 6-3A)** where the peaks were not well resolved and were overlapped. This could be due to the presence of disordered regions in PcrG. To design a PcrG construct that will yield an ideal NMR spectrum, the program PSIPRED (*13*) was used to predict the secondary structure of PcrG **(Figure 6-1B)**. The extreme N and C termini of PcrG were predicted by PSIPRED to be random coils **(Figure 6-1B)**. To remove the disordered terminal residues and include the structured regions of PcrG while maintaining the hydrophilic terminal residues for solubility, a PcrG truncation was subcloned with residues Glu-9 to Ser-76 (PcrG$^{9\text{-}76}$) fused to a C-terminal His_6-tagged GB1 domain.

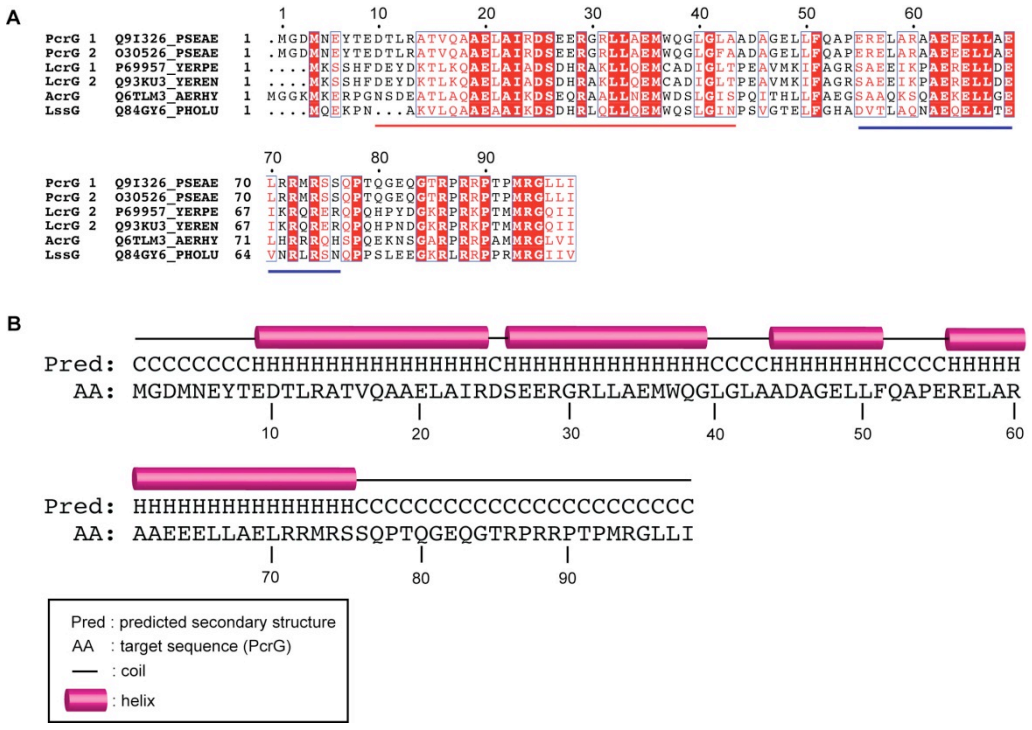

Figure 6-1. Multiple sequence alignment (MSA) of PcrG (UNIPROT ID: Q9I326_PSEAE) family of tip chaperones and secondary structure prediction for PcrG. **(A)** MSA of PcrG family of proteins using CLUSTALW. The homologous proteins were obtained from BLAST and denoted as PcrG2 (different strain of *P. aeruginosa*), LcrG1 (*Y. pestis*), LcrG2 (*Y. enterocolitica*), AcrG1 (*A. hydrophila*) and LssG (*P. luminescens*). The red line denotes the region homologous to the reported binding domain of LcrV on LcrG (*14*). The blue line denotes the region homologous to the C-terminus of LcrG, which was perturbed upon binding to LcrV by NMR studies (Chapter 5). **(B)** Result of secondary structure prediction for PcrG by PSIPRED (*13*). "C" or "H" denotes residues in random coil or helical regions, respectively. A cartoon representation is also provided where the helices and random coils are represented as pink cylinders and black lines respectively.

6.2.2 Protein Expression and Purification

Both the PcrG constructs ($PcrG^{FL}$ and $PcrG^{9-76}$) and PcrV (the design of the PcrV construct is discussed in section 2.1.4) were overexpressed in *E. coli* and purified under native conditions by Ni^{2+}-affinity chromatography. Purified fractions were then cleaved by a His_6-tagged TEV protease and products were loaded onto a Ni^{2+}-affinity column to separate $PcrG^{FL}$, $PcrG^{9-76}$ or PcrV from the GB1 tag. All the purified proteins produced yields in milligram quantities that facilitated NMR studies.

6.2.3 Circular Dichroism and Thermal Denaturation

Circular dichroism (CD) spectra of $PcrG^{FL}$ and $PcrG^{9-76}$ showed alpha helical content based on the minima at 222nm and a significant amount of disorder based on the predominant minima at 208nm. Nevertheless, comparison of the two CD spectra **(Figure 6-2A)** confirmed that $PcrG^{FL}$ and $PcrG^{9-76}$ have nearly identical secondary structures because their CD spectra were nearly superimposable. Thus the $PcrG^{9-76}$ truncation did not produce any appreciable changes to the secondary structure of PcrG. The thermal denaturation curves of $PcrG^{FL}$ and $PcrG^{9-76}$ **(Figure 6-2B)** showed that they unfolded in a non-cooperative manner without showing any clear inflection points.

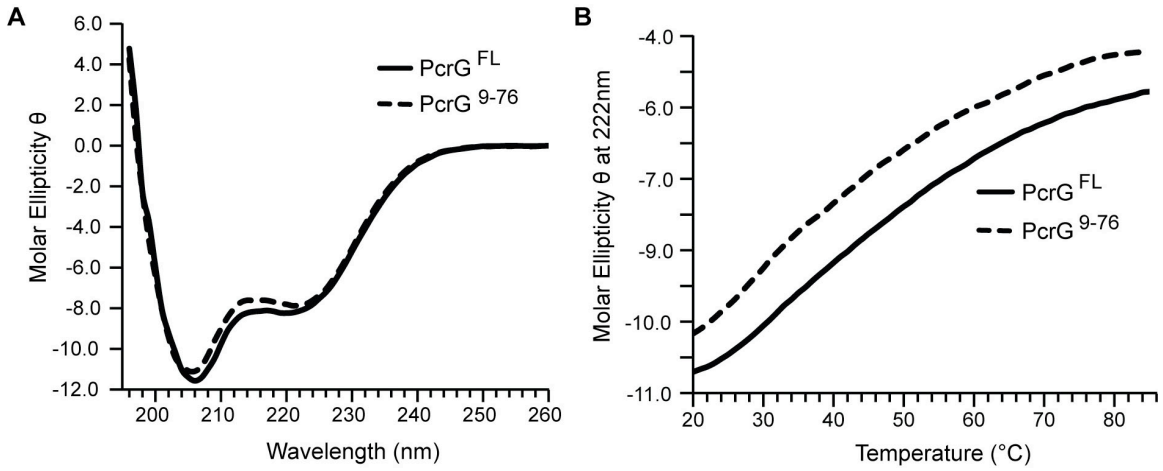

Figure 6-2. CD and thermal denaturation spectra of the PcrG constructs. **(A)** CD spectra acquired at 25° C for $PcrG^{FL}$ and $PcrG^{9-76}$. **(B)** Thermal denaturation plots of $PcrG^{FL}$ and $PcrG^{9-76}$. (Molar ellipticity $\theta = (deg \cdot cm^2 \cdot dmol^{-1}) \times 10^{-5}$).

6.*2.4 PcrG NMR spectra and backbone assignments*

$PcrG^{FL}$ and $PcrG^{9-76}$ were soluble at high concentrations and afforded millimolar amounts of purified protein. The 2D ^{1}H-^{15}N HSQC spectrum for $PcrG^{FL}$ **(Figure 6-3A)** showed a non-ideal NMR spectrum with broad and overlapped peaks, with many more peaks expected from a 98-residue protein. On the other hand, the $PcrG^{9-76}$ truncation afforded a spectrum suitable for NMR characterization based on the presence of sharp and well-resolved peaks **(Figure 6-3B)**. Hence 3D NMR datasets were acquired on $PcrG^{9-76}$ to assign the backbone resonances of $PcrG^{9-76}$. The two-dimensional ^{1}H-^{15}N HSQC spectrum of $PcrG^{9-76}$ was assigned with the correct number of peaks expected for a 68-residue protein using the 3D HNCACB experiment. The backbone amides of the 67 non-proline residues of $PcrG^{9-76}$ were assigned as well as all 8 residues of the C-terminal cloning artifact GSENLYFQ **(Figure 6-4)**. The overlapping peaks are indicated in the figure with asterisks **(Figure 6-4)**. Examples of the carbon backbone connectivity of some of the representative PcrG residues are illustrated in **Figure 6-5**.

Analysis of the secondary Cα and Cβ chemical shifts suggested the presence of α-helices from residues Val-16 to Gly-41 and Glu-55 to Ser-76 **(Figure 6-6A, B)** with short interspersed residues with low helical content and few lack any apparent secondary structure.

6.2.5 PcrG Backbone dynamics

To assess the backbone dynamics of PcrG, the steady state heteronuclear $\{^{1}H\}$-^{15}N NOE and ^{15}N backbone R_1 and R_2 relaxation rates for $PcrG^{9-76}$ were acquired.

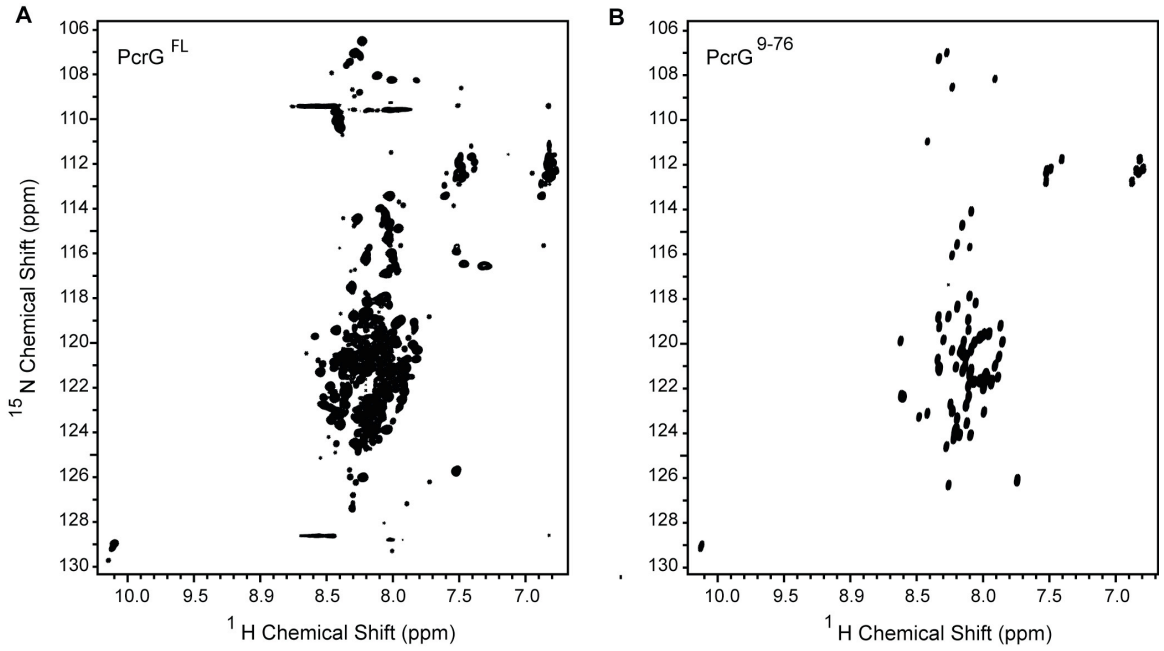

Figure 6-3. 2D ^{1}H-^{15}N HSQC spectra of **(A)** PcrG^{FL} and **(B)** truncated PcrG$^{9-76}$.

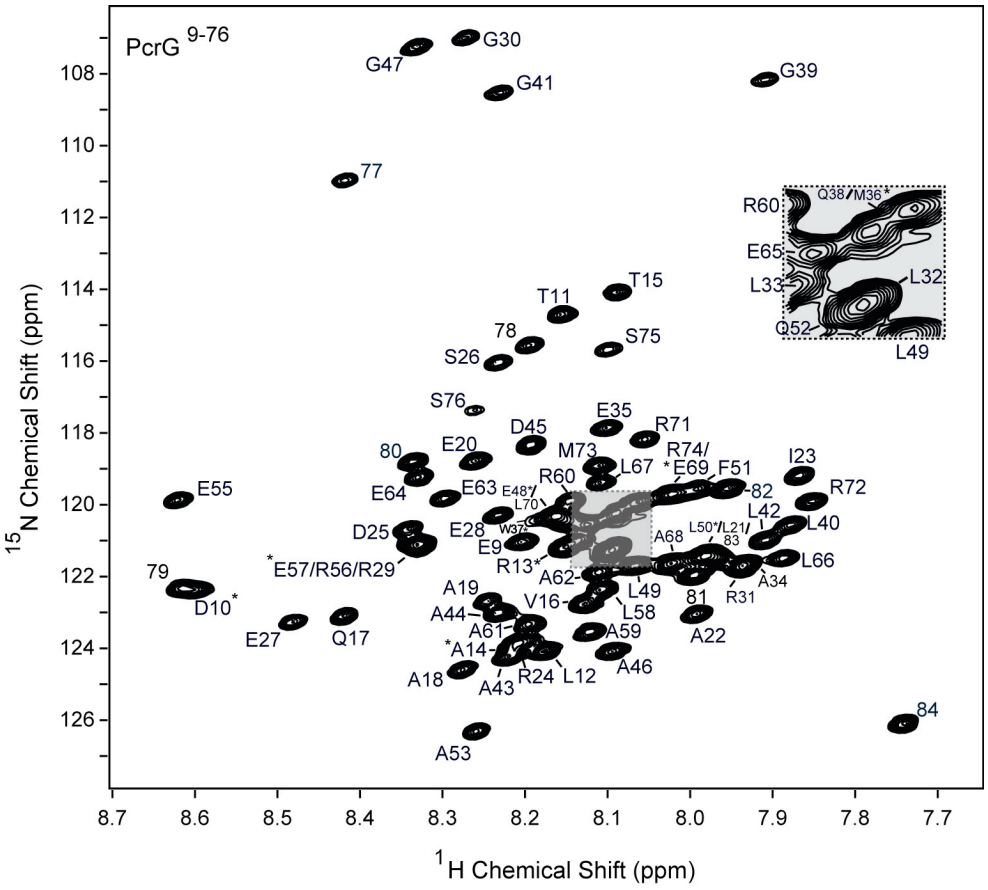

Figure 6-4. Assigned 2D ^{1}H-^{15}N HSQC spectrum of PcrG$^{9-76}$. Residues are indicated next to their corresponding peaks. Overlapped peaks are indicated with asterisks (L50* overlapped with L21 and F83; R13* overlapped with L33; and E48* overlapped with L70; D10* overlapped with E79; E69* overlapped with R74; E57* overlapped with R56 and R29; A14* overlapped with R24; M36* overlapped with Q38. W37* was not well resolved). The W37 side chain peak is not shown. Residues 77-84 (G_{77}SENLYFQ$_{84}$) are cloning artifacts.

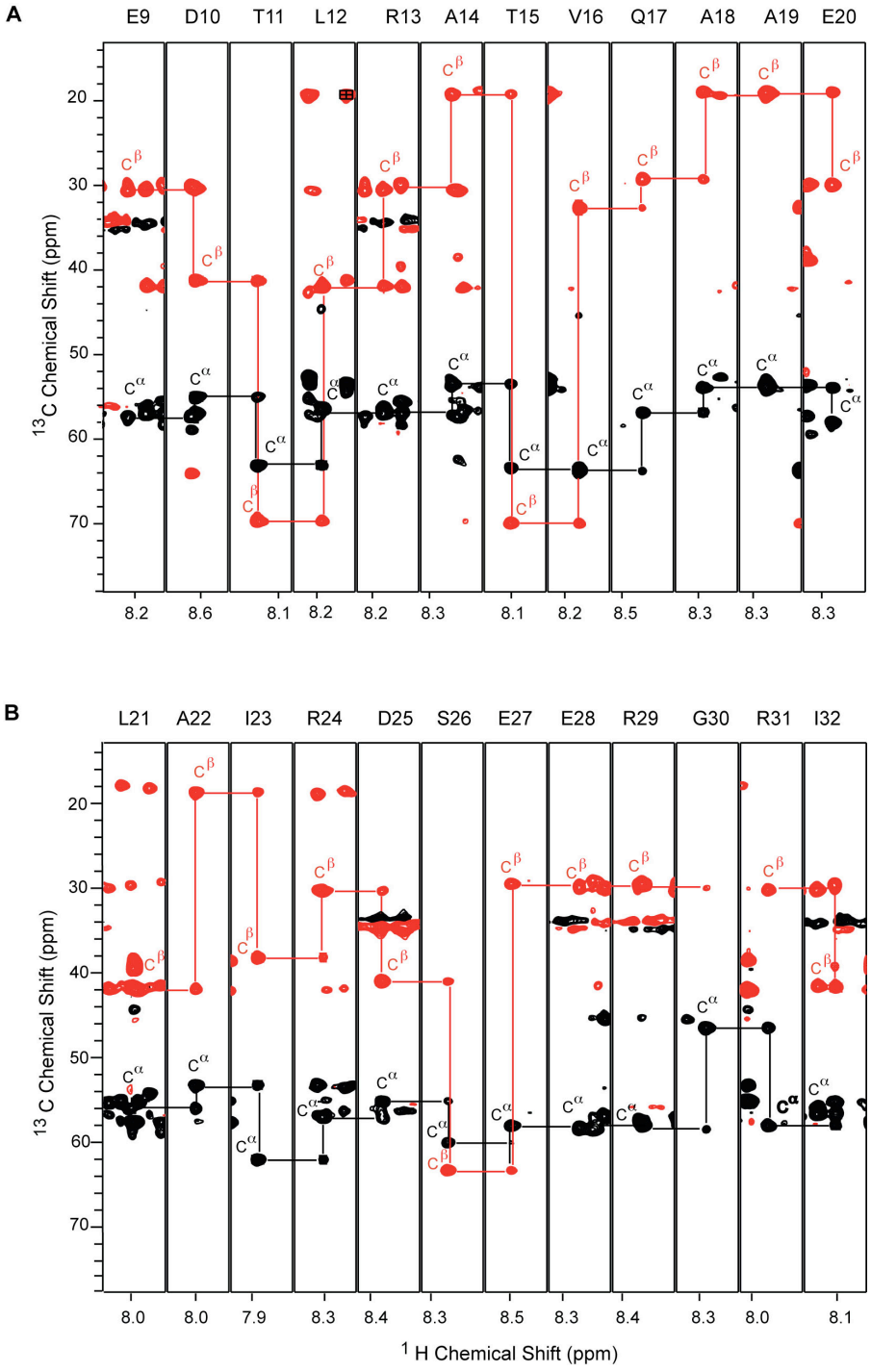

Figure 6-5. Representative strips of the 3D HNCACB spectrum of $^{15}N/^{13}C$ PcrG$^{9-76}$ spanning residues E9 to E20 (top) and L21 to I32 (bottom) to illustrate the backbone connectivity identified for PcrG$^{9-76}$.

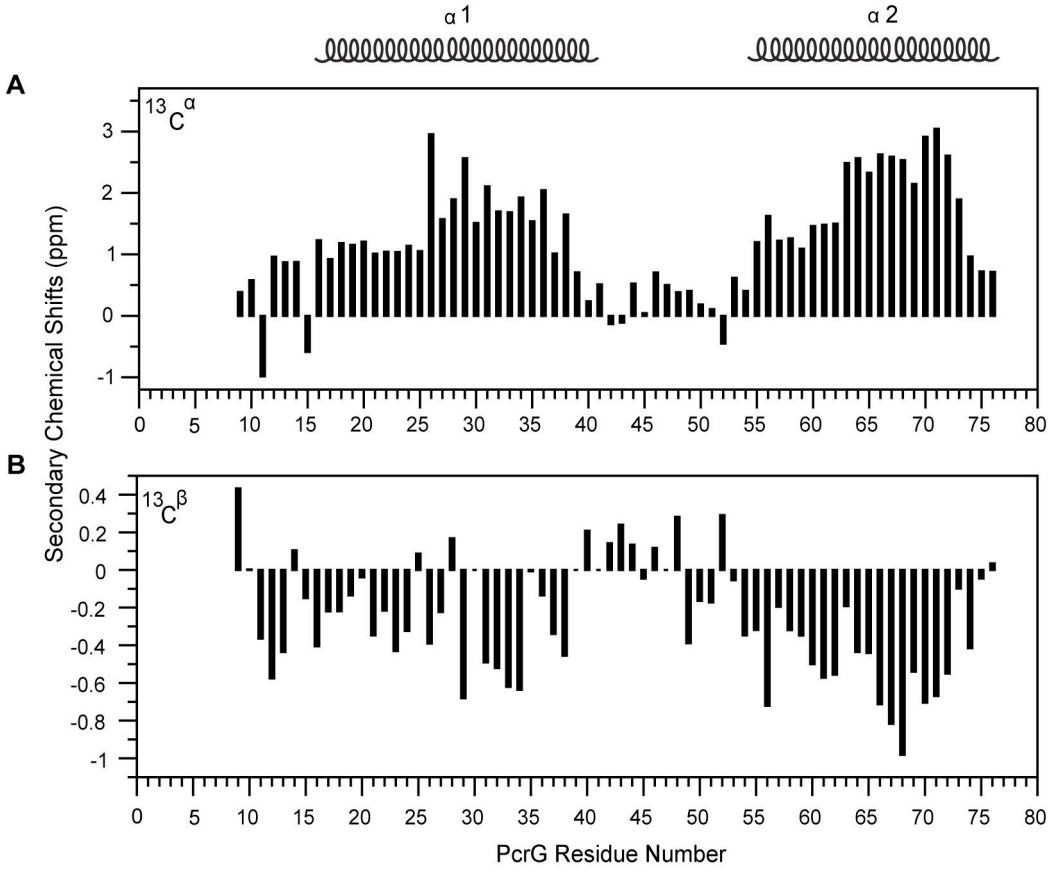

Figure 6-6. **(A)** Cα and **(B)** Cβ secondary chemical shifts of PcrG$^{9-76}$ suggested the presence of two α-helical regions. If the Cα chemical shifts are consistently positive, it is denoted as a α-helix. The positions of the helices are indicated. The random coil chemical shifts are determined as described in Chapter 2 (section 2.3.3).

The heteronuclear $\{^1H\}$-^{15}N NOE provides insight into the backbone dynamics of proteins at picoseconds to nanoseconds time scales. Heteronuclear $\{^1H\}$-^{15}N NOE values above 0. 6 indicate well-structured regions and can be qualitatively described as being rigid. Heteronuclear $\{^1H\}$-^{15}N NOE values between 0.4-0.6 can be qualitatively described as semi-rigid flexibility, whereas, $\{^1H\}$-^{15}N NOE values below 0.2 indicate completely unstructured regions, as in random coils. Most of the residues in the two α-helices showed $\{^1H\}$-^{15}N NOEs between 0.4 to 0.6 **(Figure 6-7A)**. The $\{^1H\}$-^{15}N NOEs of residues outside of these two helices were mostly at or below 0.4 except a few of them were above 0.4. Only one residue (Leu-12) had a $\{^1H\}$-^{15}N NOE of slightly below 0. 2 indicating random coil flexibility. Interestingly, some residues within the two helices showed $\{^1H\}$-^{15}N NOEs values above 0. 6.

The ^{15}N backbone relaxation rates (R_1 and R_2) indicated that the two helices in PcrG behaved with nearly similar backbone amide dynamics **(Figure 6-7B, C)**. For both the datasets, there was no appreciable difference in the relaxation rates from the beginning to the end of the protein. This indicated that PcrG tumbles as a single entity in solution, as opposed to, for example, helix α1 tumbling at a different rate compared to helix α2. The gaps in the datasets are due to the overlapping peaks that have been omitted from the analyses.

6.2.6 NMR titrations with ^{15}N PcrG$^{9-76}$

NMR chemical shift mapping was used to characterize the PcrG-PcrV interaction. Purified ^{15}N-labeled PcrG$^{9-76}$ was titrated with increasing amounts of PcrV (at PcrV:PcrG molar ratios of 0.0, 0.25, 0.5, 1.0, 2.0 and 4.0) in NMR buffer.

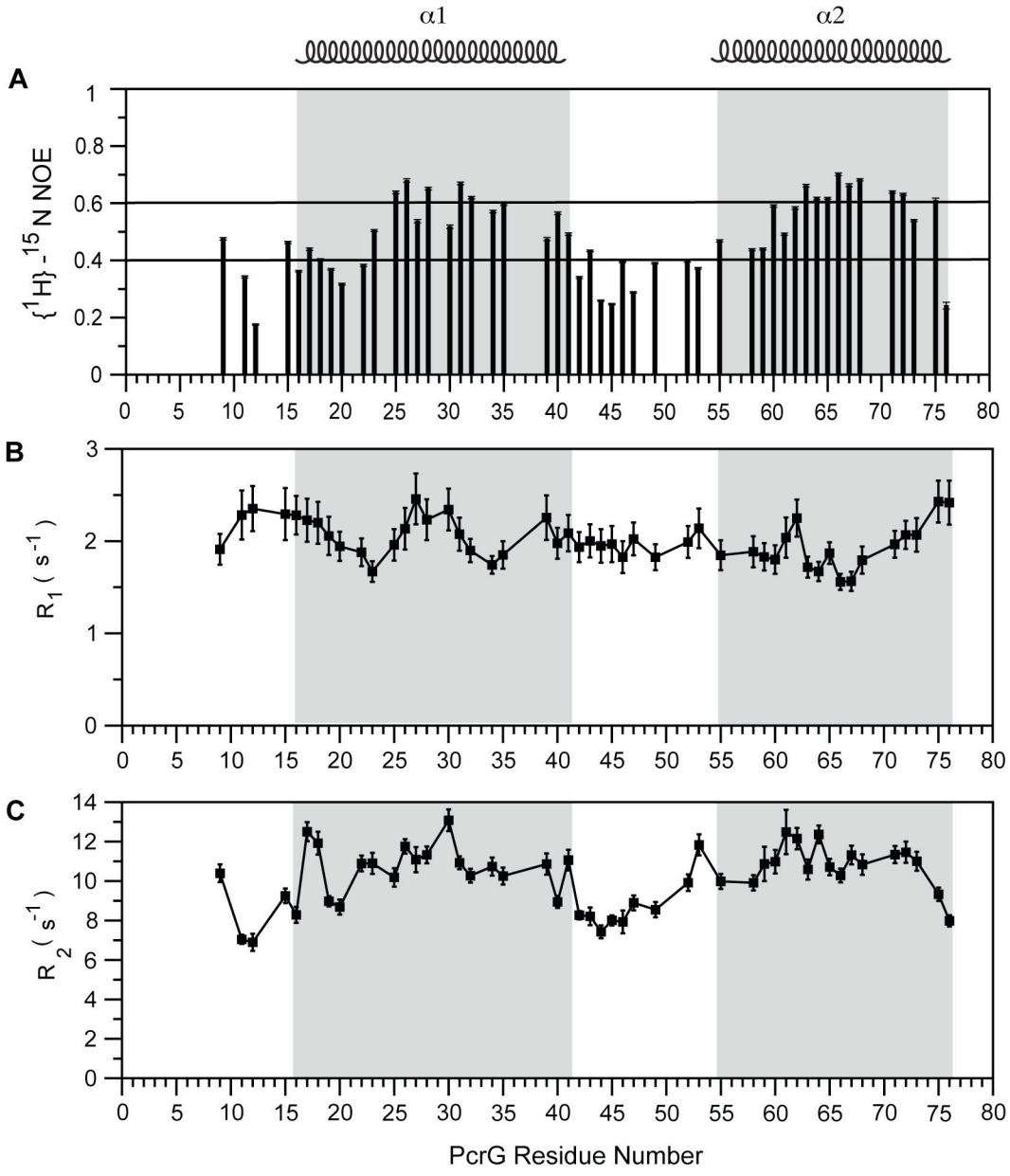

Figure 6-7. (A) Heteronuclear $\{^1H\}$-^{15}N NOEs, **(B)** R_1 and **(C)** R_2 relaxation data for $PcrG^{9-76}$. The helical regions are shaded.

The changes were monitored by acquiring 2D ^{1}H-^{15}N HSQC spectra. The 2D ^{1}H-^{15}N HSQC spectrum for each titration ratio was overlayed to determine the changes in the ^{1}H-^{15}N HSQC of PcrG as it binds to PcrV **(Figure 6-8)**. With the exception of only 7 of the 75 backbone amide peaks (including the C-terminal cloning artifact), nearly all peaks showed significant reduction in peak intensities with increasing molar ratios of PcrV. The 7 peaks that did not show any change in peak intensities throughout the titration corresponded to the cloning artifact residues (Ser-78, Glu-79, Asn-80, Leu-81, Tyr-82, Gln-84) and one PcrG residue Leu-50. However, one of the cloning artifact residues Gly-77 appeared to be in fast exchange time scale on titration with PcrV.

6.2.7 NMR titrations with ^{13}C-ILV PcrG$^{9-76}$

A second NMR titration was performed using purified ^{13}C-ILV PcrG$^{9-76}$ combined with increasing molar ratios of PcrV. The advantages of the ILV labeling technique have been explained in section 5.2.3 (Chapter 5). The positions of the methyl groups of Ile, Leu and Val (ILV) of PcrG$^{9-76}$ are indicated in the two-dimensional ^{1}H-^{13}C HSQC spectrum of ^{13}C ILV-PcrG$^{9-76}$ **(Figure 6-9A)**. The ILVs are well distributed throughout PcrG as shown in **Figure 6-9B**. 2D ^{1}H-^{13}C HSQC spectra were acquired at each PcrV:PcrG molar ratio (0.0, 0.25, 0.5, 1.0, 2.0, and 3.0) and then overlayed **(Figure 6-10)** to monitor the changes in the HSQC spectra of ^{13}C ILV-PcrG$^{9-76}$ upon binding to PcrV. As the concentration of PcrV increased, many peaks in PcrG were reduced in intensity (indicated by asterisks in **Figure 6-10**) upon binding to PcrV.

To identify the residues of PcrG that were perturbed upon complex formation with PcrV, the mutational approach (described in section 5.2.3) was used to assign the methyl groups of ILVs.

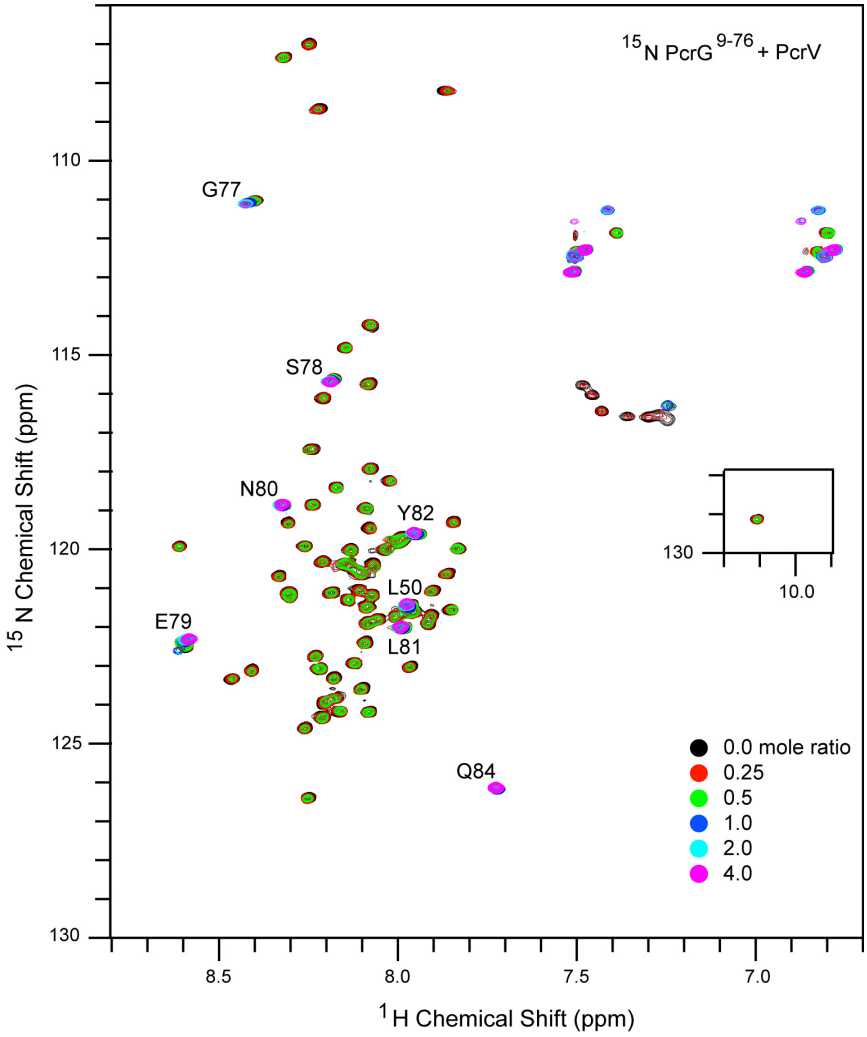

Figure 6-8. **(A)** Six overlaid 2D ^{1}H-^{15}N HSQC spectra of PcrG$^{9-76}$ with increasing ratios of PcrV. Assigned backbone amide peaks that remained unperturbed by the titration are labeled.

This approach was rather challenging for PcrG due to the significant number of overlapping peaks and conformational heterogeneity. The methyl groups of Val-16, Ile-20, and Leu-66 could be assigned unambiguously. These three residues underwent reduction in peak intensities upon binding to PcrV **(Figure 6-10)**. The presence of two peaks for Ile-20 and Val-16 indicated conformational heterogeneity of PcrG **(Figure 6-10)**. Interestingly only one conformation of Ile-20 and Val-16 of PcrG were perturbed (indicated with asterisks) upon complex formation with PcrV. Based on the NMR secondary chemical shift mapping, the residues Ile-20 and Val-16 lie in the helix α-1, and the residue Leu-66 lies in the helix α-2 of PcrG. Thus, both the helices of PcrG were perturbed on binding to PcrV.

6.2.8 NMR titrations with ^{13}C-ILE PcrV

Another set of titration experiments was carried out using ^{13}C ILE-PcrV combined with increasing molar ratios of unlabeled PcrG$^{9-76}$. Similarly, 2D ^{1}H-^{13}C HSQC spectra were acquired at each PcrG:PcrV molar ratios (0.0, 0.5, 1.0, 2.0 and 3.0) and then superimposed. This same set of titration experiments was also done with unlabeled PcrG^{FL}. For comparison of the results for PcrG^{FL} and PcrG$^{9-76}$, spectra from two molar ratios (0.0 and 1.0) are shown for clarity **(Figure 6-11)**. In both the datasets (showing the PcrV isoleucines), there were two new peaks (shown as boxes) and two peaks that disappeared from the spectra (shown with arrows) upon complex formation **(Figure 6-11)**. Although the PcrV isoleucine spectrum is not assigned, the important point to note is that the same sets of PcrV residues were affected when titrated with PcrG^{FL} or PcrG$^{9-76}$.

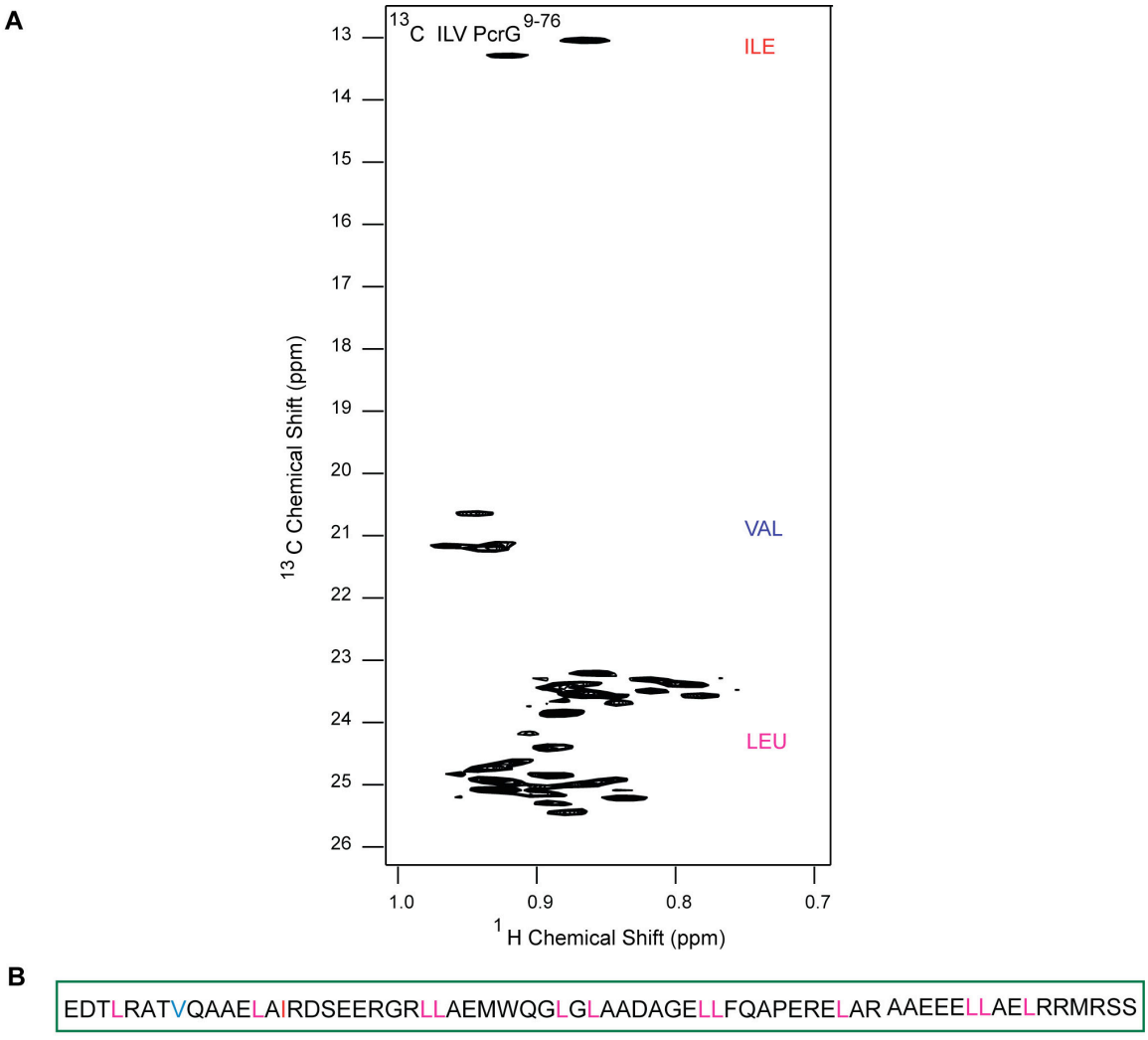

Figure 6-9. **(A)** Two-dimensional ^{1}H-^{13}C HSQC spectrum of ^{13}C-ILV PcrG$^{9-76}$ where the positions of the ^{13}C methyl groups of Ile, Leu and Val are indicated. **(B)** Amino acid sequence of PcrG$^{9-76}$ showing the distribution of Ile (red), Leu (pink), and Val (blue).

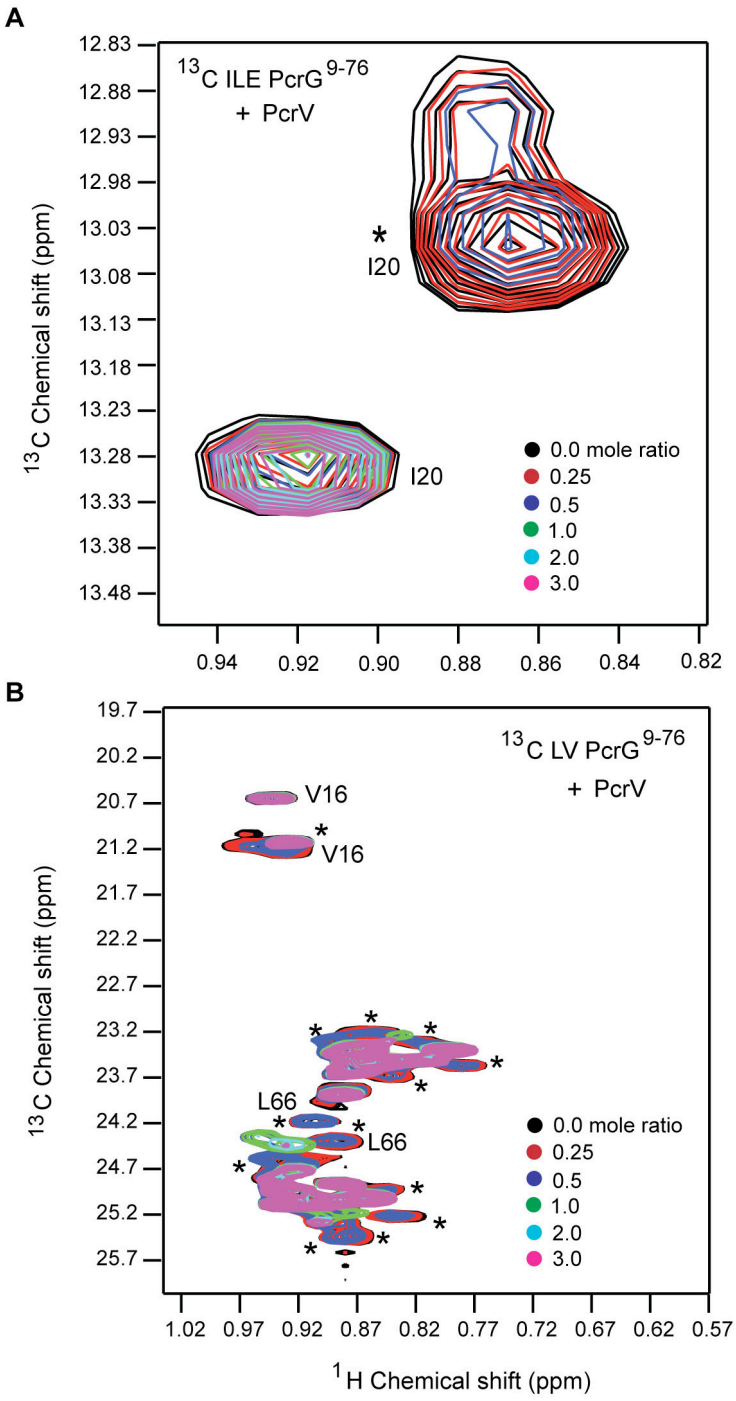

Figure 6-10. Six overlaid 2D ^{1}H-^{13}C HSQC spectra of **(A)** ^{13}C- ILE PcrG$^{9-76}$ and **(B)** ^{13}C-LV (leucine and valine) PcrG$^{9-76}$ with increasing ratios of PcrV. Peaks that reduced in intensities are marked with asterisks. The three assigned methyl groups of Ile-20, Val-16, and Leu-66 are indicated next to their peak positions.

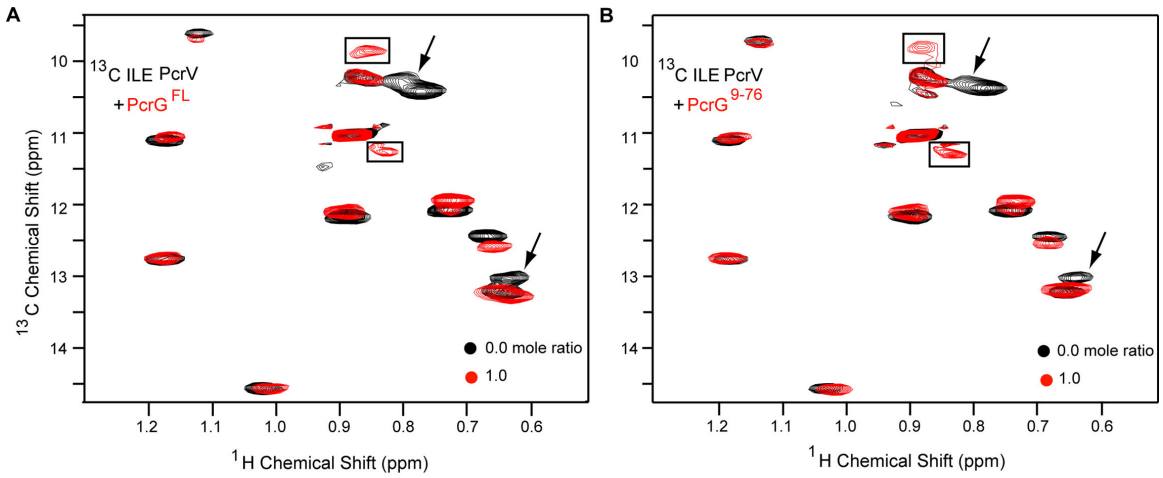

Figure 6-11. Two overlaid 2D ^{1}H-^{13}C HSQC spectra of ^{13}C ILE-PcrV in complex with **(A)** PcrG^{FL} and **(B)** PcrG$^{9-76}$ in a 1:1 molar ratio. New peaks, and the peaks, which decreased in intensity and disappeared from the spectra upon complex formation are indicated with boxes and arrows respectively.

Thus, both $PcrG^{FL}$ and $PcrG^{9-76}$ bind similarly to PcrV. In other words, the truncation did not alter the ability of PcrG to bind to PcrV.

6.2.9 Surface Plasmon Resonance Spectroscopy

Surface plasmon resonance (SPR) was used to determine the binding affinity and binding kinetics between PcrV and PcrG. PcrG constructs were fused to a C-terminal GB1-His_6 tag to facilitate immobilization to anti-His_6 antibody coated CM5 flow cells. Injection of PcrV into flow cells with immobilized PcrG produced a clear binding response that increased proportionally with increasing analyte concentration. The SPR data for the interaction between PcrV and $PcrG^{FL}$ was best fitted to a 1:1 Langmuir model (χ^2 = 0. 314) **(Figure 6-12)**. The K_d for this interaction was calculated to be 26.5 nM, which is very similar to that previously described by Nanao *et al. (9)* in which SPR was used to evaluate binding between full length proteins, PcrG and PcrV. Thus, the N-terminal 24-residue truncation of PcrV had little effect on the interaction. The binding also occurred with rapid kinetics, with $k_a = 5.62 \times 10^5\ M^{-1}s^{-1}$ and $k_d = 1.53 \times 10^{-2}\ s^{-1}$.

The truncations made in $PcrG^{9-76}$ did not appear to have a significant effect in its PcrV binding capacity. In fact, the sensorgram for PcrV binding to immobilized $PcrG^{9-76}$-GB1-His_6 was fit to a 1:1 Langmuir model (*15*) (χ^2 = 2.53) and the calculated binding affinity was slightly higher than that for $PcrG^{FL}$ (23.7 nM) **(Figure 6-12)**. Also, the binding kinetics were found to be more rapid than seen for $PcrG^{FL}$, though less than an order of magnitude, with $k_a = 1.02 \times 10^6\ M^{-1}s^{-1}$ and $k_d = 2.42 \times 10^{-2}\ s^{-1}$. These minimal changes in binding suggested that truncated $PcrG^{9-76}$ retained the regions needed for interaction with PcrV.

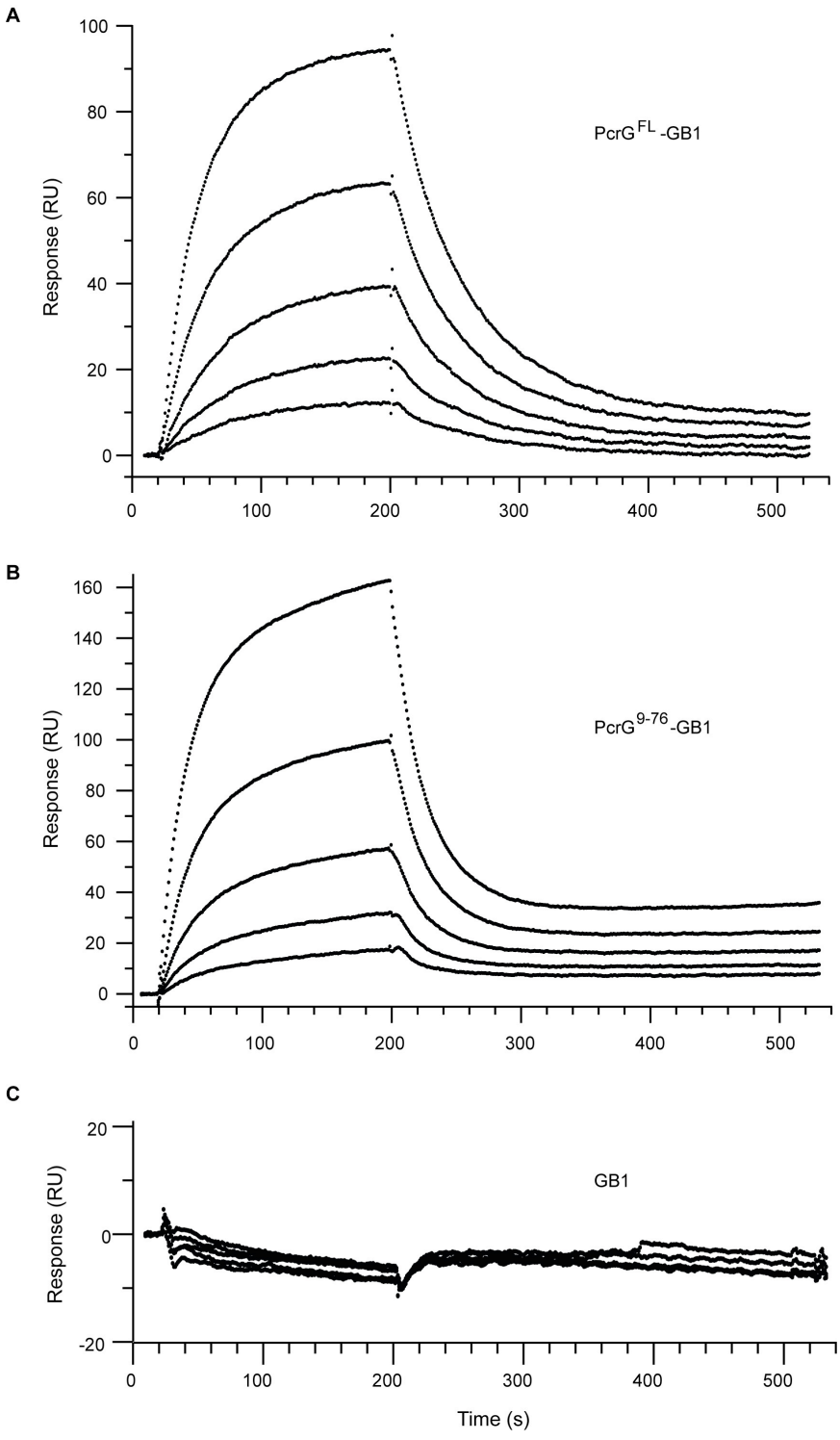

Figure 6-12. SPR sensorgrams for PcrV binding to **(A)** $PcrG^{FL}$-GB1-His_6, **(B)** $PcrG^{9-76}$-GB1-His_6, and **(C)** GB1-His_6 fusion tag.

The SPR data is consistent with the NMR titration experiment using ^{13}C ILE-PcrV, which showed that both the truncated and full length PcrG bind similarly to PcrV.

To account for possible interference of the GB1-His_6 tag with the PcrG-PcrV interaction, a control sensorgram was collected with identical conditions from the previous experiment, but with GB1-His_6 as the ligand **(Figure 6-12)**. The binding response to PcrV was insignificant and did not increase with increasing PcrV concentration. Therefore, the GB1-His_6 tag remained inert in the interaction. This observation also pointed to the specificity of the PcrG-PcrV interaction.

6.3 Discussion

LcrG is the most closely related homolog of PcrG and shares with it a 41% sequence identity **(Figure 6-1A)**. Results of yeast two-hybrid suggested that the LcrG N-terminal residues, Asp7 to Thr-40 (corresponding to Asp-10 to Ala-43 in PcrG), are required for LcrV interaction (*14*). The results of the NMR titrations (Chapter 5) suggested that the C-terminus of LcrG from residues Ser-52 to Arg-73 (corresponding to Glu-55 to Ser-76 in PcrG) was also perturbed upon complex formation with LcrV (Chapter 5). While *in vivo* substitutions of PcrG for LcrG in *Y. pestis* have been unable to transcomplement normal T3SS regulation, both proteins bind LcrV (*14*). Thus, PcrG likely maintains the LcrG binding motif for its respective adaptor protein, PcrV.

6.3.1 PcrG is a partially folded protein

Due to the non-ideal NMR spectrum of $PcrG^{FL}$, a PcrG truncation ($PcrG^{9-76}$) was constructed for NMR studies. The use of truncated PcrG was validated with different experimental approaches, and results show that both the full length and truncated PcrG behaved similarly with respect to

binding PcrV. CD spectroscopy showed that both $PcrG^{9-76}$ and $PcrG^{FL}$ spectra maintained similar ratios of the composition of secondary structure **(Figure 6-2)**. Results from SPR confirmed that the PcrG truncation showed similar binding affinity and binding kinetics for PcrV **(Figure 6-12)**. In fact, the binding affinity was slightly higher than that of $PcrG^{FL}$, which might be attributed to the removal of non-participating residues that may otherwise reduce binding accessibility. GB1-His_6 fusion proteins were used for SPR studies because anti-polyhistidine antibodies were used to coat the surface of the flow cells by amine coupling. Another NMR titration using ^{13}C ILE-PcrV showed that both $PcrG^{9-76}$ and $PcrG^{FL}$ bind to the same surface of PcrV, as the same set of isoleucine residues were affected in PcrV upon titration with $PcrG^{9-76}$ or $PcrG^{FL}$ **(Figure 6-11)**.

CD spectroscopy and thermal denaturation, which showed the absence of a clear melting temperature (Tm) **(Figure 6-2)**, indicated that PcrG is a helical protein without any well-ordered tertiary structure. Nanao *et al.* (*9*) also observed that PcrG does not display a clear Tm, which is consistent with our observation. Additionally, the $\theta_{222/208}$ ratio of 0.7 is indicative of a partially folded helical protein with loosely packed helices. The results of CD are consistent with the narrow proton chemical shift range (<1 ppm) of PcrG in the 2D ^{1}H-^{15}N HSQC spectra **(Figure 6-3)** which suggested that the protein might be highly α-helical or unstructured. Similarly, the 2D ^{1}H-^{13}C HSQC spectrum of PcrG where the methyl groups of Ile, Leu and Val were labeled also showed poor chemical shift dispersion with conformational heterogeneity and broad overlapping peaks **(Figure 6-9A)**. This too is indicative of relatively loose packing of the hydrophobic regions in PcrG.

For the NMR characterization of $PcrG^{9-76}$, the full 2D ^{1}H-^{15}N HSQC spectrum of $PcrG^{9-76}$ was assigned by 3D NMR experiments. The secondary Cα and Cβ chemical shifts suggested that the

secondary structure of PcrG is essentially dominated by two α-helices **(Figure 6-6)**. The heteronuclear $\{^1H\}$-^{15}N NOE experiment showed that the helices do not form well-structured (rigid) regions, but instead have semi rigid flexibility **(Figure 6-7A)**. Interestingly, some of the residues in the helices have $\{^1H\}$-^{15}N NOEs above 0.6, which suggest they may have backbone dynamics approaching a well-structured state. The residues that lie outside the helices have $\{^1H\}$-^{15}N NOEs at or below 0.4, suggesting higher flexibility in these regions. The ^{15}N backbone relaxation rates (R_1 and R_2) showed that the α-helices behaved with similar backbone dynamics and the whole protein tumbles as a single unit in solution **(Figure 6-7B, C)**. Thus overall, NMR data presented herein suggested that PcrG, like LcrG has secondary structure but lacks a compact tertiary structure, and hence can be best described as a partially folded helical protein.

Direct binding between PcrG and PcrV has been demonstrated previously (*9, 10*), but a defined PcrV binding region on PcrG has yet to be identified. The NMR titration experiments **(Figure 6-8, 6-10)** using $PcrG^{9-76}$ indicated that PcrV induced a global change in PcrG structure that may likely result from a combination of both PcrV-binding interactions and binding-induced conformational changes within PcrG. As noted for LcrG-LcrV binding interaction in Chapter 5, the size difference between PcrV (33KDa) and $PcrG^{9-76}$ (8KDa) makes the wrapping of PcrG around PcrV a likely scenario providing a large surface area for interaction and thus increasing the stability of the PcrG-PcrV complex.

6.3.2 Significance of PcrG as a partially folded protein

In conclusion, the NMR, CD, and SPR data presented here provided the first structural characterization of PcrG, showing that the PcrG chaperone family adopts a partially folded α-

helical conformation lacking a compact tertiary structure. Earlier results have pointed out multiple putative roles for PcrG towards control of secretion and translocation of effector proteins in *P. aeruginosa* T3SS (*7, 8*), as well as serving as a chaperone to the tip protein PcrV (*7, 8*). The results showing an inherent structural flexibility for PcrG may aid in functional versatility of this protein, and is likely a hallmark of the PcrG/LcrG family of V-tip chaperones. Overall, the LcrG/PcrG family of proteins contributes to a growing list of partially folded proteins that play important roles in the bacterial type III secretion system.

6.4 References

1. Lyczak, J. B., Cannon, C. L., and Pier, G. B. (2000) Establishment of *Pseudomonas aeruginosa* infection: lessons from a versatile opportunist, *Microbes Infect. 2*, 1051-1060.
2. Engel, J., and Balachandran, P. (2009) Role of Pseudomonas aeruginosa type III effectors in disease, *Curr Opin Microbiol 12*, 61-66.
3. Hauser, A. R. (2009) The type III secretion system of Pseudomonas aeruginosa: infection by injection, *Nat. Rev. Microbiol. 7*, 654-665.
4. Yahr, T. L., Vallis, A. J., Hancock, M. K., Barbieri, J. T., and Frank, D. W. (1998) ExoY, an adenylate cyclase secreted by the Pseudomonas aeruginosa type III system, *Proc. Natl. Acad. Sci. USA 95*, 13899-13904.
5. Dacheux, D., Epaulard, O., de Groot, A., Guery, B., Leberre, R., Attree, I., Polack, B., and Toussaint, B. (2002) Activation of the Pseudomonas aeruginosa type III secretion system requires an intact pyruvate dehydrogenase aceAB operon, *Infect. Immun. 70*, 3973-3977.

6. Goure, J., Pastor, A., Faudry, E., Chabert, J., Dessen, A., and Attree, I. (2004) The V antigen of *Pseudomonas aeruginosa* is required for assembly of the functional PopB/PopD translocation pore in host cell membranes, *Infect. Immun. 72*, 4741-4750.

7. Sundin, C., Thelaus, J., Broms, J. E., and Forsberg, A. (2004) Polarisation of type III translocation by Pseudomonas aeruginosa requires PcrG, PcrV and PopN, *Microb. Pathog. 37*, 313-322.

8. Lee, P. C., Stopford, C. M., Svenson, A. G., and Rietsch, A. (2010) Control of effector export by the Pseudomonas aeruginosa type III secretion proteins PcrG and PcrV, *Mol. Microbiol. 75*, 924-941.

9. Nanao, M., Ricard-Blum, S., Di Guilmi, A. M., Lemaire, D., Lascoux, D., Chabert, J., Attree, I., and Dessen, A. (2003) Type III secretion proteins PcrV and PcrG from Pseudomonas aeruginosa form a 1:1 complex through high affinity interactions, *BMC.Microbiol. 3*, 21.

10. Allmond, L. R., Karaca, T. J., Nguyen, V. N., Nguyen, T., Wiener-Kronish, J. P., and Sawa, T. (2003) Protein binding between PcrG-PcrV and PcrH-PopB/PopD encoded by the pcrGVH-popBD operon of the *Pseudomonas aeruginosa* type III secretion system, *Infect. Immun. 71*, 2230-2233.

11. Matson, J. S., and Nilles, M. L. (2001) LcrG-LcrV interaction is required for control of Yops secretion in *Yersinia pestis*, *J. Bacteriol. 183*, 5082-5091.

12. Hamad, M. A., and Nilles, M. L. (2007) Roles of YopN, LcrG and LcrV in controlling Yops secretion by *Yersinia pestis*, *Adv. Exp. Med. Biol. 603*, 225-234.

13. McGuffin, L. J., Bryson, K., and Jones, D. T. (2000) The PSIPRED protein structure prediction server, *Bioinformatics 16*, 404-405.

14. Matson, J. S., and Nilles, M. L. (2002) Interaction of the *Yersinia pestis* type III regulatory proteins LcrG and LcrV occurs at a hydrophobic interface, *BMC Microbiol. 2*, 16.

15. Masel, R. I. (1996) *Principles of adsorption and reaction on solid surfaces.*, Wiley-Interscience.

CHAPTER 7: Summary

The type III secretion system (T3SS) is utilized by a number of Gram-negative pathogenic bacteria to deliver effector proteins into the targeted host cells (*1*). In addition to the structural proteins that form the needle apparatus, chaperones play many important roles in type III secretion (*1*). These include stabilization of their binding partners in the cytoplasm, prevention of premature interactions with other partners, and facilitating secretion of the substrates (*2, 3*). These chaperones have been categorized into three classes depending on their T3SS substrates and these classes have been characterized structurally (*4-6*). Class I chaperones help in maintaining the effector proteins in a secretion competent state (*1*). Class II chaperones assist the hydrophobic translocators by neutralizing their toxicity while inside the bacterial cytoplasm (*1*). Lastly, Class III chaperones prevent the premature polymerization of the needle protein inside the bacterial cytosol (*1*). The T3SS tip proteins also require chaperones, but they have not been classified into any of the above three classes primarily because much less is known about their atomic structures.

Comparison of the structures of T3SS tip proteins has highlighted the absence of the N-terminal α-helical hairpin domain in the structure of the V-tip proteins. The N-terminal α-helical hairpin serves as a self-chaperone for the tip proteins IpaD and BipD (*7*). It has been suggested that LcrG and PcrG form a coiled coil structure analogous to the self-chaperoning domains of the other tip proteins (*7, 8*). However, the atomic structure of the LcrG/PcrG family of chaperones remains unknown. The aim of the research presented in this dissertation was to fill this gap by gaining insight into the solution structure and dynamics of the V-tip chaperone family using NMR spectroscopy and other biophysical techniques.

Surprisingly and contrary to the earlier hypothesis proposed by others about LcrG/PcrG forming a coiled coil (*7, 8*), data presented here show that LcrG and PcrG lack a tertiary structure (Chapters 4 and 6). The two-dimensional ^{1}H-^{15}N HSQC spectra of these chaperones displayed a narrow backbone proton chemical shift range (<1 ppm), which suggests that the protein is either highly α-helical or unstructured. CD spectroscopy and thermal denaturation showed that these chaperones are α-helical but lack a distinct melting transition, which indicate the lack of a closely packed tertiary fold. The molar ellipticity $\theta_{222/208}$ ratio of 0.7-0.8 obtained from the CD spectra of these chaperones is also indicative of a loosely packed helical protein. Similarly, the 2D ^{1}H-^{13}C HSQC spectrum of PcrG where the methyl groups of Ile, Leu and Val were ^{13}C-labeled also showed poor chemical shift dispersion with conformational heterogeneity and broad overlapping peaks. This also indicates relatively loose packing of the hydrophobic regions in PcrG. Secondary Cα and Cβ chemical shifts of the chaperones suggest that their secondary structures are dominated by two α-helices in PcrG, and three α-helices in LcrG. Characterization of the backbone dynamics of the chaperones by heteronuclear $\{^{1}H\}$-^{15}N NOE suggests that the α-helices display semi-rigid flexibility and do not form well-structured regions. However, the presence of residues within the α-helical regions with $\{^{1}H\}$-^{15}N NOE values above 0.6 implies that although the chaperones lack a well-structured three-dimensional fold, they are not completely disordered but contain residues with flexibilities approaching a more stable conformation. The ^{15}N backbone relaxation rates (R_1 and R_2) suggested that the α-helices behave with nearly similar backbone amide dynamics with respect to each other, and they tumble as a single unit in solution. Thus, the NMR and CD data presented here point towards the chaperones being highly α-helical, yet intrinsically flexible, and lacking a tertiary fold **(Figure 4-12)**.

The LcrG and PcrG chaperones are multifunctional. In addition to facilitating the secretion of their respective tip proteins (*9-11*), they play important regulatory roles in the T3SS of *Y. pestis* and *P. aeruginosa*. Both LcrG and PcrG serve as negative regulators of effector secretion (*9, 10, 12-15*). LcrG also plays a facilitative role in targeting Yop effectors into the host cells (*11, 16*). Likewise, PcrG also assists in the translocation of effector proteins into the host cells (*17*). The conformational flexibilities of the chaperones perhaps contribute to their functional versatility, which is a characteristic feature of many flexible proteins (*18, 19*). The conformationally interchangeable nature of intrinsically flexible structures like LcrG and PcrG ensures easier adaptation of distinct conformational states required for carrying out multiple roles within the cellular environment. Disordered regions confer dynamic flexibility to proteins, allowing transitions between different conformations (*20*). This increased flexibility is advantageous in the recognition of multiple binding targets (*20*). It has been suggested that disordered proteins owing to a greater capture radius can associate faster with specific binding partners as compared to globular proteins with restricticted conformational freedom (*19, 21*). Thus being partially folded proteins like the V-tip chaperone family can be particularly advantageous. Such intrinsically disordered proteins are not only associated with transcriptional regulation, translation, and cellular signal transduction (*22*), but have also become common in the T3SS. They have been observed among effectors and structural proteins (*6, 23*). The *Salmonella* inner rod protein PrgJ is an example of a partially folded α-helical protein (*23*). Among other T3SS components that also display this kind of intrinsically flexible conformation are the *Yersinia pseudotuberculosis* effector protein YopE, and the *Pseudomomas aeruginosa* translocon proteins PopB and PopD (*6, 24, 25*).

NMR titrations using ^{15}N LcrG$^{7-73}$ C34S and ^{15}N PcrG$^{9-76}$ indicated that the V-tip proteins LcrV and PcrV induced a global change in the structure of their respective chaperones upon complex formation (Chapters 5 and 6). LcrG residues Asp-7 to Arg-51 showed significant reduction in peak intensities, whereas the residues Ser-52 to Arg-73 appeared in new peak positions upon complex formation with LcrV. Likewise, PcrG residues Glu-9 to Ser-76 also showed significant reduction in peak intensities upon binding to PcrV. This suggests that the chaperones were perturbed along their entire length upon binding to the V-tip proteins. In addition to the traditional ^{15}N backbone labeling, ^{13}C methyl labeling of the side chains of isoleucines, leucines and valines (ILV) of the chaperones were also used to map the binding interface. The ILVs are well distributed along the chaperones and since hydrophobic interactions are an important component of protein-protein interactions, mapping the effects on ^{13}C-methyl labeled ILV to identify the binding interface was a reasonable alternative. NMR titrations using ^{13}C ILV-LcrG$^{7-73}$ C34S and ^{13}C ILV-PcrG$^{9-76}$ further confirmed the observation that upon complex formation, the V-tip proteins induced a global change in the structure of the chaperones. On one hand, this data agrees with the published results that showed the N-terminus of the chaperones is the binding site for the V-tip proteins (*9, 12*). On the other hand, NMR titrations reported in this dissertation also indicated that the C-terminus of the chaperones is perturbed upon binding. One likely explanation for this is that the sheer difference in size between the two binding partners (33-37 kDa for the V-tip proteins and 8 kDa for the chaperones) entails that almost the full length of the chaperones (LcrG and PcrG) is needed to form a stable binding interface. This will not be uncommon since many flexible proteins present a larger surface area for interaction as compared to globular proteins (*18*). It has also been confirmed by NMR spectroscopy that the coiled coil domain in LcrV is important in binding to LcrG.

Examples of protein folding transitions are common in the T3SS. The flexible regions of needle protomers become ordered upon needle assembly (*26*). The *Yersinia* effector protein YopE undergoes a disorder-to-order transition upon complex formation with its chaperone, SycD (*6*). However, there is an example of the *P. aeruginosa* translocon protein PopD that remains in a molten globule like conformation, both in isolation and upon complex formation with its chaperone PcrH (*25*). Data presented herein does not indicate any disorder-to-order transition of the chaperones upon complex formation with the tip proteins. The interaction of the chaperones with their cognate tip proteins seems to discount the possibility of the chaperone-tip interaction being mediated by coiled coil domains (*27*), as the structure of neither LcrG nor PcrG becomes orderd upon binding. If the interhelical contacts within the chaperones improved upon binding to their respective tip proteins it would have led to an increase in dispersion of the backbone proton chemical shift range of the ^{15}N labeled HSQC spectrum of the chaperones upon titration with the tip proteins. This kind of increased dispersion of the HSQC spectrum has been observed for a partially folded T3SS chaperone CesAB (from enteropathogenic *Escherichia coli,* EPEC) upon complex formation with the needle filament protein EspA (*28*), thereby indicating that CesAB folds upon binding to EspA. But data presented here does not support any folding event of the V-tip chaperones upon binding to the tip proteins. This may also have been one of the reasons due to which it was not possible to obtain a co-crystal of the LcrG-LcrV complex. A future possibility could be to try co-overexpression of the tip protein and chaperone and test if that makes the structure of the complex more amenable to crystallization or structure determination by NMR. Another exciting future possibility is to try and stabilize the dynamic conformation of the chaperones. An example of stabilization of a molten globule like conformation of the T3SS chaperone, CesAB comes from the work of Chen *et al.* (*28*). Chen *et*

al. (*28*) stabilized the partially folded conformation of CesAB by correcting the packing defects of the coiled coil of CesAB. However, it would be important to verify whether the artificially stabilized chaperones remain functional in the T3SS. Notably, if the chaperones lose functionality on stabilization it would be further proof that the flexibility of LcrG and PcrG is essential for its functionality. In fact the artificially stabilized CesAB chaperone led to non-functional T3SS (*28*), highlighting the importance of structural flexibility in achieving function. Additionally other chaperones from different T3SS systems have also been shown to adopt this kind of partially folded conformation (*28*), thereby providing additional support for the physiological relevance of proteins with highly dynamic confromations.

Overall the results from the NMR titrations show that both the chaperones are perturbed along their entire length upon binding to the tip proteins. More specifically, the NMR titrations using LcrG showed that the C-terminus of LcrG (Ser-52 to Arg-73) is highly perturbed upon binding to LcrV and this interaction is in slow exchange, which means tight binding. On the other hand, the interaction with N-terminus of LcrG (Asp-7 to Arg-51) with LcrV is in intermediate exchange, which means weaker binding. Thus, introspecting about the above results in plurality leads to a likely scenario where the entire length of the chaperones is involved in complex formation with the tip proteins, where the C-terminal half of LcrG binds more tightly to LcrV, while the N-terminal half binds weakly to LcrV. Due to the absence of the structure of the complex between the tip protein and chaperone, it is unclear exactly how the helices in the chaperones mediate protein-protein interactions with the coiled coil domain of LcrV. The results of the Yop secretion assay (Chapter 5) suggest that the C-terminus of LcrG from residues Ser-52 to Ile-67 plays an important role in blocking the secretion of Yop effectors. This data is further corroborated by results on the homolog PcrG, which also indicate that the C-terminus of PcrG is

important in blocking the secretion of effectors (*9*). Thus, our data suggests that the tip protein binding site and the secretion blocking site at the C-terminal region of LcrG overlap with each other. However, studies with the homolog PcrG has shown that the tip protein binding and the secretion blocking activities can be separately attributed to the two halves of PcrG, though the full length of PcrG is needed for PcrV export (*9*). The data presented here, indiactes that this might not be true for LcrG. Further experiments are required to test this possibility, by creating more drastic mutants (such as three point mutations) in both the halves of LcrG, and testing them separately for their ability to bind LcrV and block effector secretion in *Y. pestis.* This would lead to an overall understanding of how LcrG performs the dual activity of facilitating tip protein secretion and blocking secretion of effector proteins in *Y. pestis.*

Since LcrG and PcrG have multiple roles in the T3SS, it is likely that they have multiple binding partners. Characterization of the individual protein-protein interactions of these chaperones with the other components of the T3SS would improve the overall understanding of the regulation of effector secretion. Since both the chaperones plug the T3SS from the cytoplasmic face, they might be binding to the components of the base, export apparatus or the ATPase complex. The export apparatus (EA) consists of five integral membrane proteins that form the export channel in the inner membrane and are believed to recognize export substrates (*29*). Among the EA components, the cytosolic domain of *Yersinia* YscV/*Pseudomonas* PcrD presents a possible target for interaction with T3SS components and chaperones (*29*). Additionally the cytosolic domain of *Yersinia* YscU/*Pseudomonas* PscU is important in substrate switching of the T3SS components during secretion (*29*). Hence, it is tempting to speculate that the chaperones might be involved in protein-protein interaction with at least these two components at the cytoplasmic face of the T3SS. This interaction of the chaperones with the T3SS components hinders the

recognition of the effector proteins, thereby blocking secretion of the effectors. With respect to the *Yersinia* system it is not unreasonable to speculate that LcrV initially recognizes an LcrG-T3SS complex, and promotes the dissociation of LcrG by altering its interaction with the T3SS components. This is followed by the formation of an LcrG-LcrV heterodimer, which removes the negative block allowing the secretion of effectors. Thus, identification of these T3SS components would yield an improved understanding of secretion regulation by the *Yersinia* and *Pseudomomas* T3SS.

The LcrV crystal structure reported in this dissertation is at a higher resolution of 1.65 Å compared to the previous structure (*30*) (Chapter 3). Importantly, this structure does not have any mutations in the N-terminal domain of LcrV as opposed to the triple mutant K40A/D41A/K42A used to solve the original structure of LcrV (*30*). Overall, the two structures are similar but there are notable differences particularly near the site of the triple mutation. The refined structure reported here revealed a slight shift in the backbone position of residues Gly-28 to Asn-43, and displayed electron density in the loop region from residues Ile-46 toVal-63 that was disordered in the original structure. In addition, the helical region spanning residues Tyr-77 to Gln-95 adopts a different orientation. The triple mutations in 1R6F are located in the N-terminal domain of LcrV, which forms the base of the tip complex and suggested to be involved in protein-protein interaction with the translocon (*31*). Thus, the refined crystal structure of LcrV reported here with native residues in the N-terminal domain would be useful in future structural modeling of the LcrV-translocon interaction.

In conclusion, the research presented herein provides the first structural characterization of the LcrG/PcrG family of chaperone proteins from *Y. pestis* and *P. aeruginosa.* It was not possible to elucidate their three-dimensional structure because of the inherent flexibility of the chaperones,

which likely contributes to their functional versatility. Along with the characterization of their individual structures, this dissertation showed for the first time the structural effects of the interaction between the V-tip proteins of the bacterial T3SS and their cognate chaperones.

7.1 References

1. Cornelis, G. R. (2006) The type III secretion injectisome, *Nat. Rev. Microbiol. 4*, 811-825.
2. Parsot, C., Hamiaux, C., and Page, A. L. (2003) The various and varying roles of specific chaperones in type III secretion systems, *Curr Opin Microbiol 6*, 7-14.
3. Page, A. L., and Parsot, C. (2002) Chaperones of the type III secretion pathway: jacks of all trades, *Mol Microbiol 46*, 1-11.
4. Sun, P., Tropea, J. E., Austin, B. P., Cherry, S., and Waugh, D. S. (2008) Structural Characterization of the Yersinia pestis Type III Secretion System Needle Protein YscF in Complex with Its Heterodimeric Chaperone YscE/YscG, *J. Mol. Biol. 377*, 819-830.
5. Schreiner, M., and Niemann, H. H. (2012) Crystal structure of the Yersinia enterocolitica type III secretion chaperone SycD in complex with a peptide of the minor translocator YopD, *BMC Struct Biol 12*, 13.
6. Rodgers, L., Gamez, A., Riek, R., and Ghosh, P. (2008) The type III secretion chaperone SycE promotes a localized disorder-to-order transition in the natively unfolded effector YopE, *J. Biol. Chem. 283*, 20857-20863.
7. Johnson, S., Roversi, P., Espina, M., Olive, A., Deane, J. E., Birket, S., Field, T., Picking, W. D., Blocker, A. J., Galyov, E. E., Picking, W. L., and Lea, S. M. (2007) Self-chaperoning of the type III secretion system needle tip proteins IpaD and BipD, *J. Biol. Chem. 282*, 4035-4044.

8. Blocker, A. J., Deane, J. E., Veenendaal, A. K., Roversi, P., Hodgkinson, J. L., Johnson, S., and Lea, S. M. (2008) What's the point of the type III secretion system needle?, *Proc. Natl. Acad. Sci. U.S.A. 105*, 6507-6513.

9. Lee, P. C., Stopford, C. M., Svenson, A. G., and Rietsch, A. (2010) Control of effector export by the Pseudomonas aeruginosa type III secretion proteins PcrG and PcrV, *Mol. Microbiol. 75*, 924-941.

10. Matson, J. S., and Nilles, M. L. (2001) LcrG-LcrV interaction is required for control of Yops secretion in *Yersinia pestis*, *J. Bacteriol. 183*, 5082-5091.

11. Fields, K. A., Nilles, M. L., Cowan, C., and Straley, S. C. (1999) Virulence role of V antigen of Yersinia pestis at the bacterial surface, *Infect.Immun. 67*, 5395-5408.

12. Matson, J. S., and Nilles, M. L. (2002) Interaction of the *Yersinia pestis* type III regulatory proteins LcrG and LcrV occurs at a hydrophobic interface, *BMC Microbiol. 2*, 16.

13. Skrzypek, E., and Straley, S. C. (1993) LcrG, a secreted protein involved in negative regulation of the low-calcium response in *Yersinia pestis*, *J. Bact. 175*, 3520-3528.

14. Nilles, M. L., Williams, A. W., Skrzypek, E., and Straley, S. C. (1997) Yersinia pestis LcrV forms a stable complex with LcrG and may have a secretion-related regulatory role in the low-Ca2+ response, *J Bacteriol 179*, 1307-1316.

15. Nilles, M. L., Fields, K. A., and Straley, S. C. (1998) The V antigen of Yersinia pestis regulates Yop vectorial targeting as well as Yop secretion through effects on YopB and LcrG, *J Bacteriol 180*, 3410-3420.

16. Sarker, M. R., Sory, M. P., Boyd, A. P., Iriarte, M., and Cornelis, G. R. (1998) LcrG is required for efficient translocation of Yersinia Yop effector proteins into eukaryotic cells, *Infect Immun 66*, 2976-2979.

17. Sundin, C., Thelaus, J., Broms, J. E., and Forsberg, A. (2004) Polarisation of type III translocation by Pseudomonas aeruginosa requires PcrG, PcrV and PopN, *Microb. Pathog. 37*, 313-322.

18. Babu, M. M., van der Lee, R., de Groot, N. S., and Gsponer, J. (2011) Intrinsically disordered proteins: regulation and disease, *Curr Opin Struct Biol 21*, 432-440.

19. Wright, P. E., and Dyson, H. J. (2009) Linking folding and binding, *Curr Opin Struct Biol 19*, 31-38.

20. Lobley, A., Swindells, M. B., Orengo, C. A., and Jones, D. T. (2007) Inferring function using patterns of native disorder in proteins, *PLoS Comput Biol 3*, e162.

21. Shoemaker, B. A., Portman, J. J., and Wolynes, P. G. (2000) Speeding molecular recognition by using the folding funnel: the fly-casting mechanism, *Proc Natl Acad Sci U S A 97*, 8868-8873.

22. Dyson, H. J., and Wright, P. E. (2005) Intrinsically unstructured proteins and their functions, *Nat Rev Mol Cell Biol 6*, 197-208.

23. Zhong, D., Lefebre, M., Kaur, K., McDowell, M. A., Gdowski, C., Jo, S., Wang, Y., Benedict, S. H., Lea, S. M., Galan, J. E., and De Guzman, R. N. (2012) The *Salmonella* Type III Secretion System Inner Rod Protein PrgJ Is Partially Folded, *J. Biol. Chem. 287*, 25303-25311.

24. Dey, S., Basu, A., and Datta, S. (2012) Characterization of molten globule PopB in absence and presence of its chaperone PcrH, *Protein J 31*, 401-416.

25. Faudry, E., Job, V., Dessen, A., Attree, I., and Forge, V. (2007) Type III secretion system translocator has a molten globule conformation both in its free and chaperone-bound forms, *FEBS J 274*, 3601-3610.

26. Deane, J. E., Roversi, P., Cordes, F. S., Johnson, S., Kenjale, R., Daniell, S., Booy, F., Picking, W. D., Picking, W. L., Blocker, A. J., and Lea, S. M. (2006) Molecular model of a type III secretion system needle: Implications for host-cell sensing, *Proc. Natl. Acad. Sci. U.S.A. 103*, 12529-12533.

27. Lawton, D. G., Longstaff, C., Wallace, B. A., Hill, J., Leary, S. E., Titball, R. W., and Brown, K. A. (2002) Interactions of the type III secretion pathway proteins LcrV and LcrG from *Yersinia* pestis are mediated by coiled-coil domains, *J. Biol. Chem. 277*, 38714-38722.

28. Chen, L., Balabanidou, V., Remeta, D. P., Minetti, C. A., Portaliou, A. G., Economou, A., and Kalodimos, C. G. (2011) Structural instability tuning as a regulatory mechanism in protein-protein interactions, *Mol. Cell. 44*, 734-744.

29. Diepold, A., Wiesand, U., and Cornelis, G. R. (2011) The assembly of the export apparatus (YscR,S,T,U,V) of the Yersinia type III secretion apparatus occurs independently of other structural components and involves the formation of an YscV oligomer, *Mol Microbiol 82*, 502-514.

30. Derewenda, U., Mateja, A., Devedjiev, Y., Routzahn, K. M., Evdokimov, A. G., Derewenda, Z. S., and Waugh, D. S. (2004) The structure of *Yersinia pestis* V-antigen, an essential virulence factor and mediator of immunity against plague, *Structure 12*, 301-306.

31. Broz, P., Mueller, C. A., Muller, S. A., Philippsen, A., Sorg, I., Engel, A., and Cornelis, G. R. (2007) Function and molecular architecture of the Yersinia injectisome tip complex, *Mol. Microbiol. 65*, 1311-1320.